



## Collisions

Collision Cross section

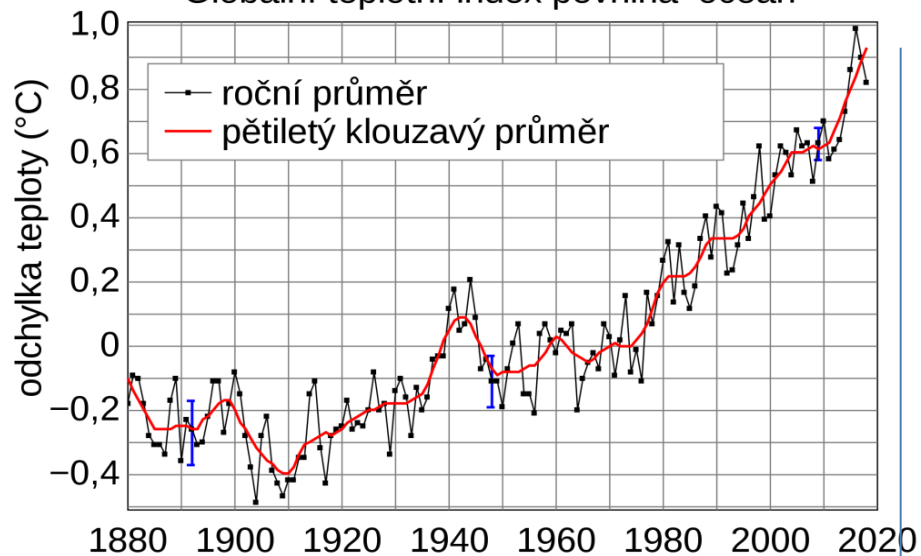
Collision rate coefficient

Reaction Cross section

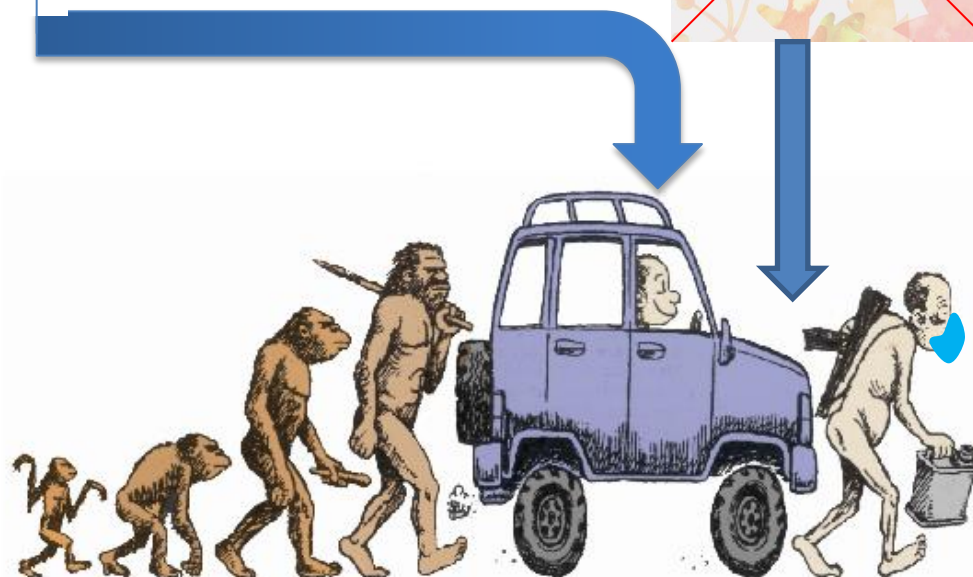
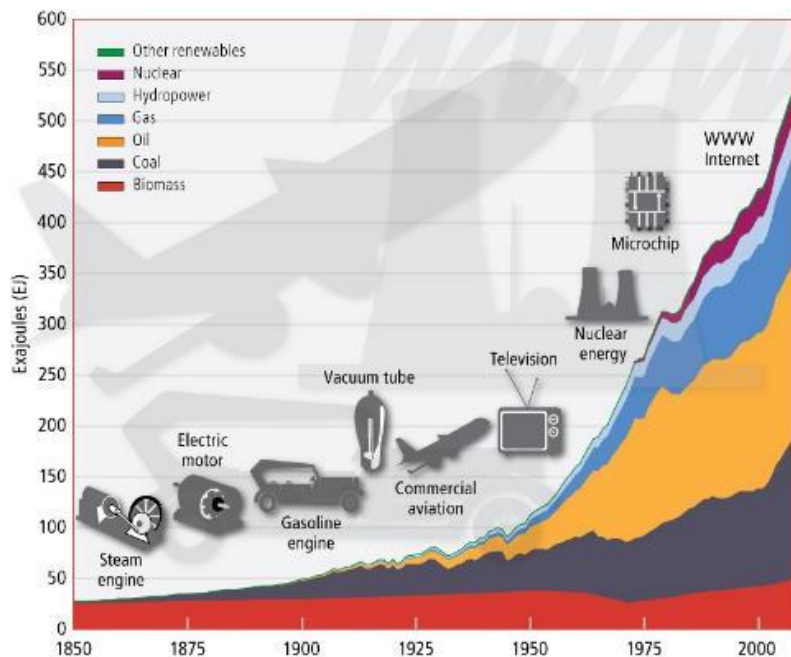
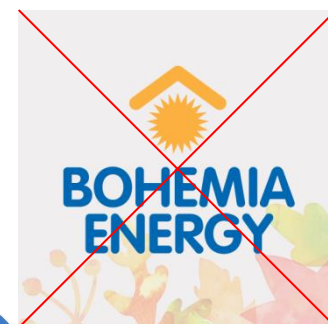
Reaction rate coefficient

Electron collisions

Globální teplotní index pevnina-oceán



Kdo z vás je bez hříchu,  
první hod' na ni kamenem

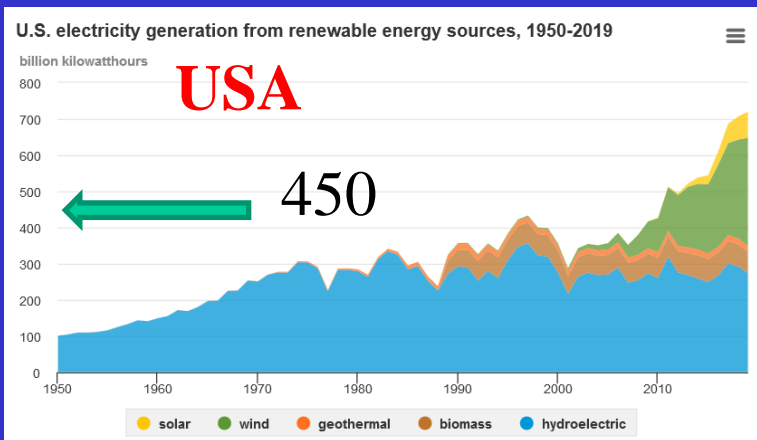
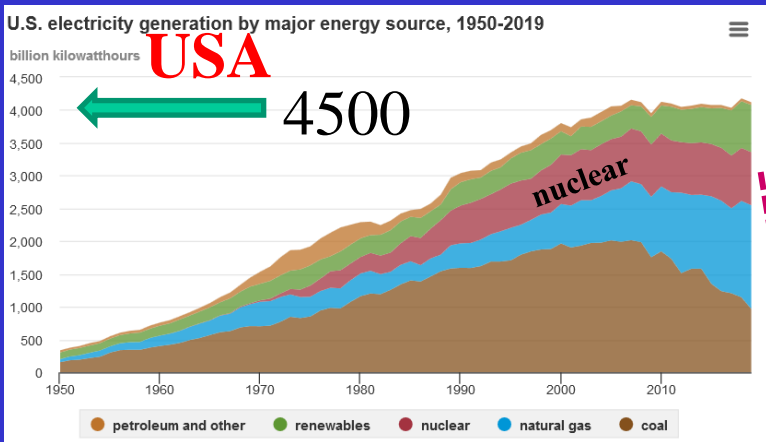


Why fusion ?

To avoid the last step, if possible! ➔

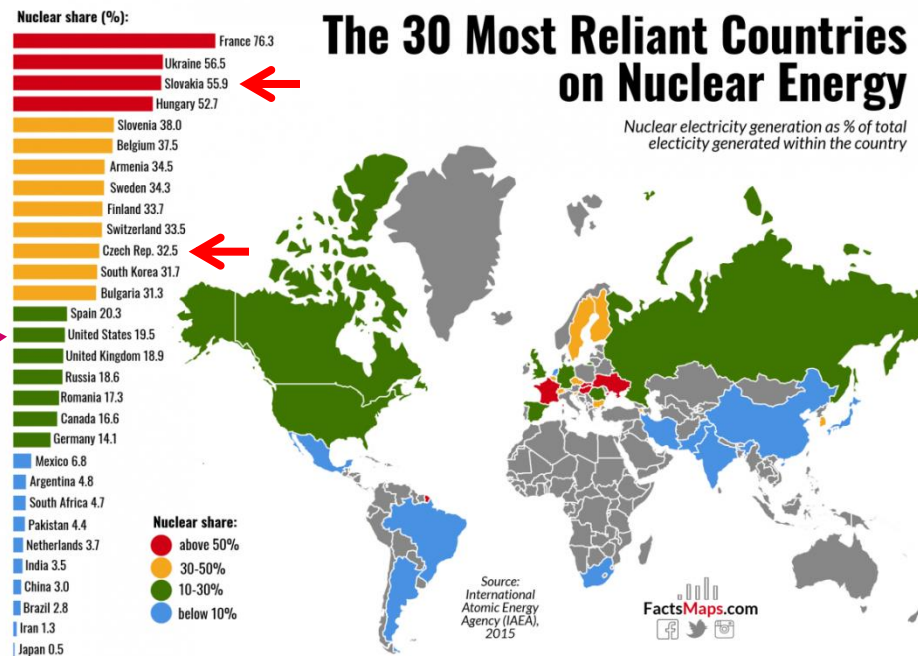
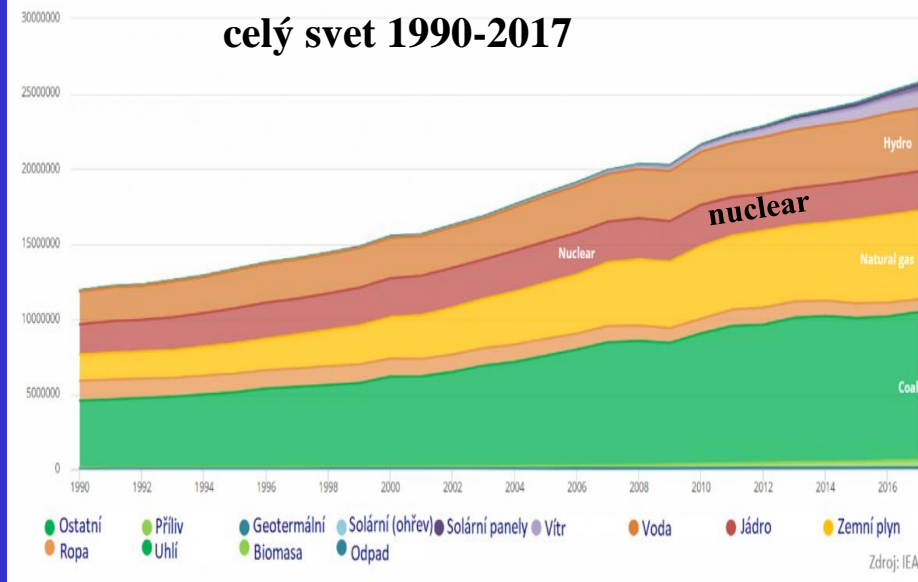


... bla...bla ... bla....



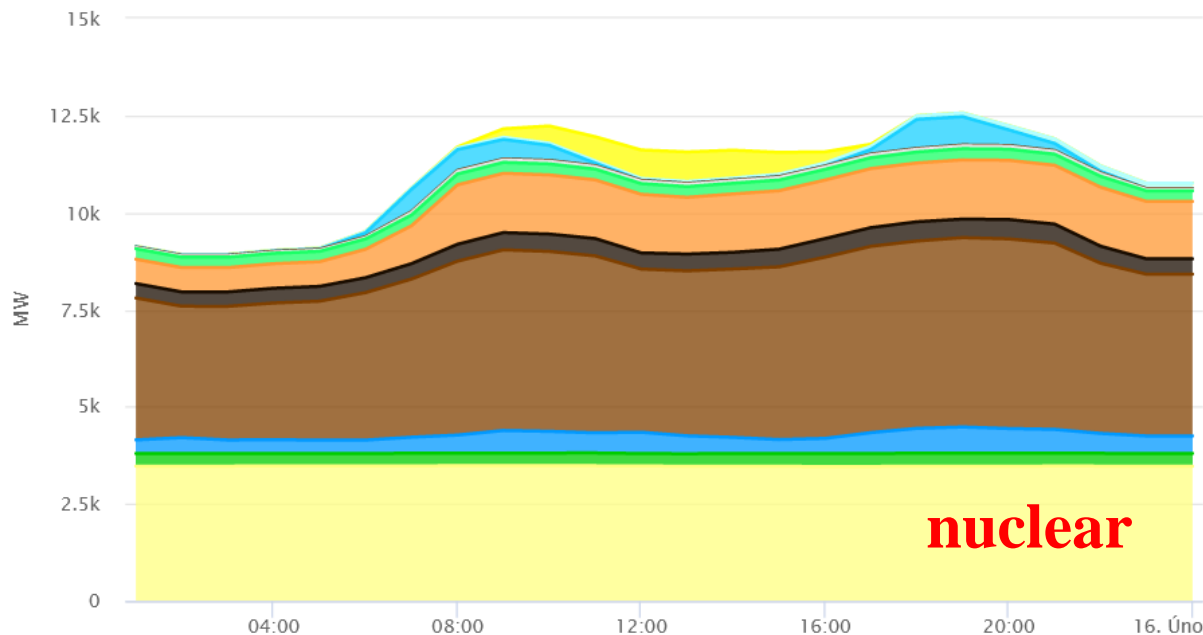
## Výroba elektřiny podle zdroje

celý svět 1990-2017



# Česká republika: Výroba elektřiny

Data od: 15. 2. 2021 do: 15. 2. 2021

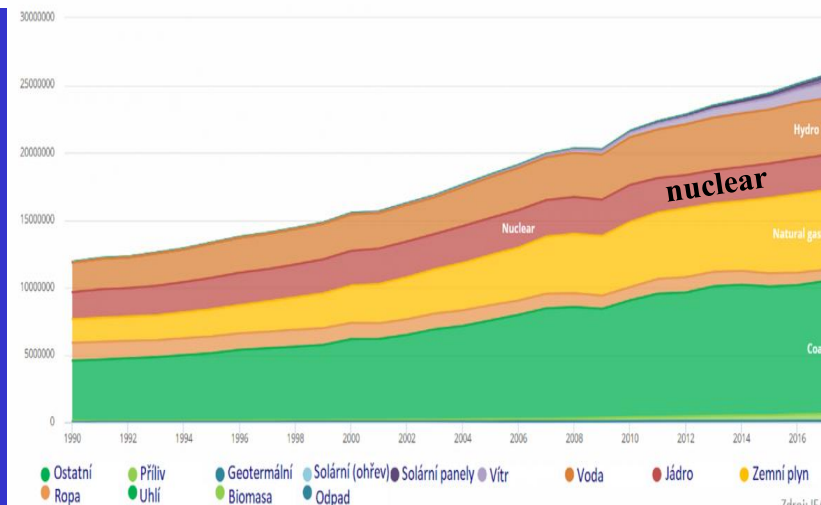


- Solární elektrárny
- Zpracování odpadu
- Plynové zdroje
- Vodní elektrárny
- Větrné elektrárny – onshore
- Ostatní
- Černé uhlí
- Biomasa
- Přečerpávací elektrárny
- Ostatní OZE
- Hnědé uhlí
- Jaderné elektrárny

**nuclear**

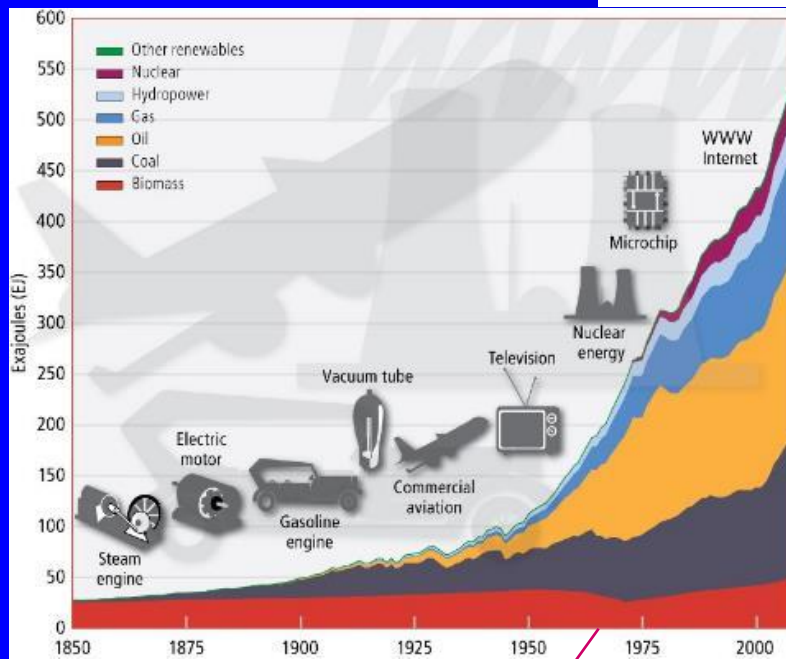
**celý svět 1990-2017**

## Výroba elektřiny podle zdroje



**nuclear**

can you see the correlations ????

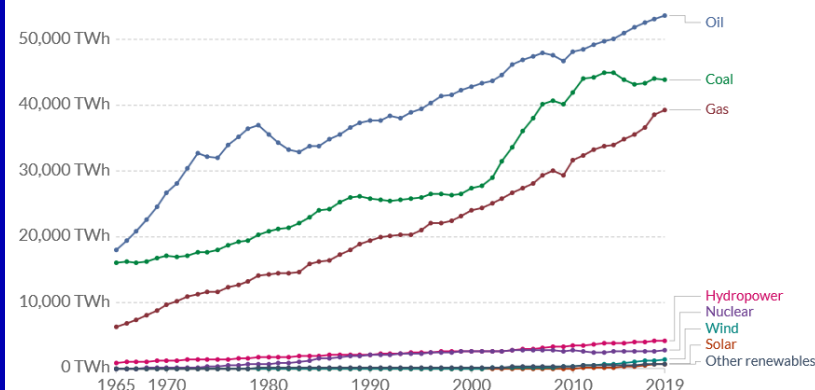


## Primary direct energy consumption by source, World

Energy consumption is shown as direct primary energy. This means this does not correct for fossil fuel inefficiencies in conversion to useful energy estimates.

Our World in Data

Change country



Source: BP Statistical Review of Global Energy  
Note: Includes only commercially-traded fuels (coal, oil, gas), nuclear and modern renewables. As such, it does not include traditional biomass sources.

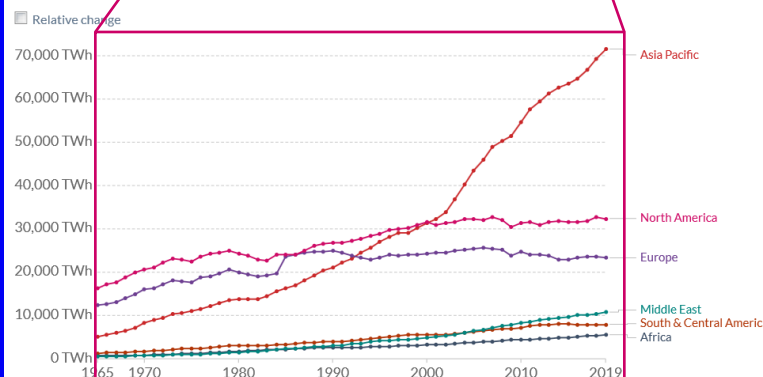
CC BY

can you see the correlations ????

## Primary energy consumption by world region

Primary energy consumption is measured in terawatt-hours (TWh). Note that this data includes only commercially-traded fuels (coal, oil, gas), nuclear and modern renewables used in electricity production. As such, it does not include traditional biomass sources.

Our World in Data

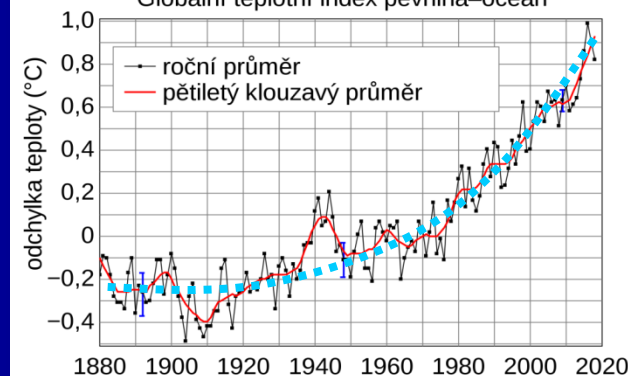


Source: BP Statistical Review of World Energy (2019)

CC BY

1965 2019  
CHART TABLE SOURCES DOWNLOAD

## Globální teplotní index pevnina-oceán

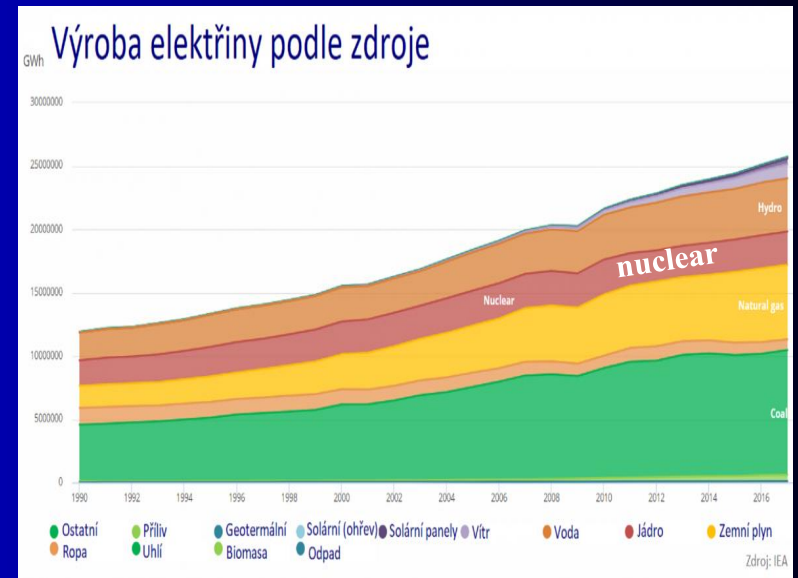






... bla...bla ... bla....

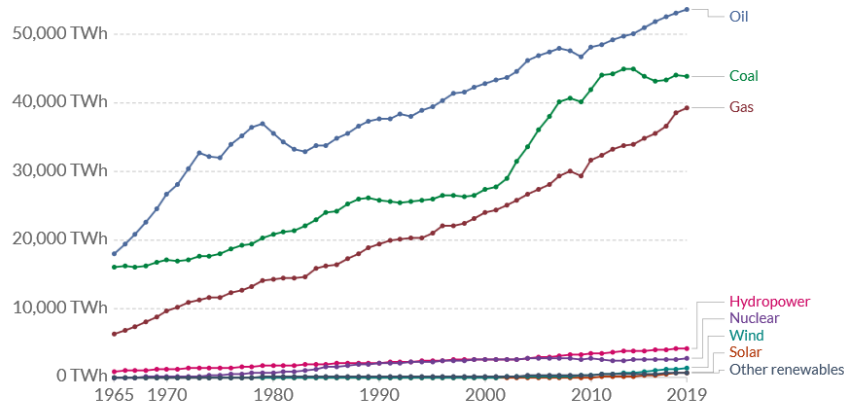
celý svet 1990-2017



## Primary direct energy consumption by source, World

Energy consumption is shown as direct primary energy. This means this does not correct for fossil fuel inefficiencies in conversion to useful energy estimates.

Change country



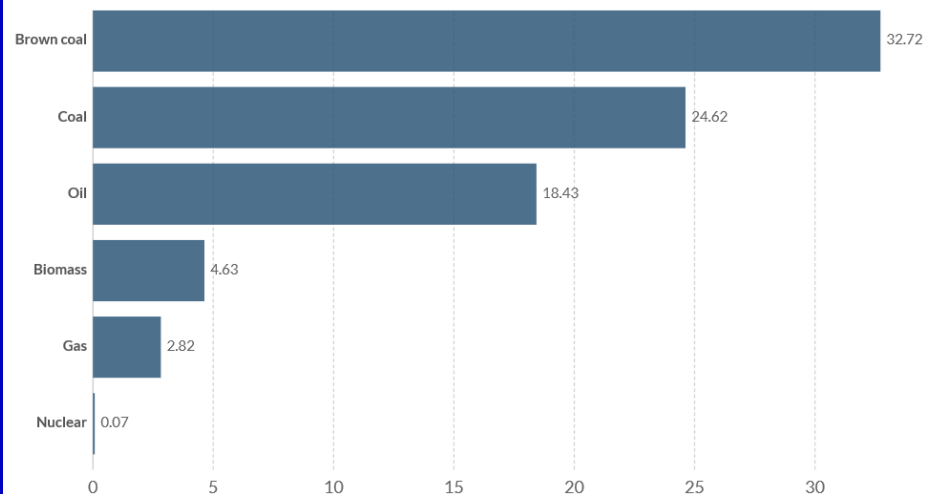
Source: BP Statistical Review of Global Energy  
Note: Includes only commercially-traded fuels (coal, oil, gas), nuclear and modern renewables. As such, it does not include traditional biomass sources.

CC BY

1965 2019

## Death rates from energy production per TWh

Death rates from air pollution and accidents related to energy production, measured in deaths per terawatt hours (TWh)



Source: Markandya and Wilkinson (2007)

Note: Figures include deaths resulting from accidents in energy production and deaths related to air pollution impacts. Deaths related to air pollution are dominant, typically accounting for greater than 99% of the total.

CC BY

# Debye shielding

$$n_e = n_\infty \exp(eV / kT_e)$$

$eV \ll kT_e$ , exponential can be approximated by linear term  $\rightarrow$

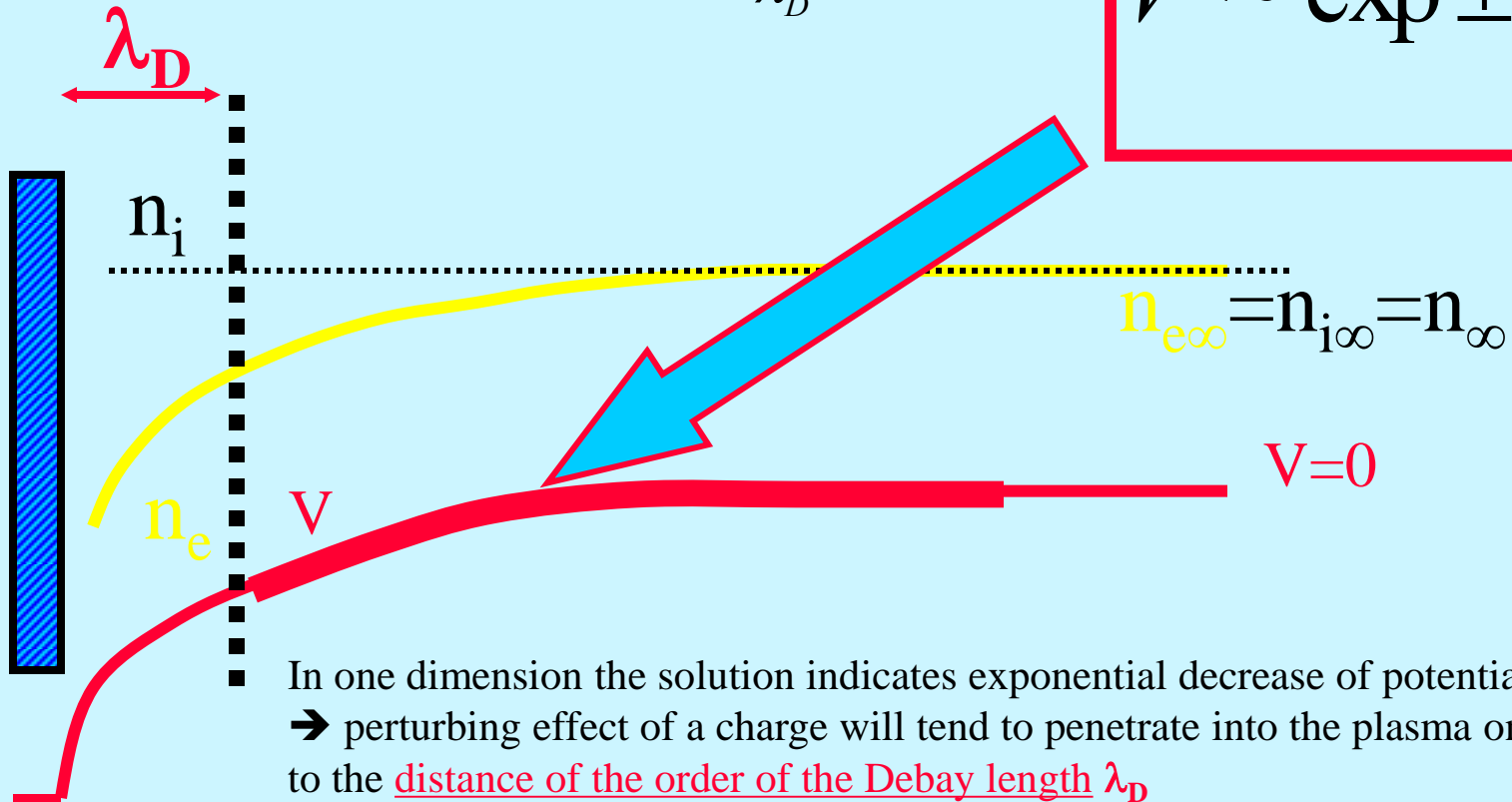
$$\nabla^2 V = \frac{-\rho}{\epsilon_0} = \frac{-e}{\epsilon_0} (n_i - n_e) = \frac{-e}{\epsilon_0} n_\infty [1 - \exp(\frac{eV}{kT_e})]$$

$$\nabla^2 V = \frac{-e}{\epsilon_0} n_\infty [\frac{-eV}{kT_e}] = \frac{e}{\epsilon_0} n_\infty \frac{eV}{kT_e} = \frac{V}{\lambda_D^2}$$

$$\lambda_D = (\epsilon_0 kT_e / e^2 n_\infty)^{1/2}$$

$$\nabla^2 V = \frac{V}{\lambda_D^2}$$

$$V \sim \exp \pm \frac{x}{\lambda_D}$$



In one dimension the solution indicates exponential decrease of potential  
 $\rightarrow$  perturbing effect of a charge will tend to penetrate into the plasma only to the distance of the order of the Debye length  $\lambda_D$

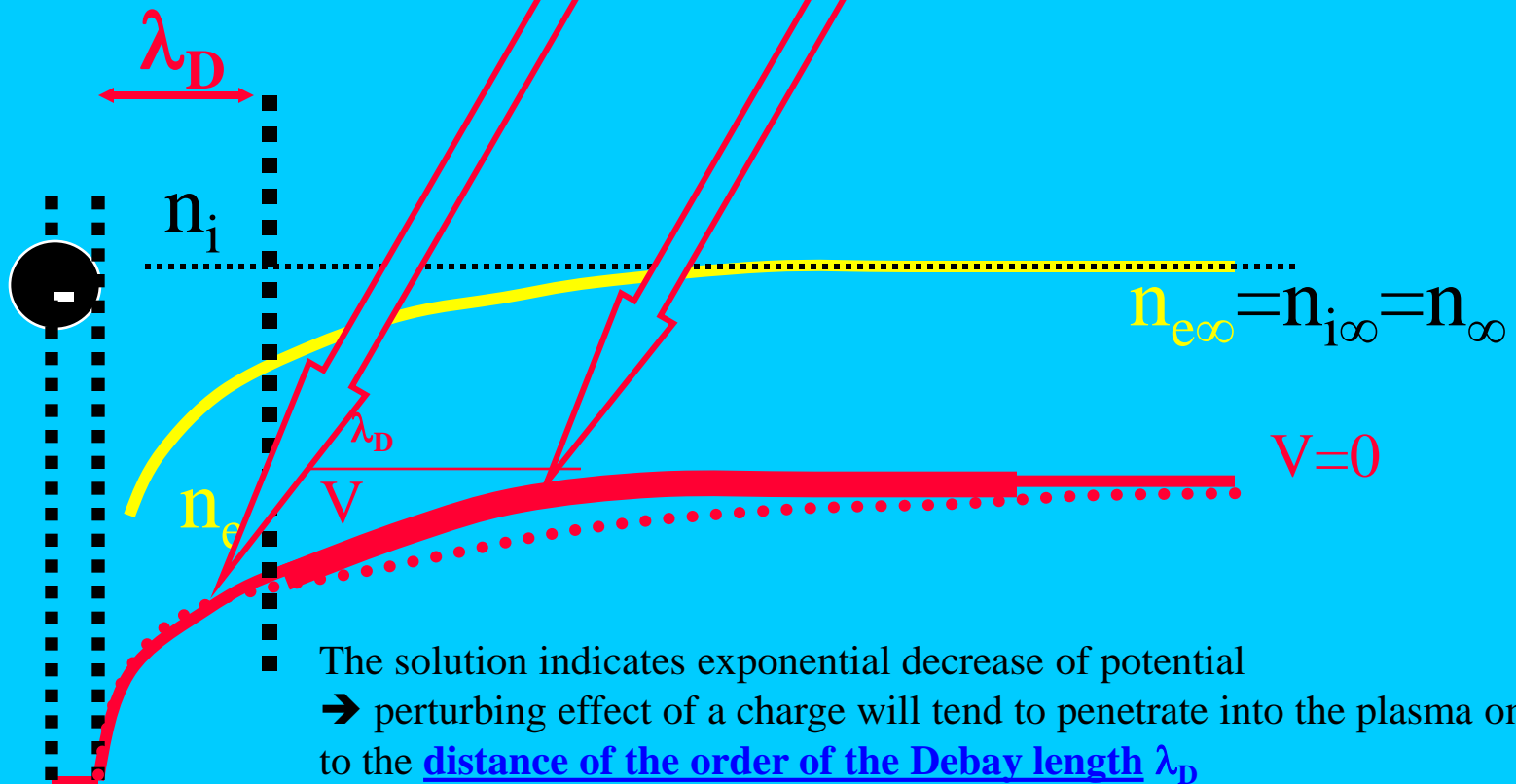
**Linear approximation just to understand problem**

# Debye shielding

## Spherical symmetry

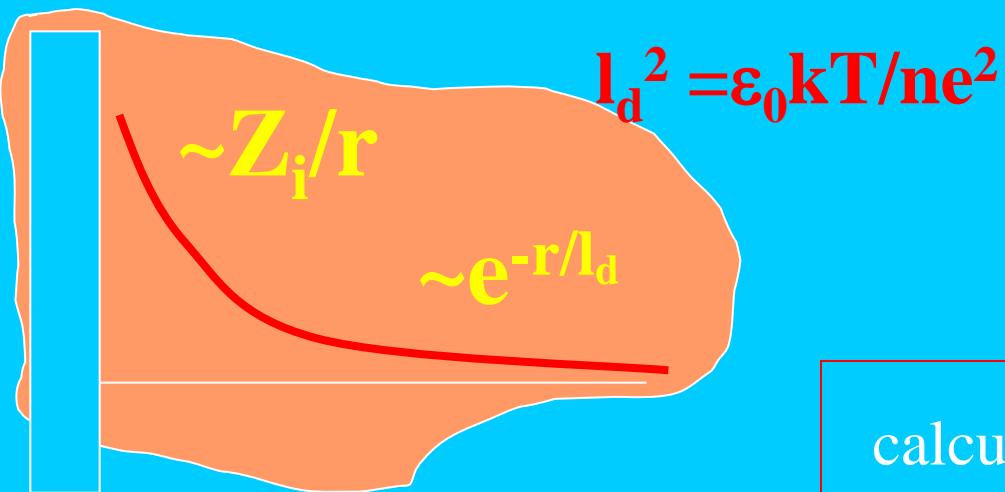
$$V = \frac{e}{r} \exp(-r / \lambda_{DX})$$

$$\lambda_{DX} = (kT_e / 4\pi e^2 n_\infty)^{1/2}$$



- The solution indicates exponential decrease of potential  
 ➔ perturbing effect of a charge will tend to penetrate into the plasma only to the distance of the order of the Debye length  $\lambda_D$





$$\phi(r) = (Z_i e / 4\pi \epsilon_0) / r * e^{-r/l_d}$$

$$\sigma_c(v) = 2\pi \int b \, db$$

Problem can be ....

calculation

$$l_d = 69 \sqrt{\frac{T}{n}}, \quad T \text{ in } K, n \text{ in } m^{-3}$$

at 1000K,  $n = 4.8 \times 10^{12} m^{-3} = 4.8 \times 10^6 \text{ cm}^{-3}$

$l_d = 1 \text{ mm} = 0.001 \text{ m}$

at 10K,  $n = 1 \times 10^{10} m^{-3} = 1 \times 10^4 \text{ cm}^{-3}$

$l_d \sim 2 \text{ mm} \sim 0.002 \text{ m}$

$$l_d = 69 \sqrt{\frac{T}{n}}, \quad T \text{ in } K, n \text{ in } m^{-3}$$

$$\lambda_{De} \equiv \sqrt{\frac{\epsilon_0 T_e}{n_e e^2}} \simeq 7434 \sqrt{\frac{T_e (\text{eV})}{n_e (\text{m}^{-3})}} \text{ m,} \quad \text{electron Debye length.}$$

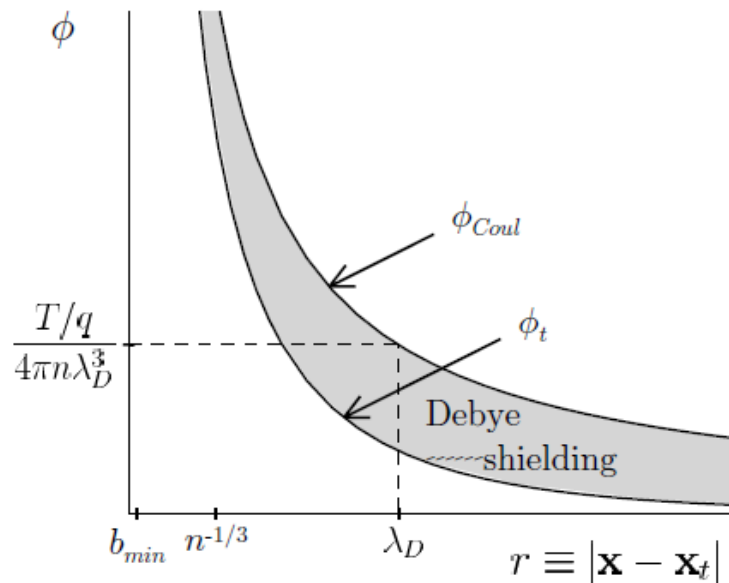


Figure 1.1: Potential  $\phi_t$  around a test particle of charge  $q_t$  in a plasma and Coulomb potential  $\phi_{Coul}$ , both as a function of radial distance from the test particle. The shaded region represents the Debye shielding effect. The characteristic distances are:  $\lambda_D$ , Debye shielding distance;  $n_e^{-1/3}$ , mean electron separation distance;  $b_{min}^{cl} = q^2 / (4\pi\epsilon_0 T)$ , classical distance of “closest approach” where the  $e\phi/T \ll 1$  approximation breaks down.

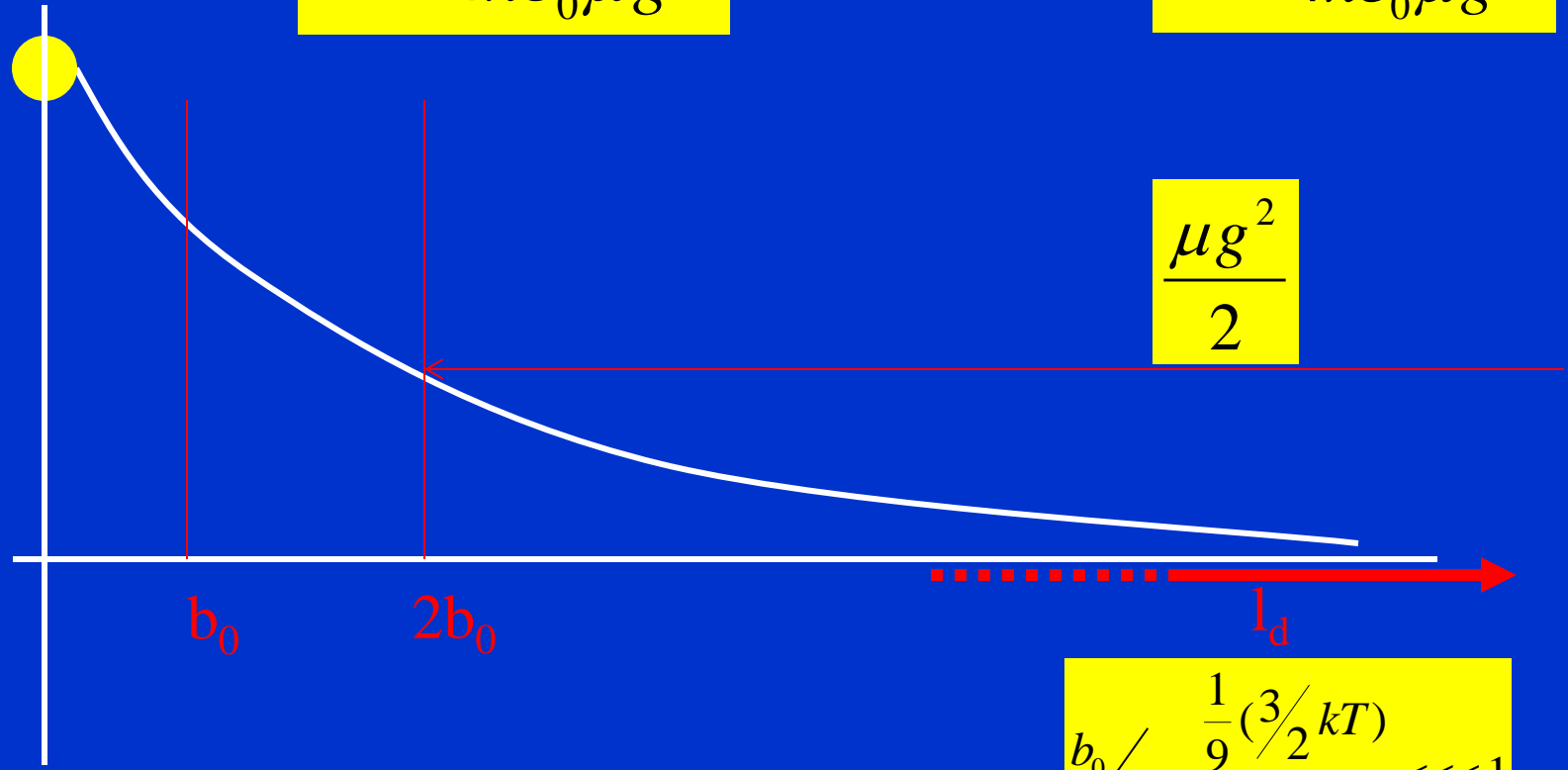
$$l_d^2 = \frac{\epsilon_0 k T_1 T_2}{e^2 (Z_1^2 n_{10} T_2 + Z_2^2 n_{20} T_1)}$$

For quasineutral plasma,  
 $n_{10} = n_{20} = n/2 =$  with  $T_1 = T_2$  we obtain

$$l_d^2 = \frac{\epsilon_0 k T}{n e^2}$$

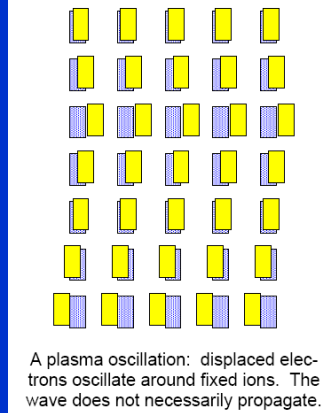
$$b_0 = \frac{Z_1 Z_2 e^2}{4 \pi \epsilon_0 \mu g^2}$$

$$b_0 = \frac{e^2}{4 \pi \epsilon_0 \mu g^2}$$



$$b_0 / l_d = \frac{\frac{1}{9} (3/2 k T)}{N^{1/2} \mu g^2} \lll 1$$

# Oscillation



Gaus equation

$$\oint_s \vec{E} \cdot d\vec{S} = Q / \epsilon_0$$

$$E = enx / \epsilon_0$$

$$m_e d^2(x) / dt^2 = -eE$$

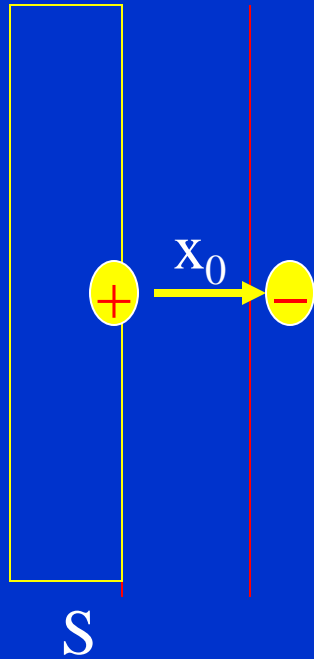
$$\omega_p = (4\pi n e^2 / m_e)^{1/2}$$

$$d^2 x / dt^2 = -\omega_p^2 x$$

Langmuir, or plasma, frequency

$$f_p = 9 \sqrt{n(10^{12} \text{ cm}^{-3})} \text{ GHz}$$

$$l_d \omega_p = (2T / m_e)^{1/2} \approx \text{thermal electron velocity}$$



## oscillations and collisions

$$\varpi_p = (4\pi n e^2 / m_e)^{1/2}$$

$$\tau_{collision} \sim 1 / \varpi_{collision}$$

## Condition of ideal plasma

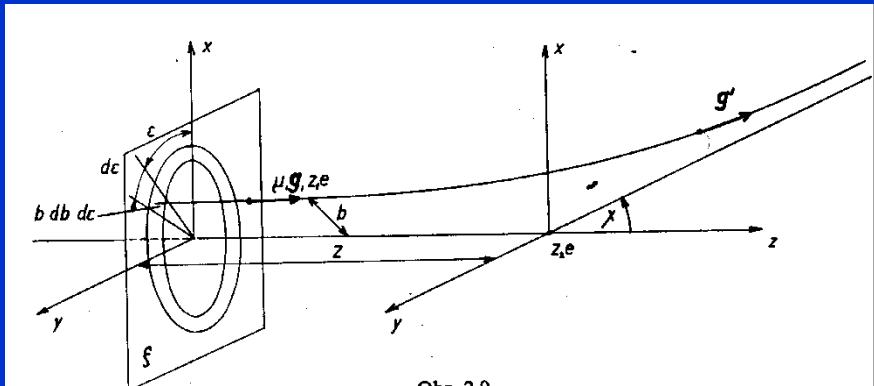
$$\varpi_p / \varpi_{collision} > 1$$

Many types of collisions .....

# Coulomb Logarithm



# Coulombic interaction



$$F = - \frac{d}{dt} \sum_{(i)} p_{1i} = - \frac{g}{g} \mu \sum_{(i)} \frac{d}{dt} g_z,$$

## Coulombovský rozptyl

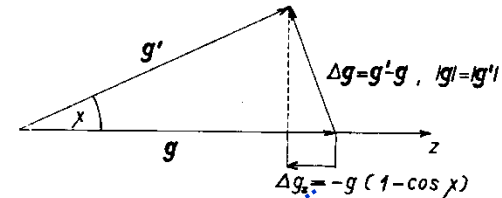
### Coulombic interaction ... formula for angle

Literatura:

„Velký Kracík“ ... čísla rovnic...

# Coulomb Logarithm

kde suma přes  $i$  značí sečítání přes všechny částice svazku. Výraz  $\sum_{(i)} (dg_z/dt)$  je možno celkem snadno určit: fyzikálně totiž znamená změnu relativní rychlosti svazku částic za jednotku času, nebo – což je totéž – změnu relativní rychlosti jedné částice svazku vlivem srážky, vynásobenou počtem srážek za jednotku času (předpokládáme, že interakci svazku můžeme rozdělit na jednotlivé binární srážky).



Obr. 2.10.

Změnu relativní rychlosti jedné částice svazku  $\Delta g_z$  určíme snadno z obr. 2.10. Snadno zjistíme, že

$$(2.136) \quad \Delta g_z = -g(1 - \cos \chi) = -2g \sin^2 \frac{\chi}{2}.$$

Počet srážek za jednotku času závisí zřejmě na průřezu svazku; za jednotku času „dosáhnou“ silového centra pouze ty částice, jejichž vzdálenost  $Z \leq g \cdot 1 \text{ sec}$ . Počet částic, které projdou elementární plochou  $b db d\epsilon$  za jednotku času a „dosáhnou“ silového centra, pak zřejmě bude

$$(2.137) \quad g n_1 b db d\epsilon,$$

kde  $n_1$  je koncentrace částic svazku. Vynásobíme-li nyní (2.136) výrazem (2.137) a integrujeme-li výsledek přes celou rovinu  $\xi$ , dostaneme, že

$$(2.138) \quad \sum_{(i)} \frac{d}{dt} g_z = \int_0^\infty db \int_0^{2\pi} d\epsilon \left( -2g \sin^2 \frac{\chi}{2} g n_1 b \right)$$

a odtud

$$(2.139) \quad F = \frac{g}{g} 2g^2 n_1 \mu 2\pi \int_0^\infty b \sin^2 \frac{\chi}{2} db.$$

Uvážíme-li nyní, že podle (2.106)  $\tan \chi/2 = b_0/b$ , můžeme dále psát, že

$$(2.140) \quad F = \frac{g}{g} \mu 4\pi n_1 g^2 b_0^2 \int_0^\infty \frac{b db}{b_0^2 + b^2}.$$

Integrál

$$(2.141) \quad L = \int_0^\infty \frac{b db}{b_0^2 + b^2}$$

$$F = \frac{g}{g} \mu 4\pi n_1 g^2 b_0^2 \int_0^\infty \frac{b db}{b_0^2 + b^2}.$$

$$L = \int_0^\infty \frac{b db}{b_0^2 + b^2}$$

$\ln(\text{E.kinetic}/\text{E.potential})$   
at distance  $l_d$

Už jsme ukázali, že platí...

$$b_0 = \frac{e^2}{4\pi\epsilon_0\mu g^2} \quad l_d^2 = \frac{\epsilon_0 kT}{ne^2}$$

$$\frac{b_0}{l_d} = \frac{\frac{1}{9}(3/2 kT)}{N^{1/2} \mu g^2} \lll 1$$

## Coulomb logarithm

logaritmicky diverguje pro velké hodnoty parametru  $b$ . Abychom dostali pro  $F$  konečné hodnoty, musíme v  $L$  nějakým způsobem omezit horní integrační mez.

V předchozím odstavci jsme si ukázali, že efektivní interakční potenciál částic je řádově dosahu  $l_d$ ; binární coulombovské srážky je pak možno uvažovat pouze pro srážkový parametr  $b \leq l_d$ . Za horní integrační mez  $L$  je tedy možno zvolit  $l_d$ . Dostaneme

$$(2.142) \quad L = \int_0^{l_d} \frac{b db}{b_0^2 + b^2} = \ln \sqrt{\left(\frac{b_0^2 + l_d^2}{b_0^2}\right)}.$$

Jestliže dále platí, že  $l_d \gg |b_0|$ , můžeme (2.142) přepsat do tvaru

$$(2.143) \quad L = \ln \left( \frac{l_d}{|b_0|} \right) = \ln \frac{l_d}{\frac{Z_1 Z_2 e^2}{4\pi\epsilon_0 \mu g^2}},$$

kde jsme za  $b_0$  dosadili (2.97) a síla  $F$ , určená rovnicí (2.140), má nyní tvar

$$(2.144) \quad F = L \frac{g}{g^3} \frac{Z_1^2 Z_2^2 e^4}{4\pi\epsilon_0} \frac{n_1}{\mu}.$$

Veličina  $L$  určená rovnicí (2.143) se nazývá coulombovský logaritmus.

Předpokládali jsme, že platí

$$(2.145) \quad l_d \gg b_0.$$

Tato podmínka však plyne přímo z předpokladů (2.120), které mají platit pro libovolné  $r$ . Položme tedy  $r = l_d$  a předpokládejme pro jednoduchost, že  $Z_1 = Z_2 = 1$ . Sečtením nerovností (2.120) ( $\varphi(r)$  bereme v prvním přiblížení jako coulombovský) dostaneme

$$(2.146) \quad \frac{2e^2}{4\pi\epsilon_0} \frac{1}{l_d} \ll k(T_1 + T_2),$$

což je možno přepsat jako

$$(2.147) \quad l_d \gg \frac{2e^2}{4\pi\epsilon_0 k(T_1 + T_2)}.$$

Protože ale  $3k(T_1 + T_2) \sim \mu g^2$ , je možno (2.147) dále přepsat na

$$(2.148) \quad l_d \gg \frac{6e^2}{4\pi\epsilon_0 \mu g^2} \sim b_0.$$

Odtud již vidíme, že nerovnost (2.145) je již splněna, platí-li (2.120), nebo jinými slovy, předpokládáme (stejně jako v 1. kapitole), že interakční energie částic je mnohem menší ve srovnání s jejich tepelnou energií. K tomuto výsledku je možno dojít ještě trochu jiným způsobem. Aby „ořezání“ integrálu  $L$  (2.141) mělo fyzikální smysl,

(2.140)

$$F = \frac{g}{g} \mu 4\pi n_1 g^2 b_0^2 \int_0^\infty \frac{b db}{b_0^2 + b^2}.$$

Integrál

(2.141)

$$L = \int_0^\infty \frac{b db}{b_0^2 + b^2}$$

(2.151)

$$|F| = \text{konst } L,$$

kde  $L$  je dáno rovnicí (2.142), resp. (2.143). Sledujme dále, jak závisí  $|F|$  na úhlu rozptylu částic. Na základě (2.106) můžeme tvrdit, že pro  $b \gg b_0$  je

(2.152)

$$\chi = \frac{2b_0}{b} \ll 1$$

a tedy rozptyl na malé úhly odpovídá dalekým průletům. Hranici mezi dalekými a blízkými průlety stanovme pro  $b = 2b_0$ . Rovnici (2.151) můžeme nyní psát ve tvaru

(2.153)

$$|F| = \text{konst} \int_0^{l_d} \frac{b db}{b_0^2 + b^2} = \text{konst} (L_{b.p.} + L_{d.p.}),$$

kde

(2.154)

**closed**

$$L_{b.p.} = \int_0^{2b_0} \frac{b db}{b_0^2 + b^2} = \ln 3 \sim 1$$

je coulombovský logaritmus odpovídající blízkým průletům a

**distant**

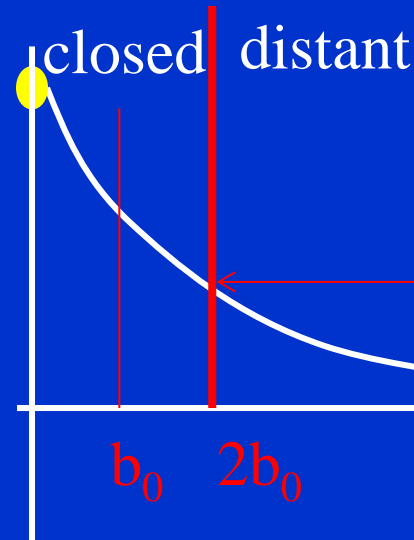
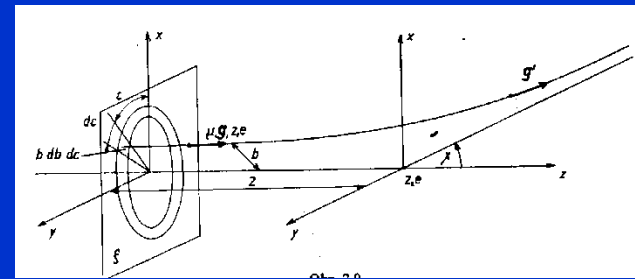
(2.155)

$$L_{d.p.} = \int_{2b_0}^{l_d} \frac{b db}{b_0^2 + b^2} = \ln \frac{l_d}{b_0} - \ln 3 \sim \ln \frac{l_d}{b_0} = L \gg 1$$

je coulombovský logaritmus odpovídající dalekým průletům. Z (2.153) je zřejmé, že střední sílu, která působí na částici 2 ze strany svazku částic 1, můžeme rozdělit na dvě části a to na sílu  $F_{b.p.}$ , odpovídající blízkým průletům, a  $F_{d.p.}$ , odpovídající dalekým průletům; pro  $F_{b.p.}$  a  $F_{d.p.}$  platí

(2.156)

$$|F_{b.p.}| \sim L_{b.p.}$$



$$b_0/l_d = \frac{1}{9} \frac{(3/2 kT)}{N^{1/2} \mu g^2} \ll 1$$

$$F_{dp}/F_{bp} \sim L \gg 1$$

# Temperature dependence

V závěru tohoto odstavce uvedeme ještě několik poznámek, týkajících se coulombovského logaritmu  $L$ . Z (2.143) vidíme, že  $L$  závisí logaritmicky na  $\mu g^2$ . V důsledku této logaritmické závislosti je možno v mnoha případech nahradit  $\mu g^2$  střední hodnotou této veličiny nebo tepelnou rychlostí částic, tj. můžeme položit  $\mu g^2 \sim \frac{3}{2}k(T_1 + T_2)$ . Abychom si utvořili představu, jak závisí  $L$  na teplotě a koncentraci, předpokládejme pro jednoduchost, že  $T_1 = T_2 = T$ . Coulombovský logaritmus má pak jednoduchý tvar

(2.159)

$$L = \ln \left[ \frac{12\pi}{n^{1/2}} \left( \frac{\varepsilon_0 k T}{e^2} \right)^{3/2} \right].$$

kl - klasický  
kv - kvantový

**Coulomb logarithm**

**$L \sim 5 - 20 \dots\dots$**

V jednoduchém případě, kdy  $\mu g^2 \sim \frac{3}{2}k(T_1 + T_2)$ ,  $T_1 = T_2 = T$  a  $|Z_1| = |Z_2| = 1$ , je možno (2.161) přepsat na tvar

$$(2.162) \quad L_{kv} = L_{kl} + \ln \left( \frac{4,2 \cdot 10^5}{T} \right)^{1/2},$$

kde  $L_{kl}$  je dáno vztahem (2.159). Hodnoty coulombovského logaritmu vypočtené z (2.159) a (2.161) jsou uvedeny v tab. 1; nejsou zde uvedeny hodnoty coulombovského logaritmu pro vysoké koncentrace a nízké teploty, protože v těchto případech je námi uvedená teorie neplatná.

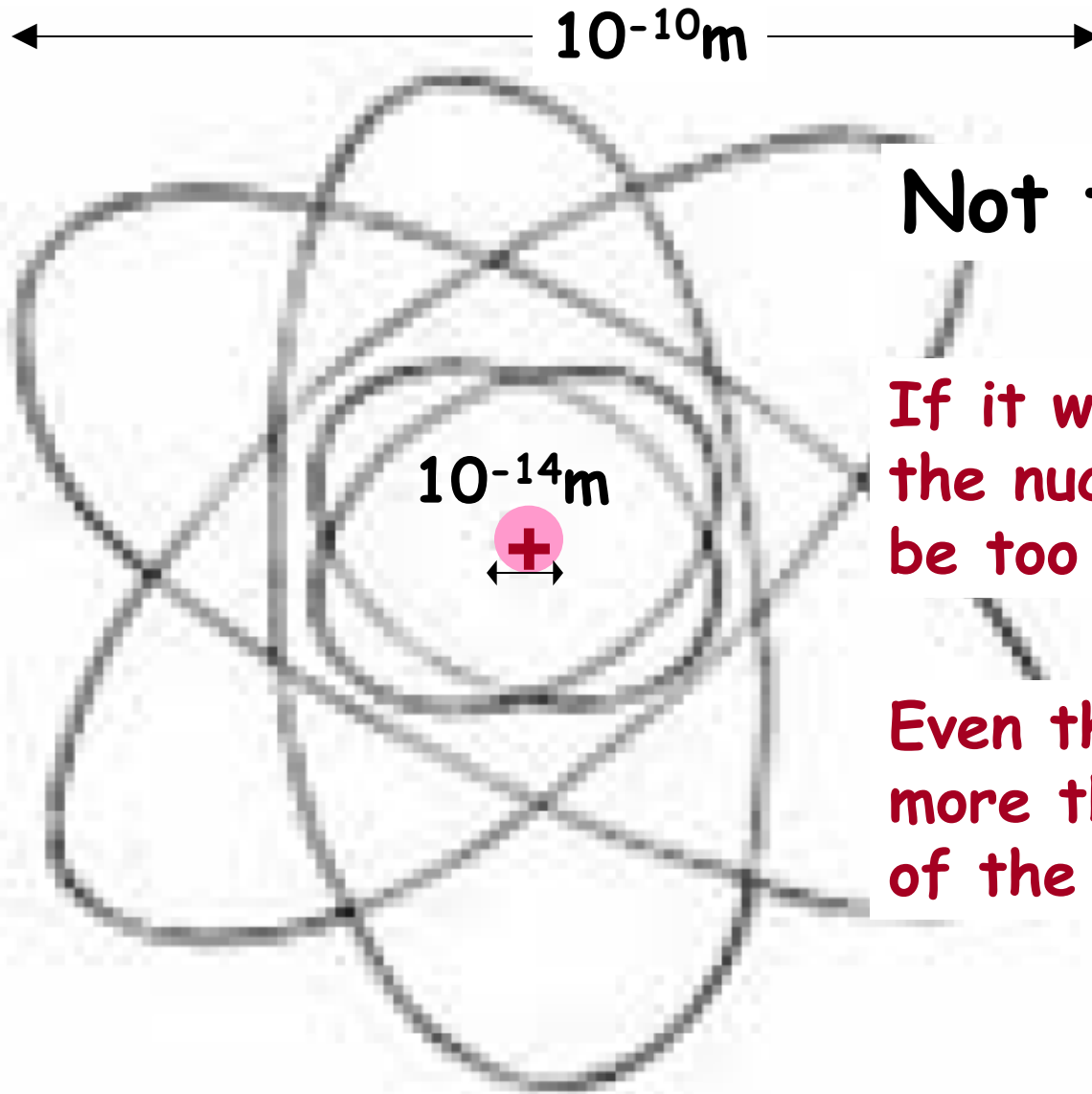
Tabulka 1 Hodnoty coulombovského logaritmu  $L$ .

Koncentrace elektronů [m <sup>-3</sup> ]	Teplota K									
	50	100	5.10 <sup>2</sup>	10 <sup>3</sup>	5.10 <sup>3</sup>	10 <sup>4</sup>	5.10 <sup>4</sup>	10 <sup>5</sup>	5.10 <sup>5</sup>	10 <sup>6</sup>
10 <sup>10</sup>	10,69	11,73	14,14	15,18	17,60	18,63	21,05	22,09	24,42	25,11
10 <sup>11</sup>	9,54	10,58	12,99	14,03	16,44	17,48	19,88	20,94	23,26	23,96
10 <sup>12</sup>	8,39	9,42	11,84	12,88	15,29	16,33	18,75	19,79	22,11	22,81
10 <sup>13</sup>	7,23	8,27	10,69	11,73	14,14	15,18	17,60	18,63	20,96	21,65
10 <sup>14</sup>	6,08	7,12	9,54	10,58	12,99	14,03	16,44	17,48	19,81	20,50
10 <sup>15</sup>	4,93	5,97	8,39	9,42	11,84	12,88	15,29	16,33	18,66	19,36
10 <sup>16</sup>	—	4,82	7,23	8,27	10,69	11,73	14,14	15,18	17,51	18,20
10 <sup>17</sup>	—	—	6,08	7,12	9,54	10,58	12,99	14,03	16,36	17,05
10 <sup>18</sup>	—	—	4,93	5,97	8,39	9,42	11,84	12,88	15,21	15,90
10 <sup>19</sup>	—	—	—	4,82	7,23	8,27	10,69	11,73	14,06	14,75
10 <sup>20</sup>	—	—	—	—	6,08	7,12	9,54	10,58	12,90	13,60
10 <sup>21</sup>	—	—	—	—	4,93	5,97	8,39	9,42	11,75	12,45
10 <sup>22</sup>	—	—	—	—	—	4,92	7,23	8,27	10,60	11,30
10 <sup>23</sup>	—	—	—	—	—	—	6,08	7,12	9,45	10,14
10 <sup>24</sup>	—	—	—	—	—	—	4,93	5,97	8,30	8,99

Literatura ke kap. 2.

- JANCEL R., KAHAN TH.: Electrodynamics of plasmas. J. Wiley & Sons, London (1966).  
 DELCROIX J. L.: Plasma physics. J. Wiley & Sons, London (1965).  
 LANDAU L. D., LIFŠIC E. M.: Kvantovaja mechanika. Moskva (1963).  
 SIVUCHIN D. V.: Voprosy teorii plazmy 4., red. M. A. Leontovič, Moskva (1964).  
 TRUBNIKOV B. A.: Voprosy teorii plazmy 1., red. M. A. Leontovič, Moskva (1963).  
 SPITZER L.: Physics of fully ionized gases. Interscience, New York (1956) (ruský překlad Spitzer L.: Fizika polnostju ionizovannogo gaza. Moskva (1965)).

# Rutherford atom



**Not to scale!!!**

If it were to scale,  
the nucleus would  
be too small to see

Even though it has  
more than 99.9%  
of the atom's mass

## Collisions in plasma

## Reactions in plasma

## Interactions of particles in plasma

## Collisions of electrons with atoms

Classical or quantum approach?

**Electron:**

$$1\text{eV} \rightarrow v = 5.9 \times 10^7 \text{ cm s}^{-1}$$

$$\tau \sim a_0/v \sim 10^{-8} / 5.9 \times 10^7 = 2 \times 10^{-16} \text{ s}$$

$$\lambda \sim 2A = 2 \times 10^{-8} \text{ cm de Broglie}$$

**Ar+:**

$$1\text{eV} \rightarrow v = 2 \times 10^5 \text{ cm s}^{-1}$$

$$\tau \sim a_0/v \sim 10^{-8} / 2 \times 10^5 \sim 6 \times 10^{-14} \text{ s}$$

$$\lambda \sim 9 \times 10^{-11} \text{ cm de Broglie}$$

$$\lambda_e(4K) \sim 540 \text{ A} \sim 54 \times 10^{-9} \text{ m}$$



# De Broglie wave length

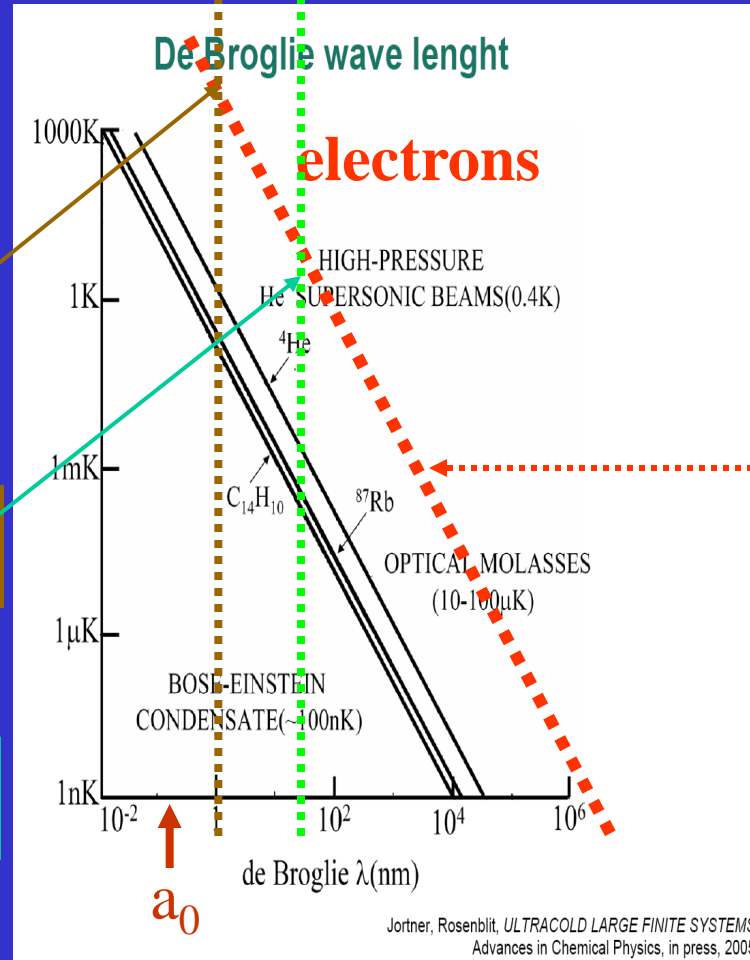
$$\lambda_{DB} = \frac{h}{p} = \frac{h}{Mv} \sim \frac{h}{\sqrt{MT}}$$

1eV

$$\lambda_{eDB}(1eV) \sim 11.6 \text{ \AA} \sim 1.16 \times 10^{-9} \text{ m}$$

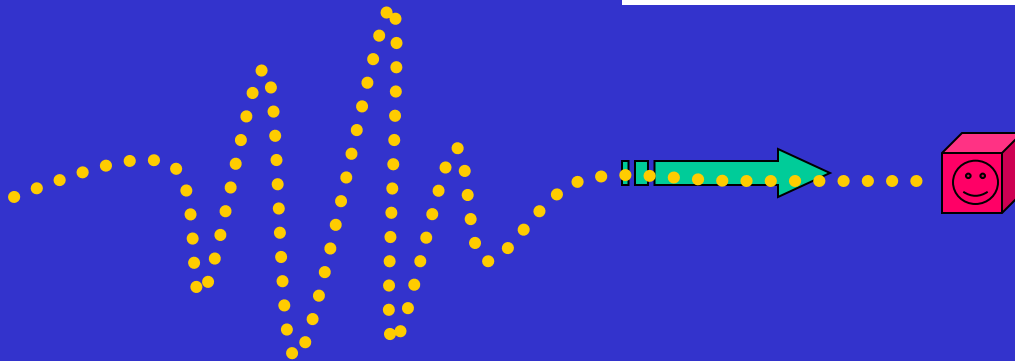
4K

$$\lambda_{eDB}(4K) \sim 540 \text{ \AA} \sim 54 \times 10^{-9} \text{ m}$$



$$\lambda_{DB} = \frac{h}{m_e v_e} \sim \frac{h}{\sqrt{m_e T}}$$

$$T \sim \frac{1}{\lambda_{DB}^2}$$



# “Electron-Driven Processes: Scientific Challenges and Technological Opportunities”

## *Current Status and Future Perspectives of Electron Interactions with Molecules, Clusters, Surfaces, and Interfaces*

1. Workshop on “Fundamental Challenges in Electron-Driven Chemistry”,  
Berkeley, October 9 & 10, 1998

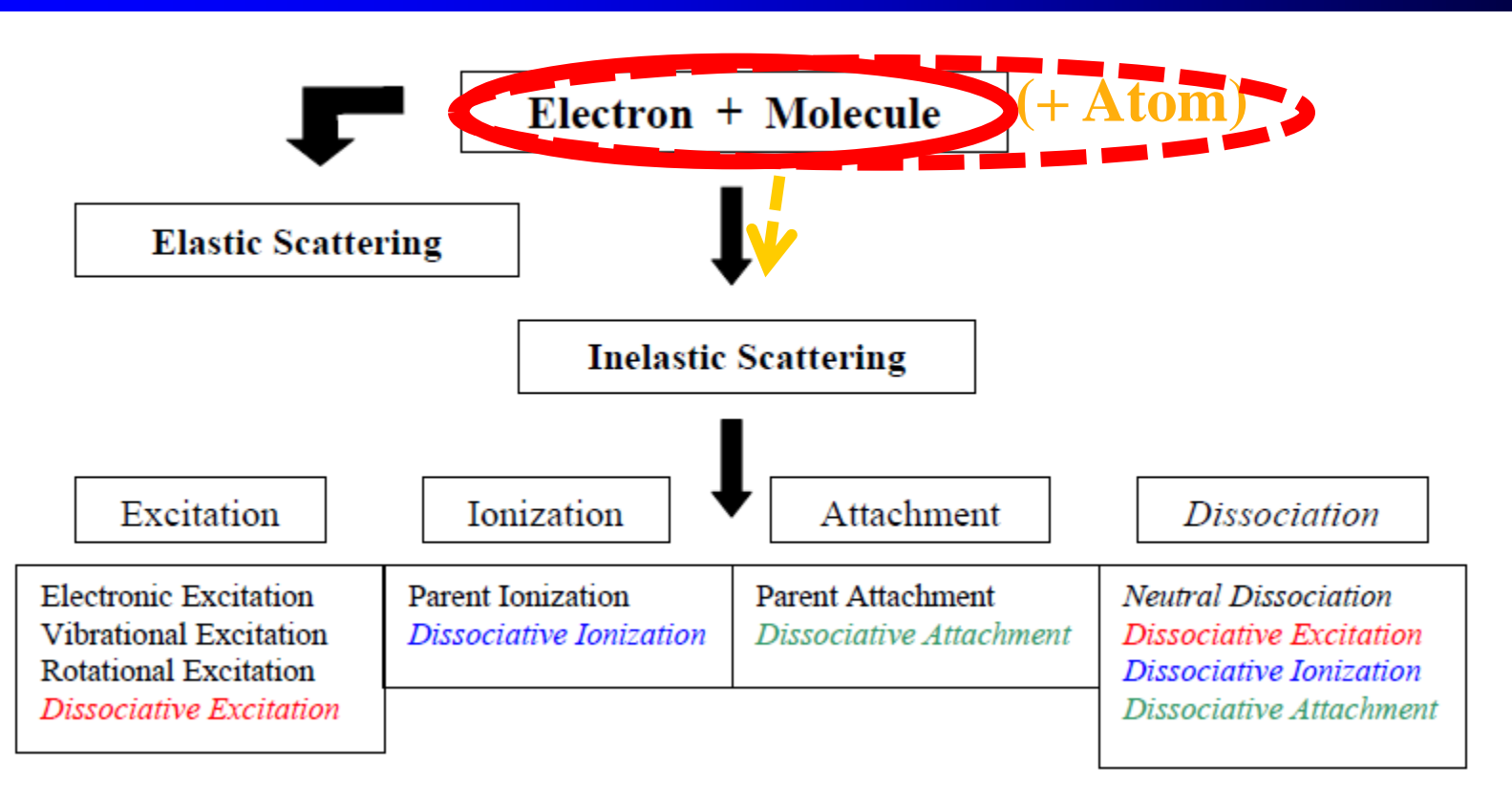
Organizers: C. William McCurdy, Lawrence Berkeley National Laboratory  
Thomas N. Rescigno, Lawrence Livermore National Laboratory

(1998)

Kurt H. Becker, Stevens Institute of Technology (SIT)  
C. William McCurdy, Lawrence Berkeley National Laboratory (LBNL)  
Thomas M. Orlando, Pacific Northwest National Laboratory (PNNL)  
Thomas N. Rescigno, Lawrence Livermore National Laboratory (LLNL)  
and Lawrence Berkeley National Laboratory (LBNL)

This report can be found on the World Wide Web at:  
<http://attila.stevens-tech.edu/physics/People/Faculty/Becker/EDP>

Other related reports can be found at the following web sites:  
[http://www.lbl.gov/ICSD/mccurdy/epic\\_home.htm](http://www.lbl.gov/ICSD/mccurdy/epic_home.htm)  
<http://www.er.doe.gov/production/bes/chm/RadRprt.doc>



# Details of interaction of electron with H<sub>2</sub> (1990)

Probability .....

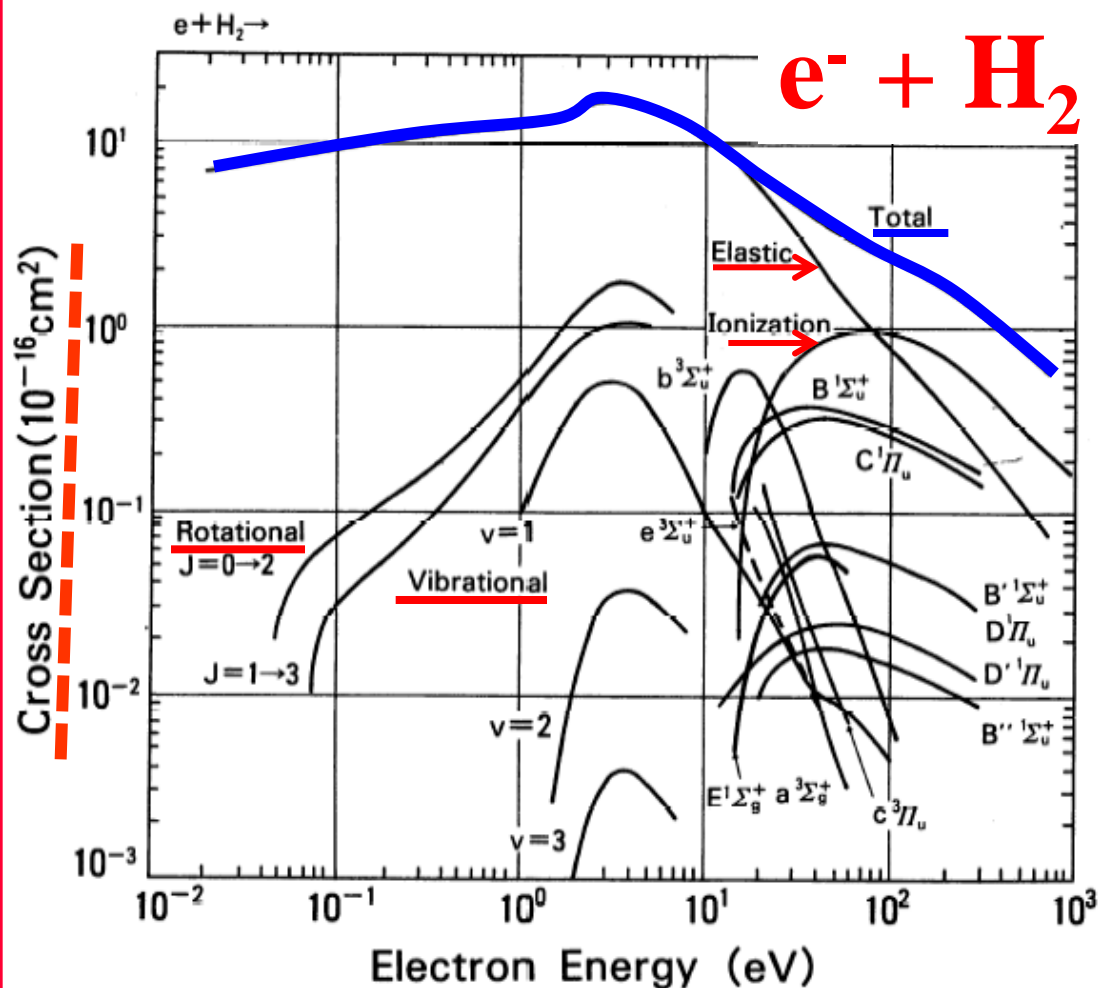


FIG. 2. Comparison of cross sections for various collision processes in neutral H<sub>2</sub>. Also for comparison, cross sections of ionization of atomic hydrogen are shown. These data are taken at room temperatures.

(1990)

## Cross Sections and Related Data for Electron Collisions with Hydrogen Molecules and Molecular Ions<sup>a)</sup>

H. Tawara, Y. Itikawa,<sup>b)</sup> H. Nishimura,<sup>c)</sup> and M. Yoshino<sup>d)</sup>

National Institute for Fusion Science,<sup>a)</sup> Nagoya 464-01, Japan

(Received July 5, 1989; revised manuscript received November 1, 1989)

Data are compiled and evaluated for collision processes of excitation, dissociation, ionization, attachment, and recombination of hydrogen molecules and molecular ions (H<sub>2</sub><sup>+</sup>, H<sub>3</sub><sup>+</sup>) by electron impact as well as for properties of their collision products.

Key words: electron impact; hydrogen molecule; hydrogen molecular ion; scattering; elastic integral; vibrational excitation; rotational excitation; dissociation; ionization; photon emission; cross section.

# Cross sections for vibrational excitation, dissociation, ionization...H<sub>2</sub>

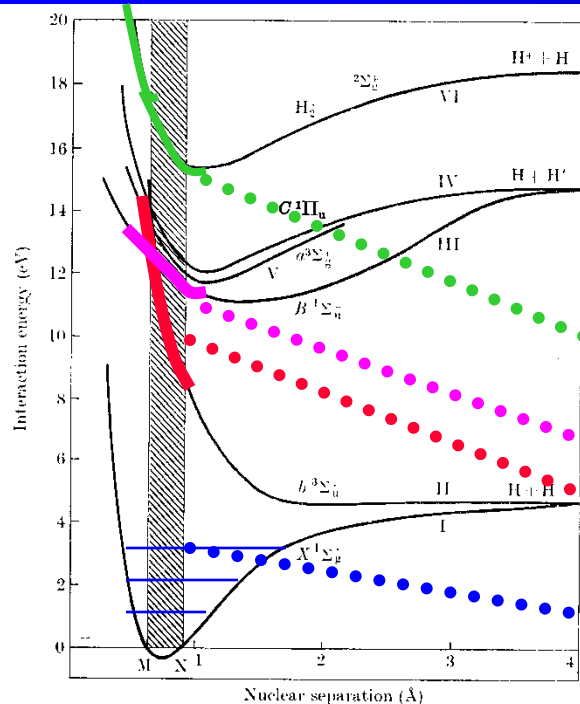


FIG. 13.1. Potential energy curves for electronic states of H<sub>2</sub> and H<sub>2</sub><sup>+</sup> lying within 20 eV of the ground state.

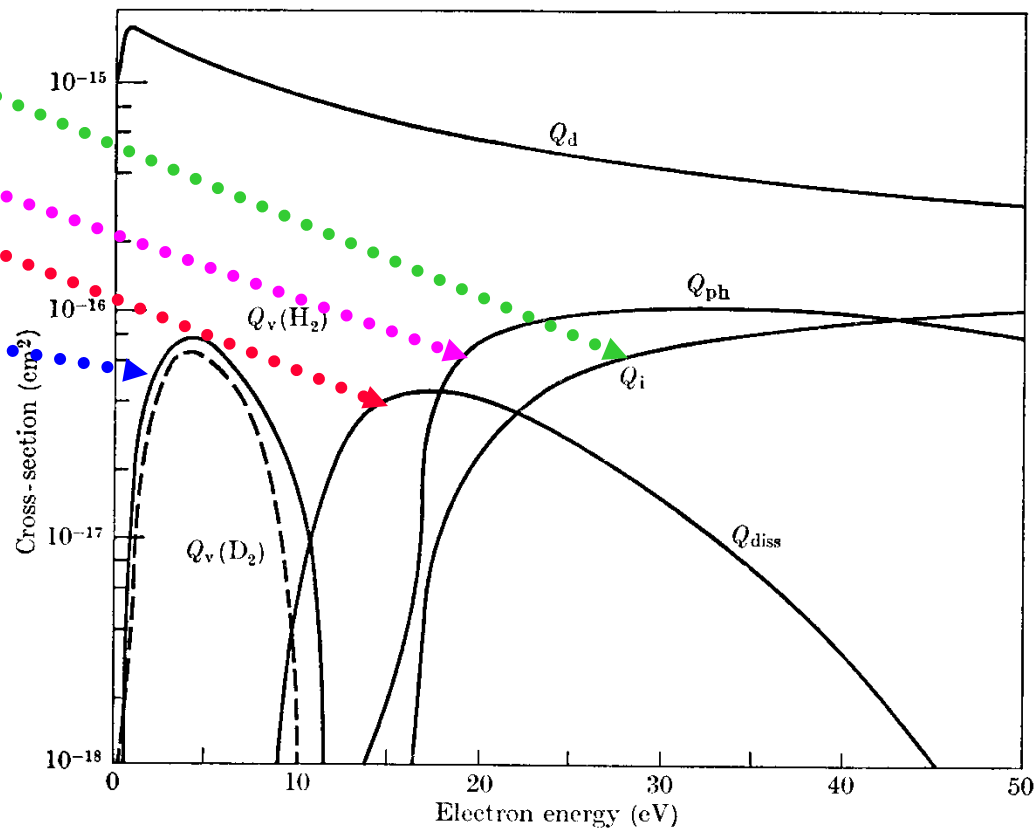
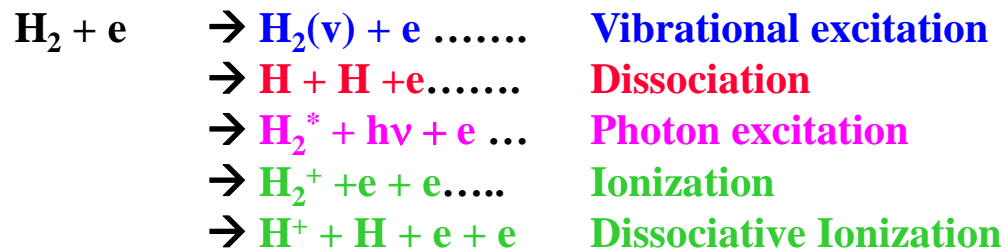
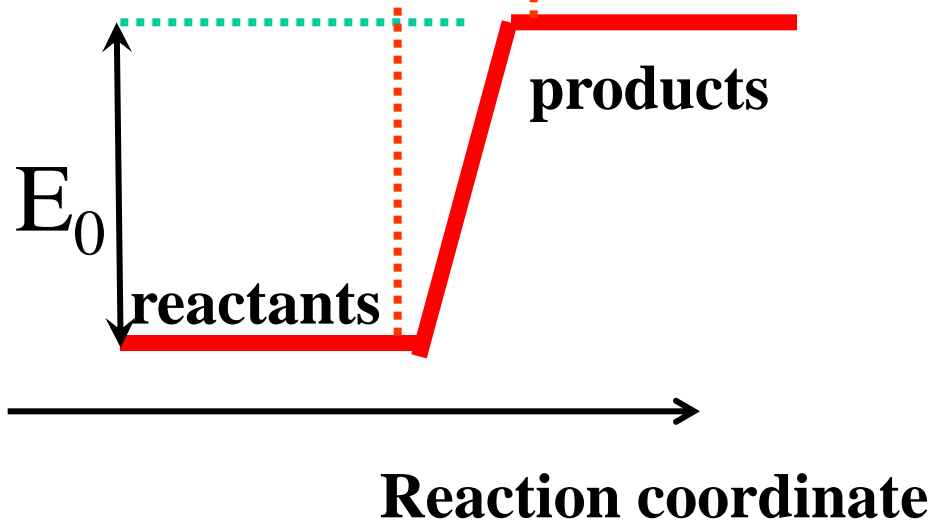
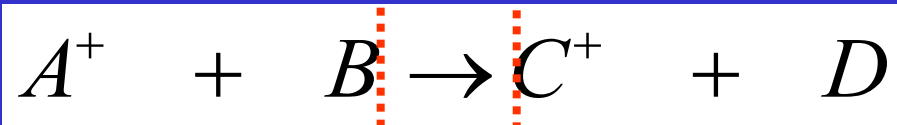


FIG. 13.37. Cross-sections assumed by Engelhardt and Phelps in their analysis of swarm data in H<sub>2</sub> and D<sub>2</sub> for electrons of characteristic energy greater than 1 eV.  $Q_d$  momentum-transfer cross-section,  $Q_i$  ionization cross-section,  $Q_{diss}$  dissociation cross-section,  $Q_{ph}$  photon excitation cross-section,  $Q_v$  vibrational excitation cross-section (— H<sub>2</sub>, --- D<sub>2</sub>).

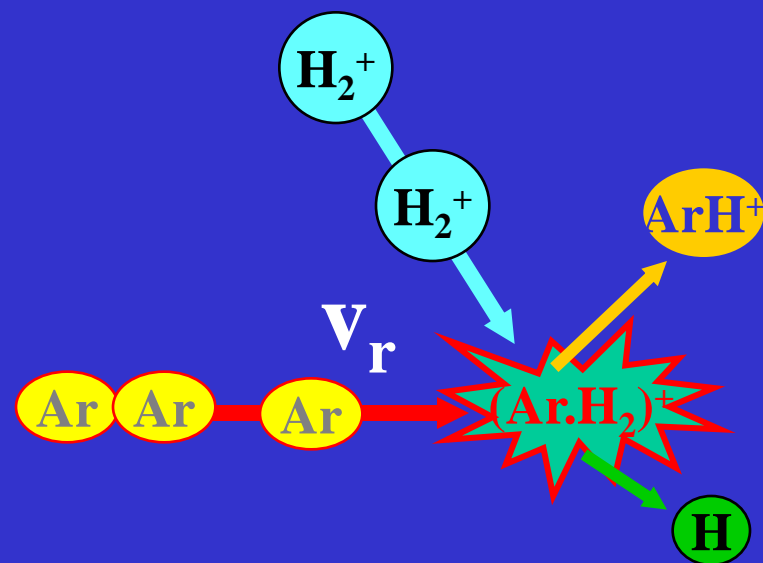
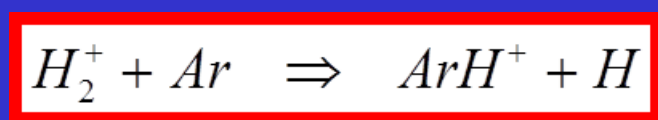
# Cross section



**Reaction cross section**

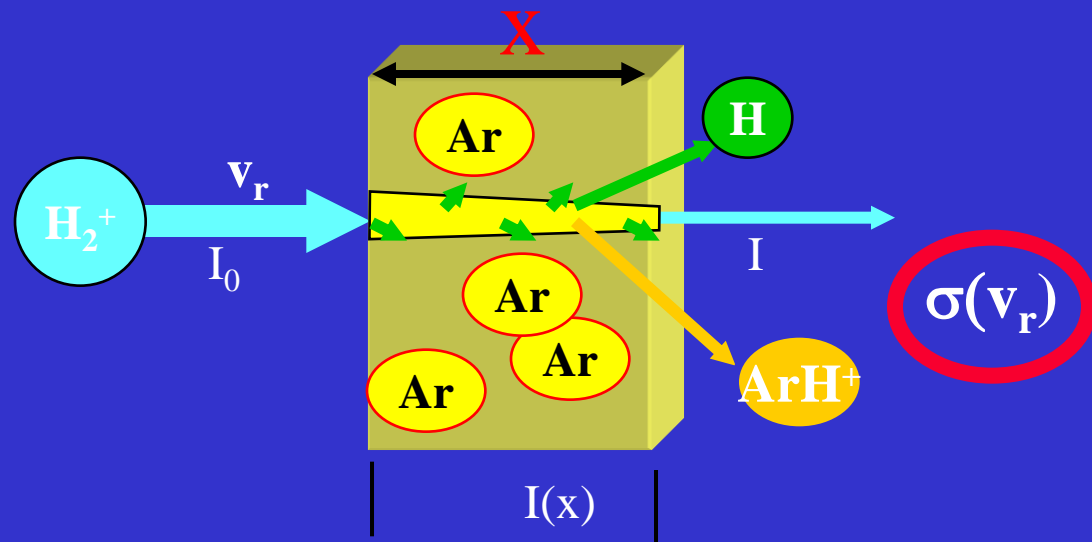
**Collisional cross section**

Single collision



Reaction cross section

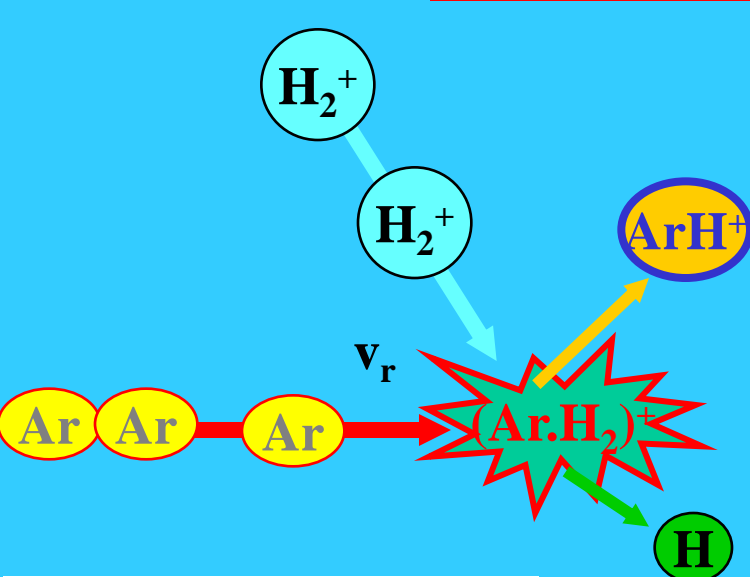
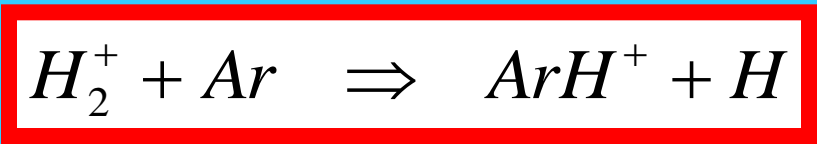
Collisional cross section



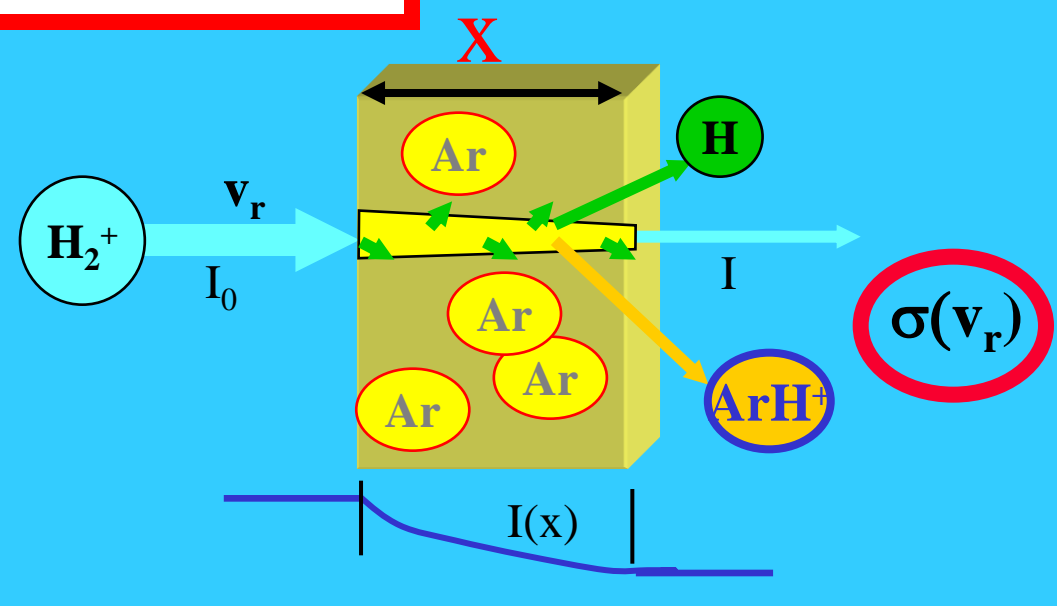
$$I = I_0 \exp(-\sigma n_{Ar} X)$$



Single collision



reaction cross section

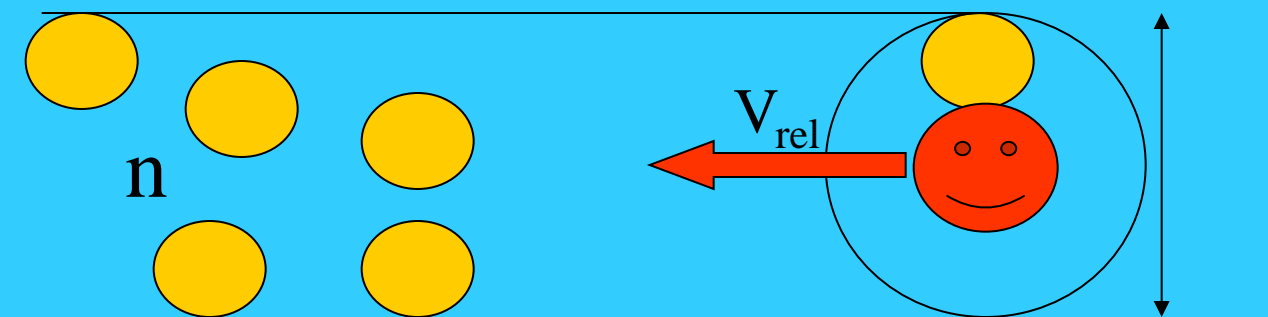


$$I=I_0\exp(-\sigma n_{Ar}x)$$

$$v_{coll} = +nV_{rel} = +nvS = +nv\pi\delta^2 = \mp nv\sigma$$

Collisional cross section

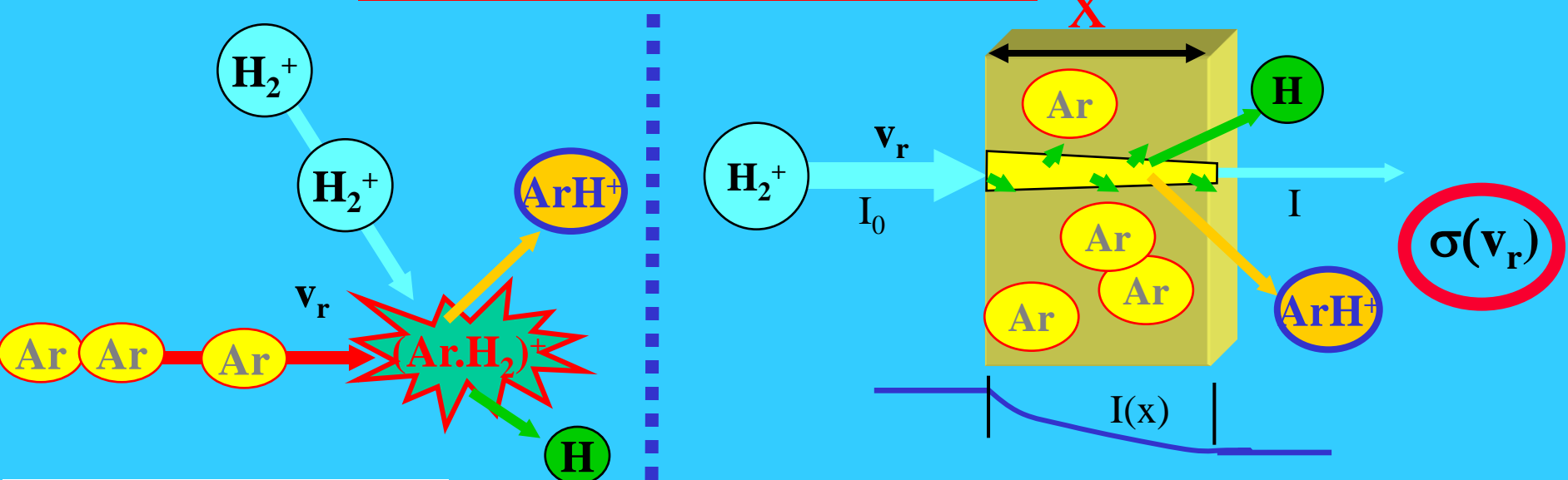
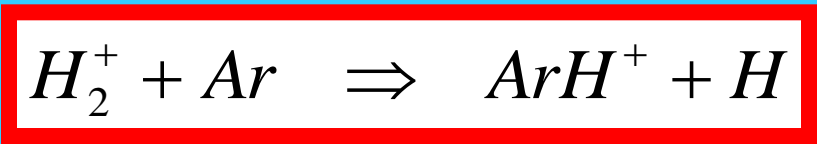
$$\frac{dI}{dt} = -\frac{I}{\tau_{coll}} = -Iv_{coll}$$



$$I(t) = I_0 \exp(-v_{coll}t) = I_0 \exp(-\sigma n v_{rel}t)$$

$$I=I_0\exp(-\sigma n_{Ar}x)$$

Single collision



reaction cross section

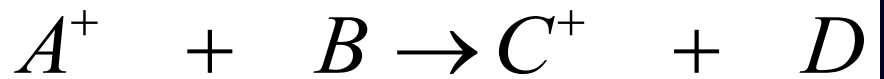
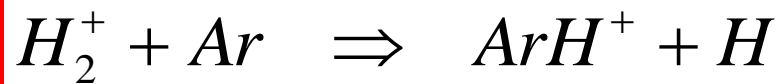
$$I = I_0 \exp(-\sigma n_{Ar} x)$$

Proportionality factor

$$\frac{dI}{dx} \sim -INx \qquad \frac{dI}{dx} = -\sigma INx$$

$$\frac{dI}{Idx} = \frac{d \ln(I)}{dx} = -\sigma Nx$$

$$I(x) = I_0 \exp(-\sigma Nx)$$



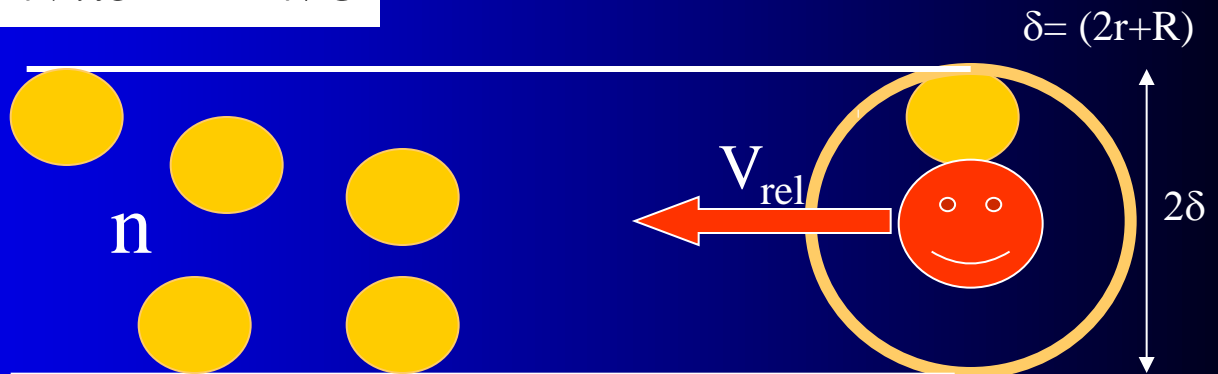
$$\frac{dA^+}{dt} = -k_{BIN} A^+ B$$

$$[A^+]_t = [A^+]_{t=0} \cdot e^{-k[B]t}$$

reaction cross section

$$\nu_{coll} = -nV_{rel} = -n v S = -n v \pi \delta^2 = -n v \sigma$$

$$\frac{dI}{dt} = -\frac{I}{\tau_{coll}} = -I \nu_{coll}$$



$$I(t) = I_0 \exp(-\nu_{coll} t) = I_0 \exp(-\sigma n v_{rel} t)$$

$$I = I_0 \exp(-\sigma n_{Ar} x)$$

## 2.3. Electron impact ionization

The electron impact ionization is the most fundamental ionization process for the operation of ion sources.

### Why?

- The cross section for the impact ionization is by orders of magnitudes higher than the cross section for the photo ionization.
- The cross section depends on the mass of the colliding particle. Since the energy transfer of a heavy particle is lower, a proton needs for an identical ionization probability an ionization energy three orders of magnitudes higher than an electron

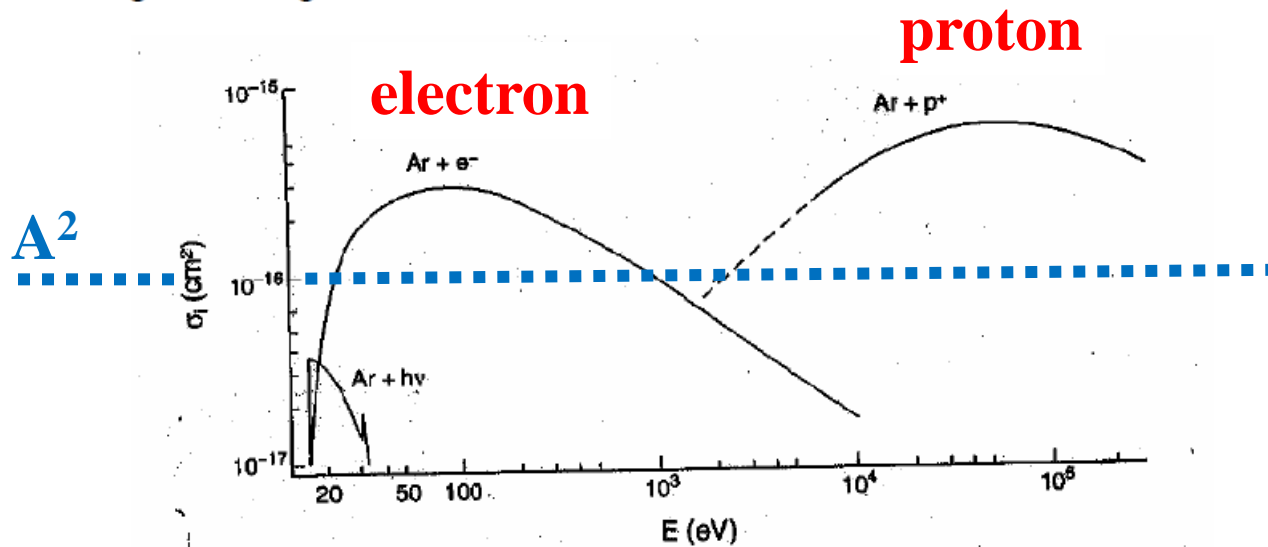


**FIGURE 4**  
Ionization cross sections as functions of energy for ionizing collisions with fast electrons, protons, and photons. (From Winter, H., in *Experimental Methods in Heavy Ion Physics*, Springer-Verlag, 1979. With permission.)

# Cross sections for vibrational excitation, dissociation, ionization...H<sub>2</sub>

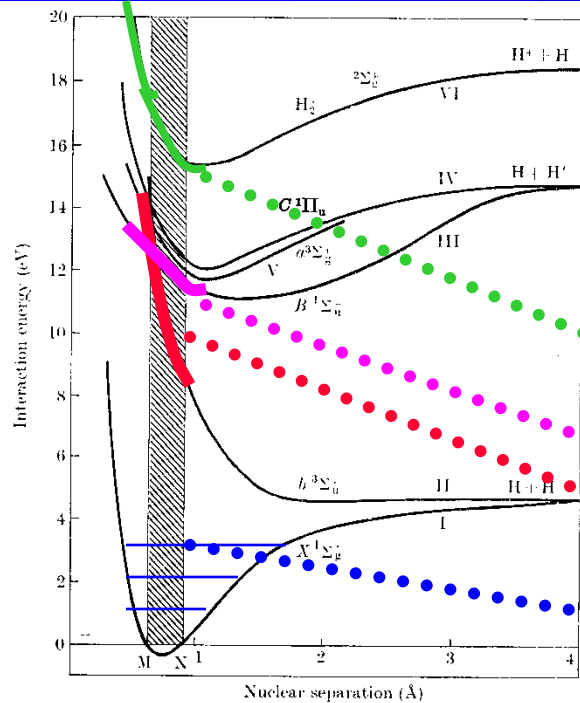


FIG. 13.1. Potential energy curves for electronic states of H<sub>2</sub> and H<sub>2</sub><sup>+</sup> lying within 20 eV of the ground state.

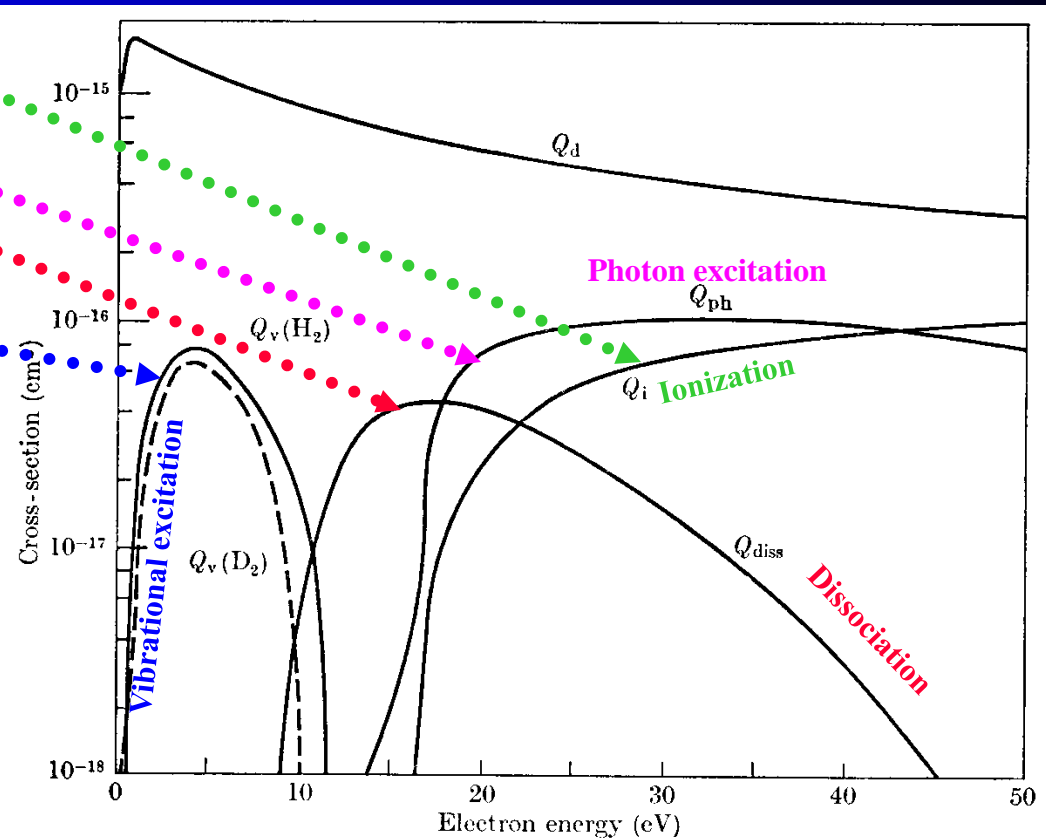
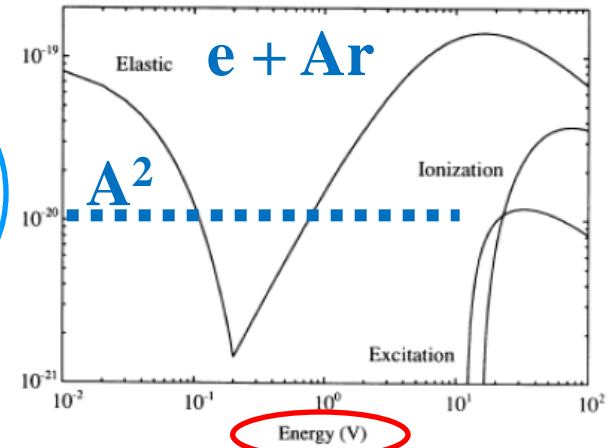
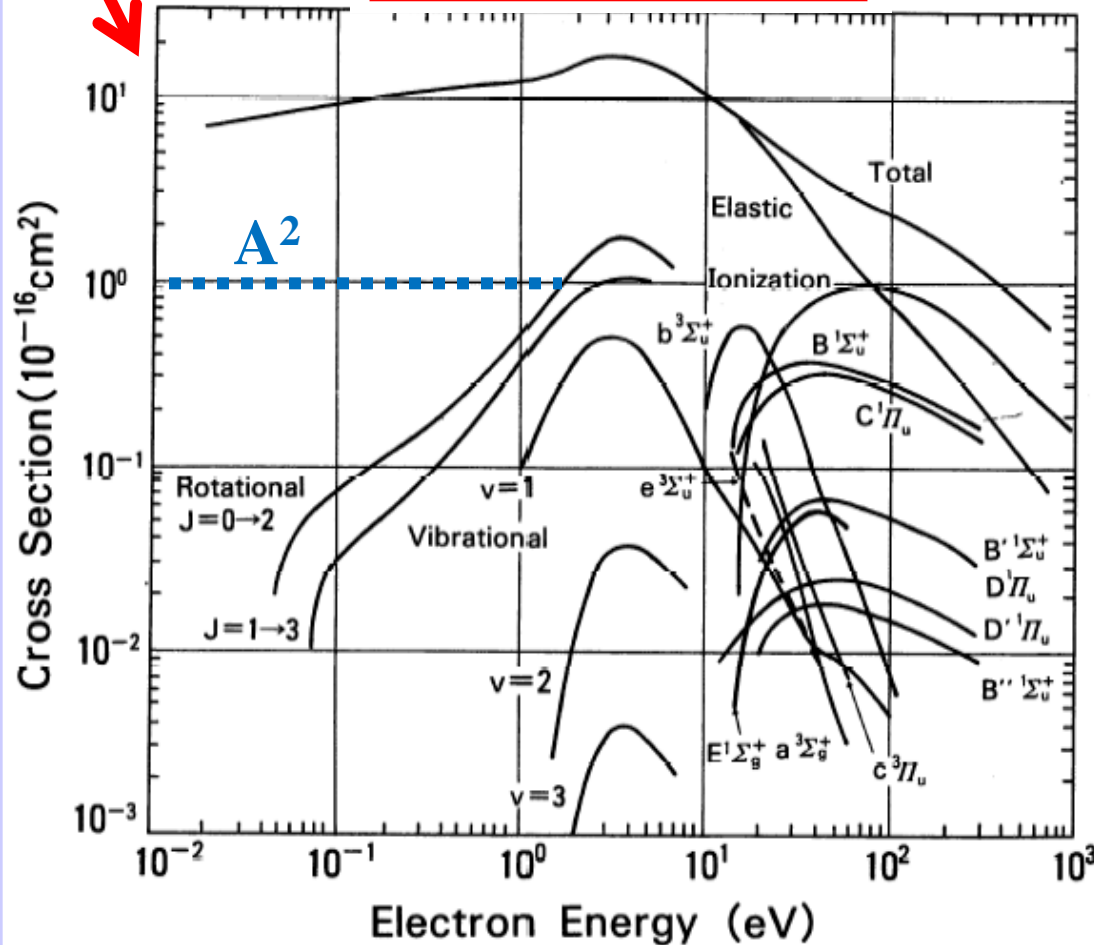


FIG. 13.37. Cross-sections assumed by Engelhardt and Phelps in their analysis of swarm data in H<sub>2</sub> and D<sub>2</sub> for electrons of characteristic energy greater than 1 eV. Q<sub>d</sub> momentum-transfer cross-section, Q<sub>i</sub>, ionization cross-section, Q<sub>diss</sub> dissociation cross-section, Q<sub>ph</sub> photon excitation cross-section, Q<sub>v</sub> vibrational excitation cross-section (— H<sub>2</sub>, --- D<sub>2</sub>).

# Electron scattering cross-section on Ar

$e + H_2$

Collisions with electrons



3. Ionization, excitation and elastic scattering cross sections for electrons in argon gas compiled by Vahedi, 1993).

FIG. 2. Comparison of cross sections for various collision processes in neutral  $H_2$ . Also for comparison, cross sections of ionization of atomic hydrogen are shown. These data are taken at room temperatures.



# Cross sections for vibrational excitation, dissociation, ionization...H<sub>2</sub>

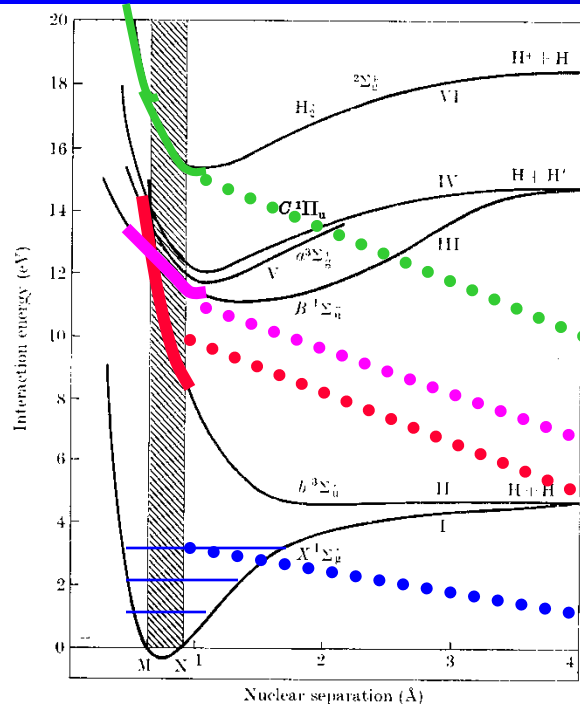


FIG. 13.1. Potential energy curves for electronic states of H<sub>2</sub> and H<sub>2</sub><sup>+</sup> lying within 20 eV of the ground state.

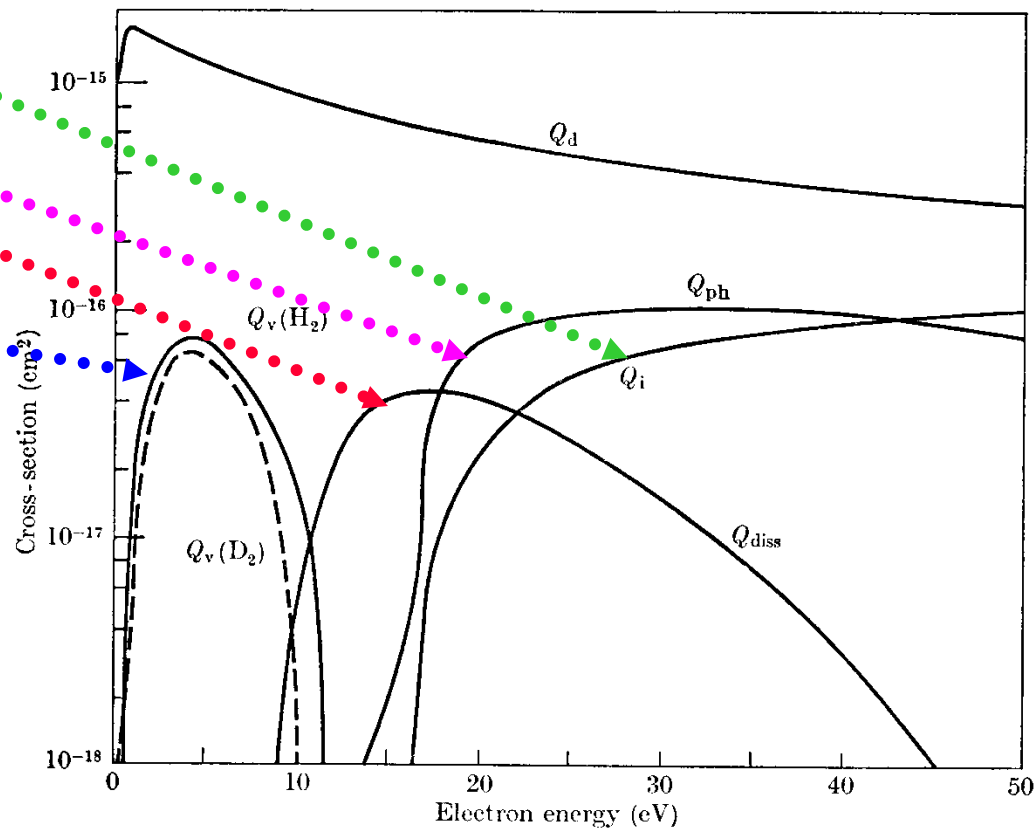
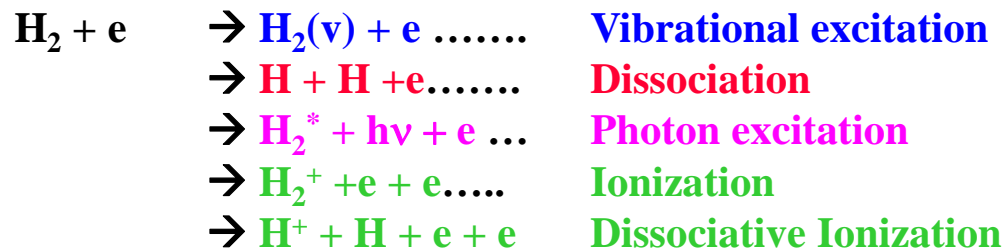
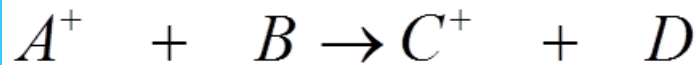
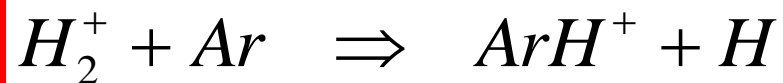


FIG. 13.37. Cross-sections assumed by Engelhardt and Phelps in their analysis of swarm data in H<sub>2</sub> and D<sub>2</sub> for electrons of characteristic energy greater than 1 eV.  $Q_d$  momentum-transfer cross-section,  $Q_i$  ionization cross-section,  $Q_{diss}$  dissociation cross-section,  $Q_{ph}$  photon excitation cross-section,  $Q_v$  vibrational excitation cross-section (— H<sub>2</sub>, --- D<sub>2</sub>).

# Kinetics of elementary process

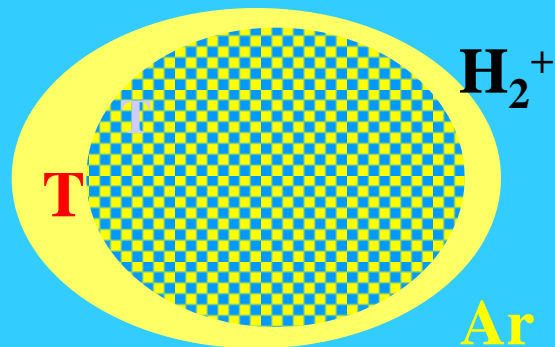


$$\frac{dA^+}{dt} = -k_{BIN} A^+ B$$

$$[A^+]_t = [A^+]_{t=0} \cdot e^{-k[B]t}$$

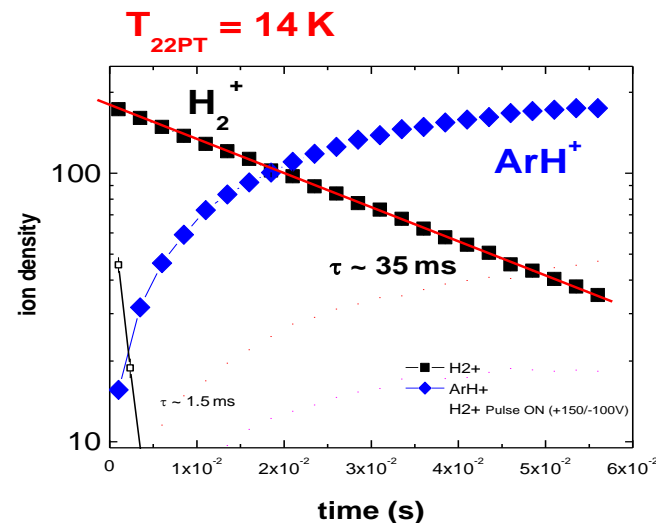
## Multiple collision

@ T



reaction rate coefficient

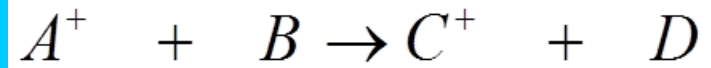
$$d(n_{H_2^+})/dt = -k n_{H_2^+} \cdot n_{Ar}$$



$k(T)$

$$n_{H_2^+} = (n_{H_2^+})_0 \exp(-kn_{Ar}t)$$

## reactions



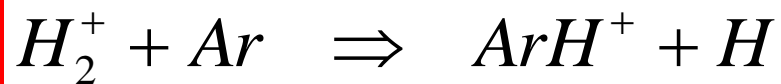
$$\frac{dA^+}{dt} = -k_{BIN} A^+ B$$

$$[k_{BIN}] = \text{cm}^3 \text{s}^{-1}$$

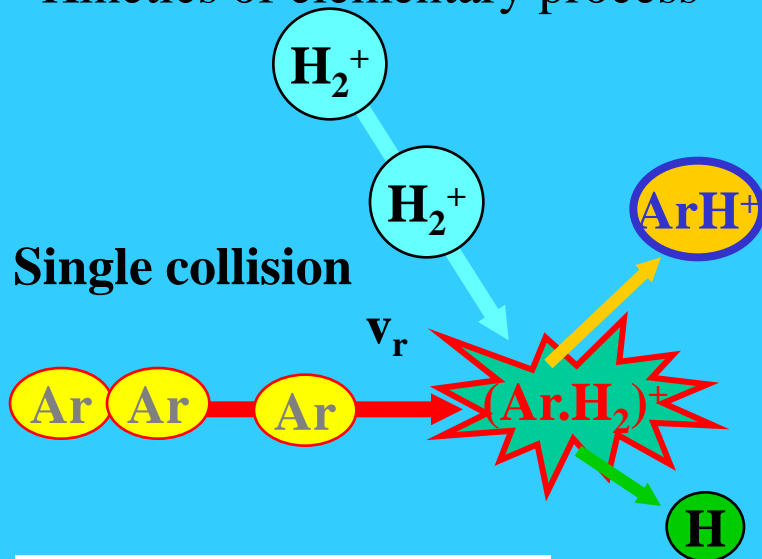
$$1/\tau = k_{BIN}[B] = \dots n v \rho \dots = [B] v \rho \dots [B] \langle v \rho \rangle$$

$$k_{BIN} = \langle v \rho \rangle$$

# Kinetics of elementary process



## Single collision

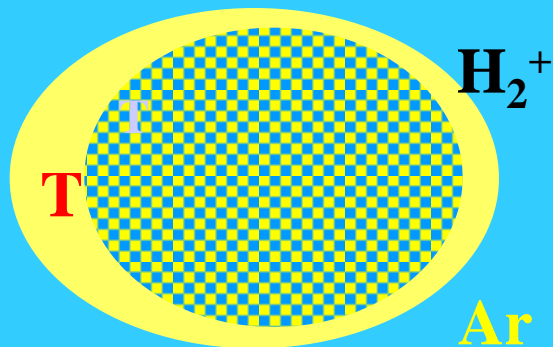


reaction cross section

$$I = I_0 \exp(-\sigma n_{Ar} x)$$

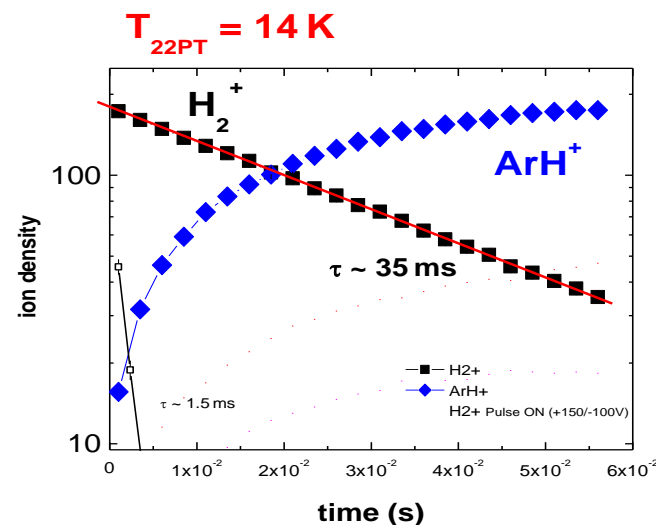
## Multiple collision

@ T



reaction rate coefficient

$$d(n_{H_2^+})/dt = -k n_{H_2^+} \cdot n_{Ar}$$

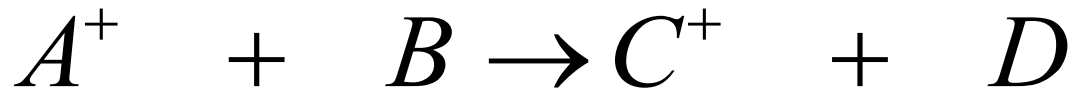


$$n_{H_2^+} = (n_{H_2^+})_0 \exp(-k n_{Ar} t)$$

$\sigma(v_r)$

$k(T) = \langle v \sigma \rangle$

$k(T)$



$$\sigma(\mathbf{v}_r)$$

$$k_{BIN} = k_{BIN}(T)$$

$$\mathbf{k}(T) = \langle \mathbf{v}_r \sigma(\mathbf{v}_r) \rangle$$

$$k = \int_v f_T(v) \cdot v \cdot \sigma(v) dv = k(T)$$

## Electron scattering cross-section on Ar

$$k = \int_{\nu} f_T(\nu) \cdot \nu \cdot \sigma(\nu) d\nu = k(T)$$

Electrons – Boltzman distribution with  $T_e$

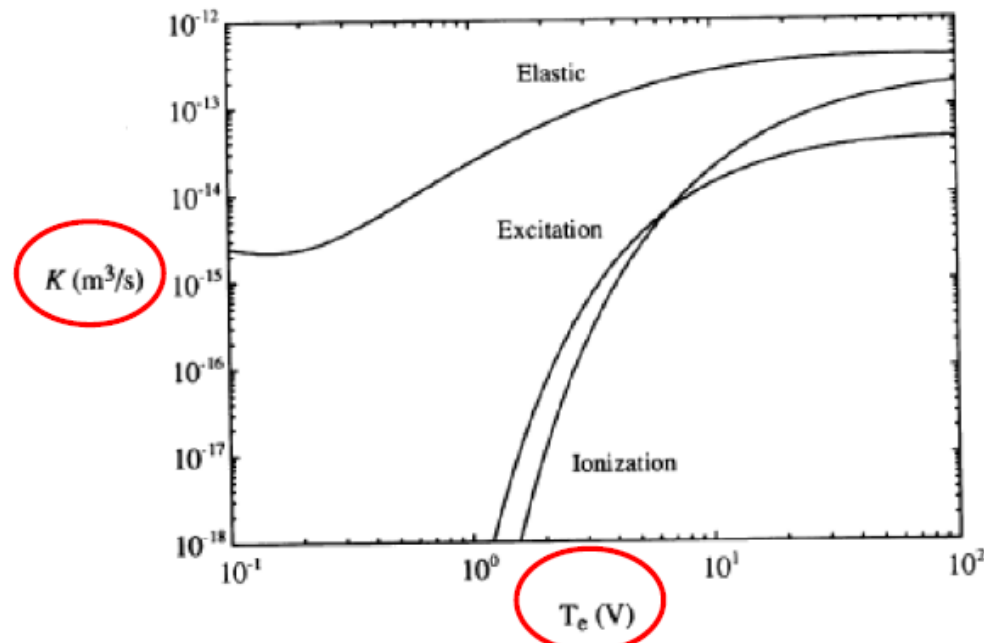
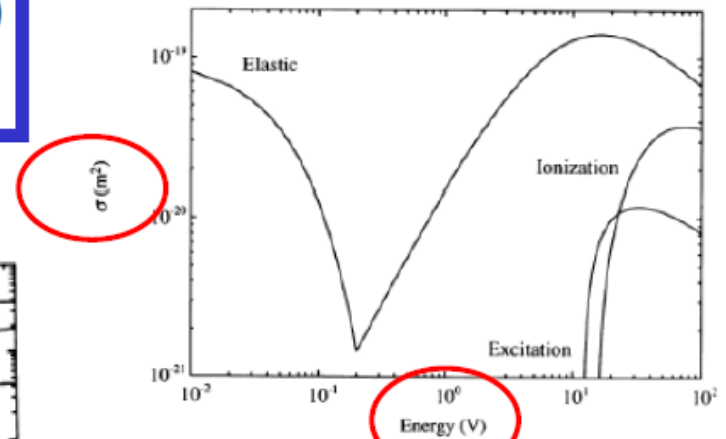


**FIGURE 3.16.** Electron collision rate constants  $K_{iz}$ ,  $K_{ex}$  and  $K_m$  versus  $T_e$  in argon gas (compiled by Vahedi, 1993).

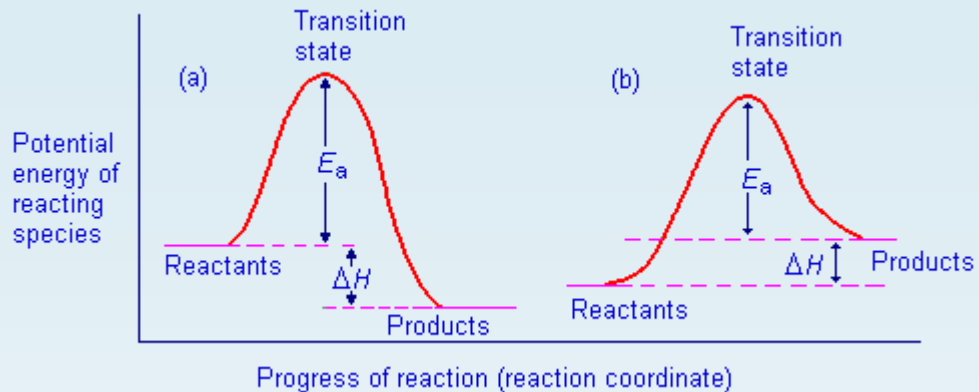
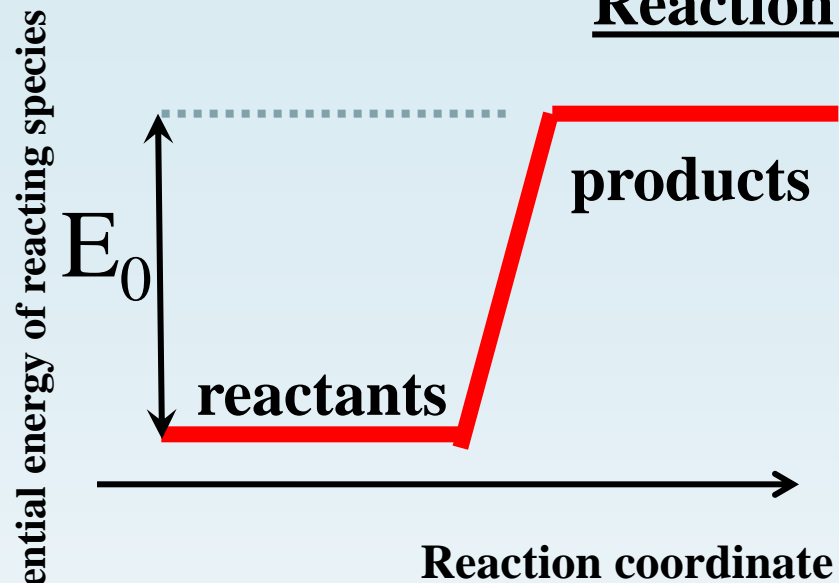


3. Ionization, excitation and elastic scattering cross sections for electrons compiled by Vahedi, 1993).

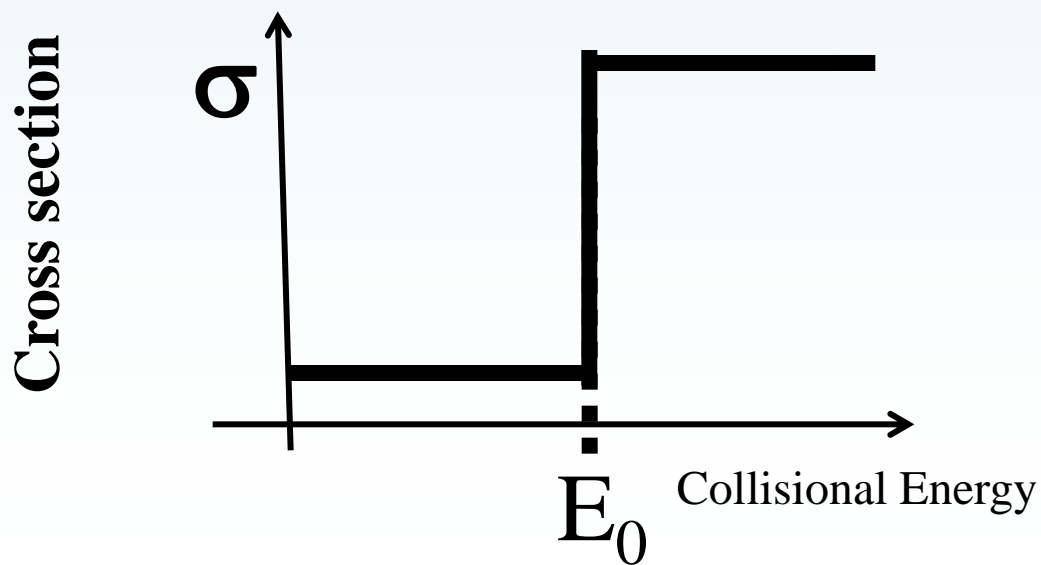
$$\alpha(T, T_e) \propto \int_0^{\infty} \sqrt{E} \sigma_w(E, T) f(E, T_e) dE$$

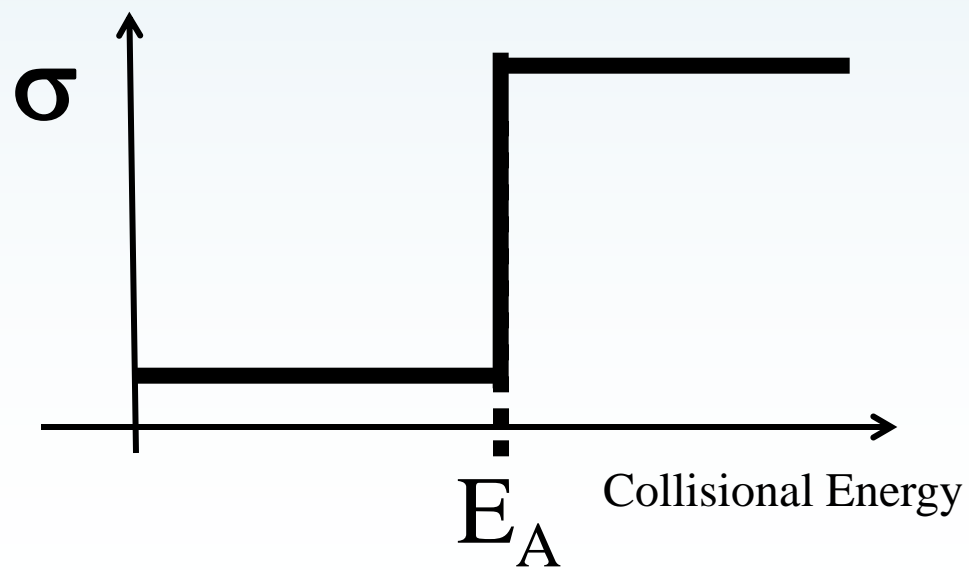
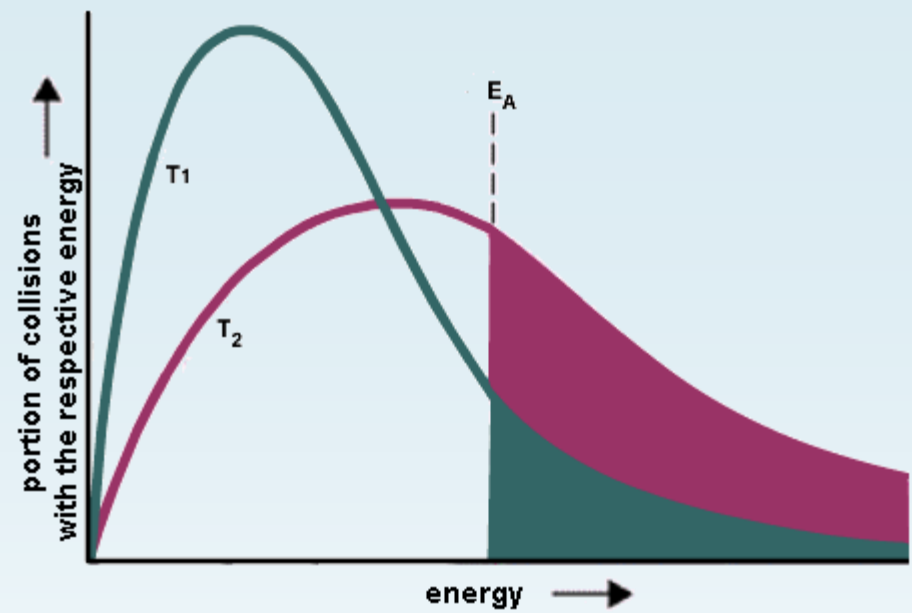
What if we have metastables?

## Reaction coordinate

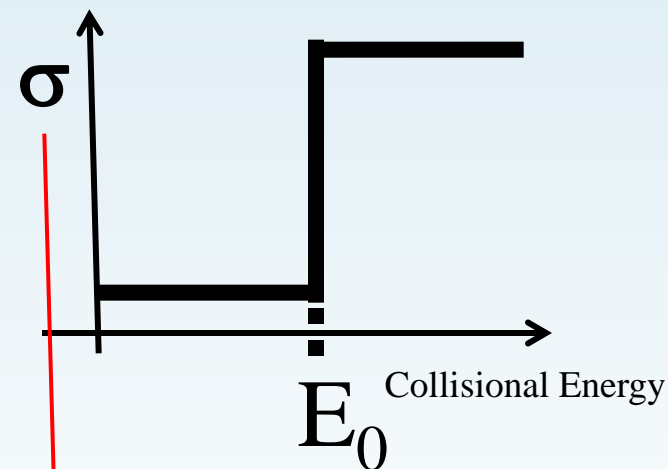
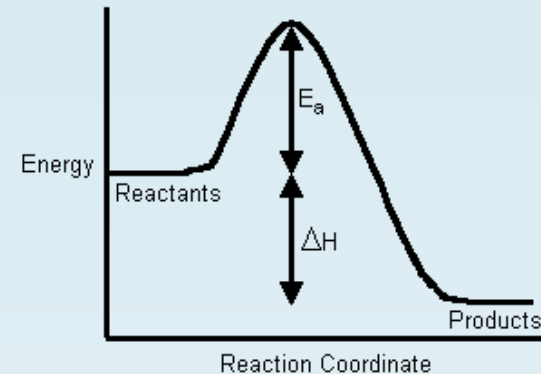
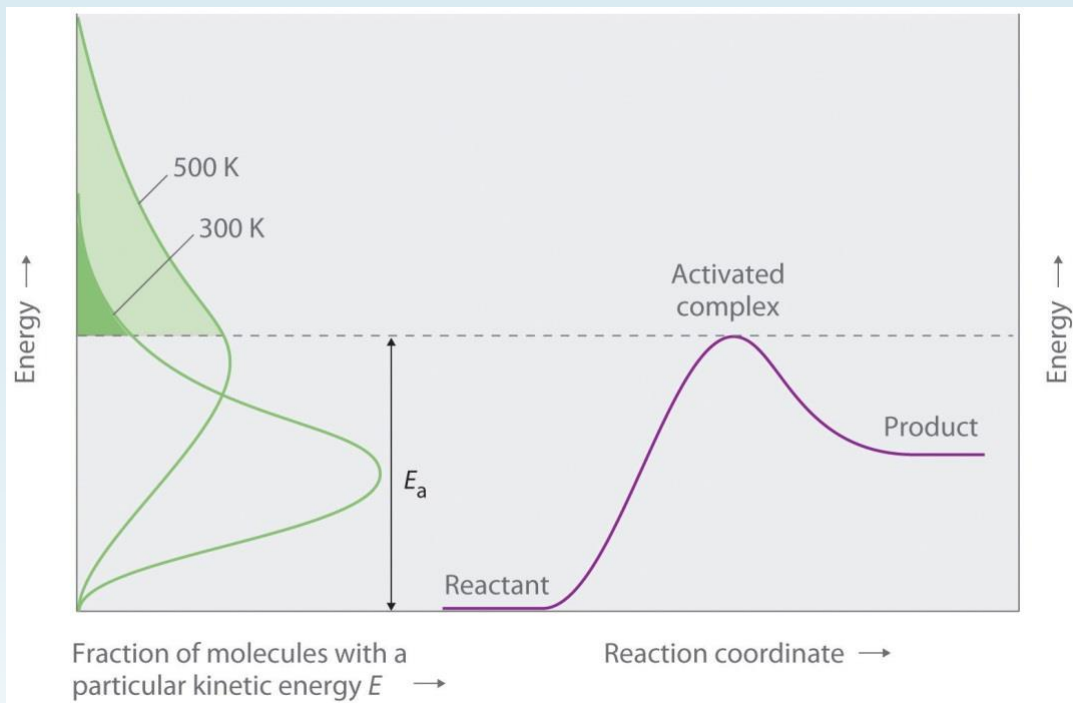


## Collisional energy









## The thermal average rate constant

## The thermal average reaction rate constant

## The reaction rate coefficient

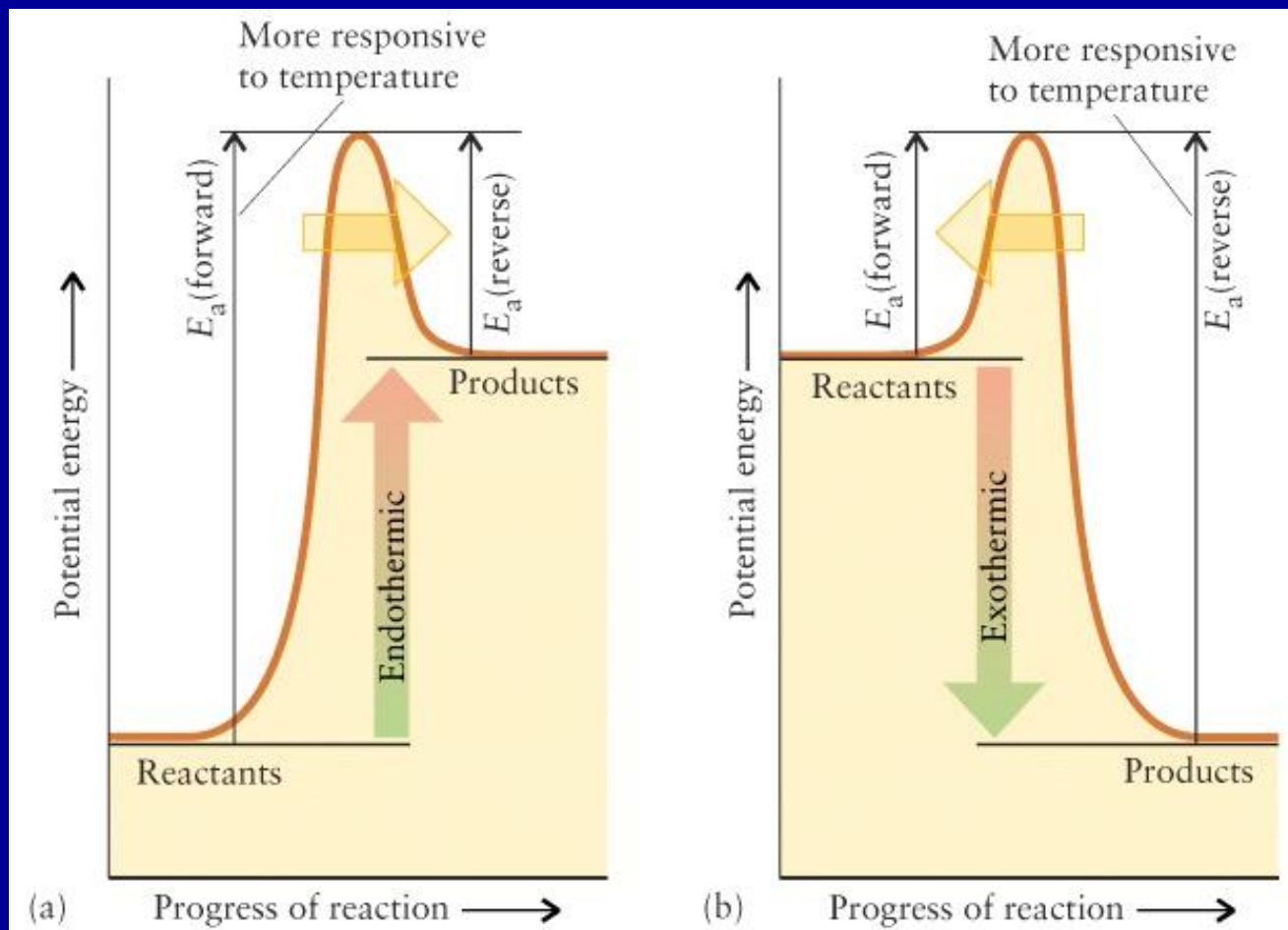
The thermally averaged rate constant  $\alpha_{th}(T)$  (in a.u.) is obtained from the energy-dependent cross-section  $\sigma(E)$  as

$$\alpha_{th}(T) = \frac{8\pi}{(2\pi kT)^{3/2}} \int_0^\infty \sigma(E_{el}) e^{-\frac{E_{el}}{kT}} E_{el} dE_{el}, \quad (4)$$

where  $T$  is the temperature. Temperature dependencies  $\alpha_{th}(T)$  for different rovibrational transitions  $v \rightarrow v'$  obtained using equation (4) are shown in Fig. 3 as solid lines.

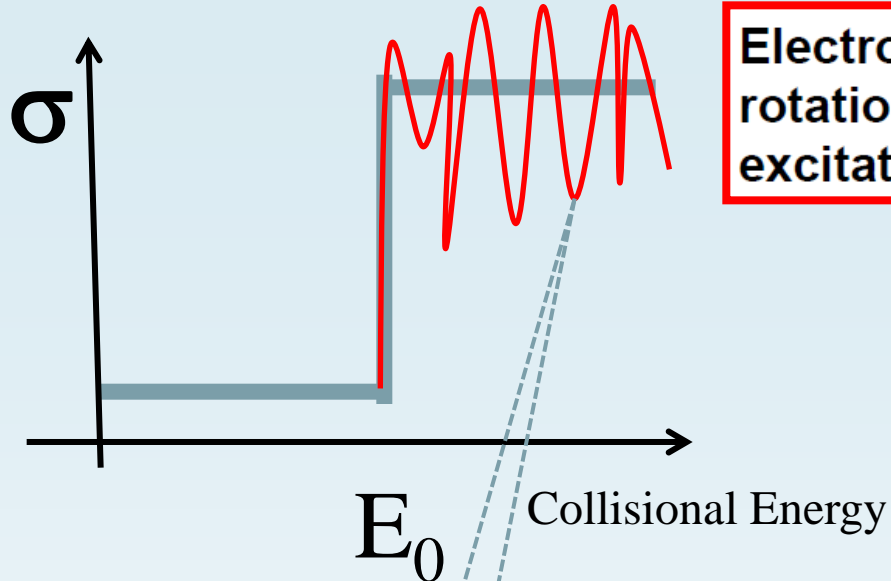
It is written for process with electron energy e.g. excitation by collisions with electrons

Higher temperatures favor products for an endothermic reaction

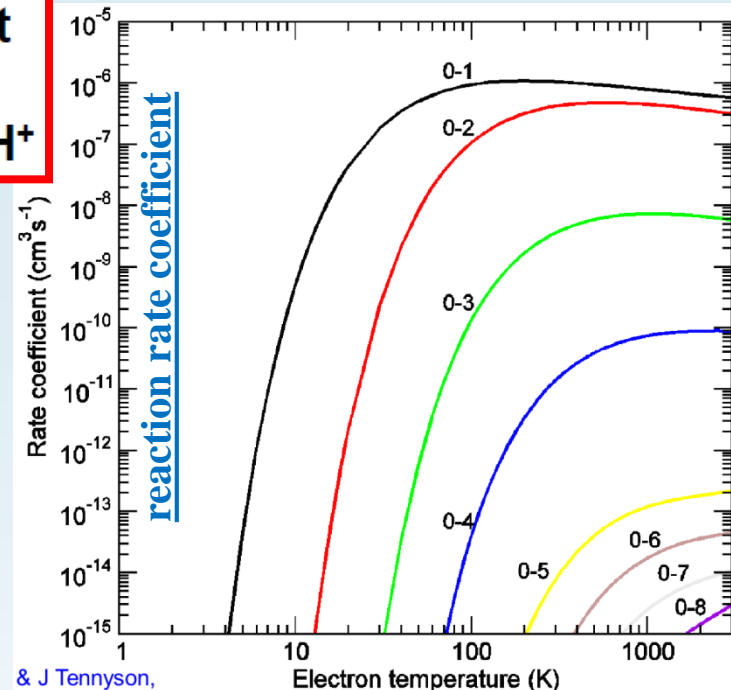


Endothermic reaction:  $E_a(\text{forward}) > E_a(\text{reverse})$

Exothermic reaction:  $E_a(\text{forward}) < E_a(\text{reverse})$



Electron impact  
rotational  
excitation of  $\text{CH}^+$



The thermally averaged rate constant  $\alpha_{\text{th}}(T)$  (in a.u.) is obtained from the energy-dependent cross-section  $\sigma(E)$  as

$$\alpha_{\text{th}}(T) = \frac{8\pi}{(2\pi kT)^{3/2}} \int_0^\infty \sigma(E_{\text{el}}) e^{-\frac{E_{\text{el}}}{kT}} E_{\text{el}} dE_{\text{el}}, \quad (4)$$

where  $T$  is the temperature. Temperature dependencies  $\alpha_{\text{th}}(T)$  for different rovibrational transitions  $v \rightarrow v'$  obtained using equation (4) are shown in Fig. 3 as solid lines.

For further discussion, it is convenient to represent the cross-section  $\sigma(E_{\text{el}})$  in the form

$$\sigma(E_{\text{el}}) = \frac{\pi}{k^2} P(E_{\text{el}}), \quad (5)$$

where  $k$  is the wave vector of the incident electron,  $P(E_{\text{el}})$  is the probability for vibrational (de-)excitation at collision energy  $E_{\text{el}}$ .

## Arrhenius dependence

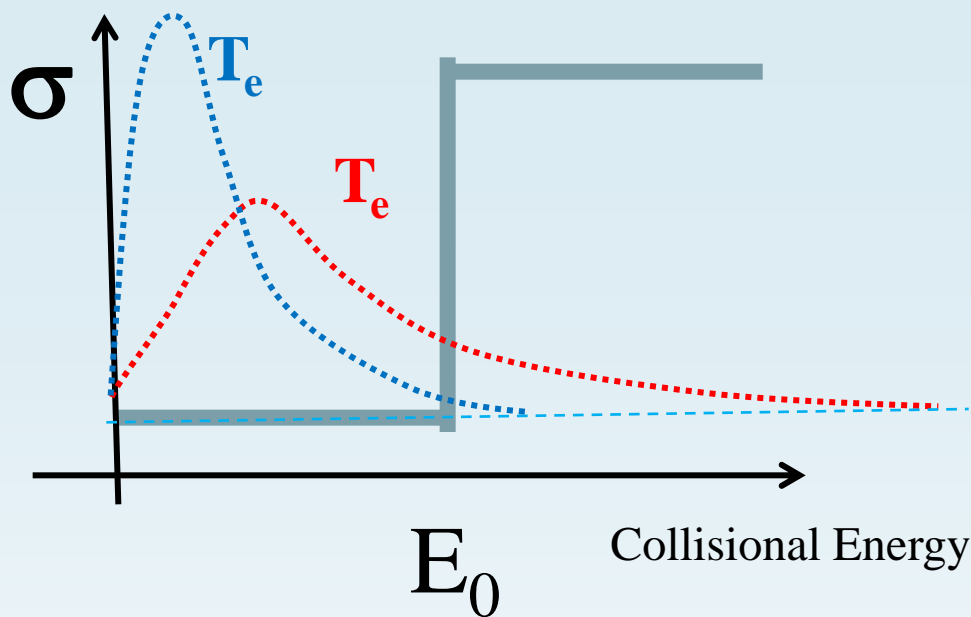
$$k = A e^{-\frac{E_a}{RT}}$$

pre-exponential factor

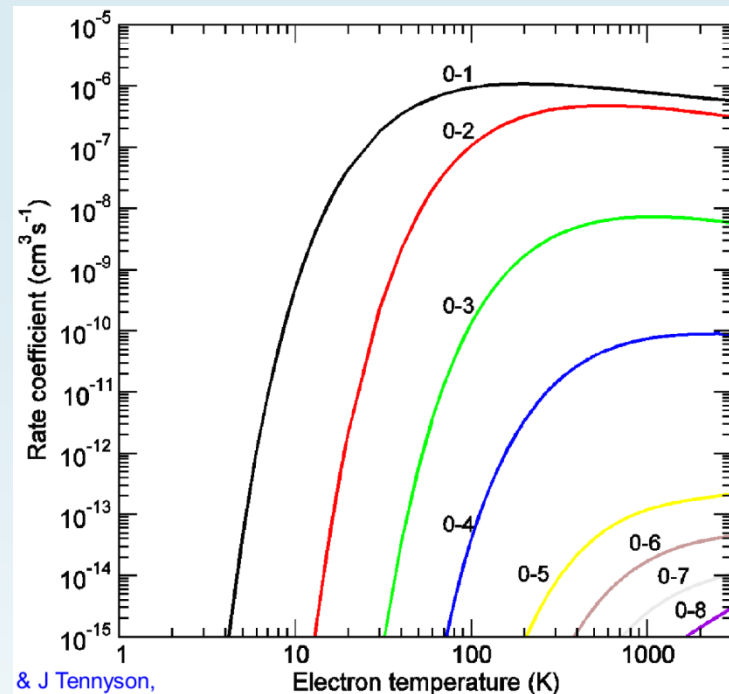
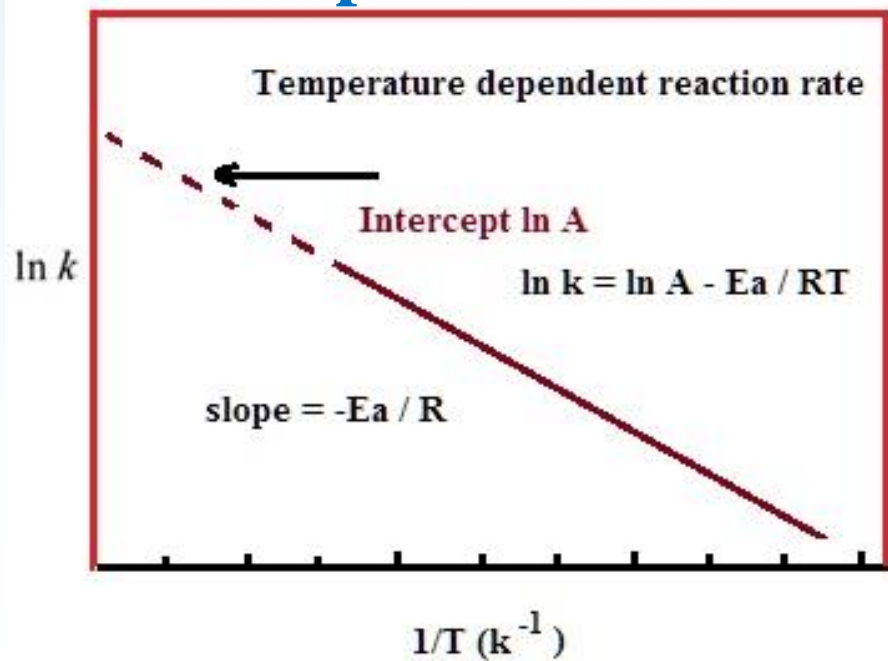
activation energy

average kinetic energy

$$\ln k = \ln A - \frac{E_a}{RT}$$



## Arrhenius plot



$$k = A e^{-\frac{E_a}{RT}}$$

pre-exponential factor

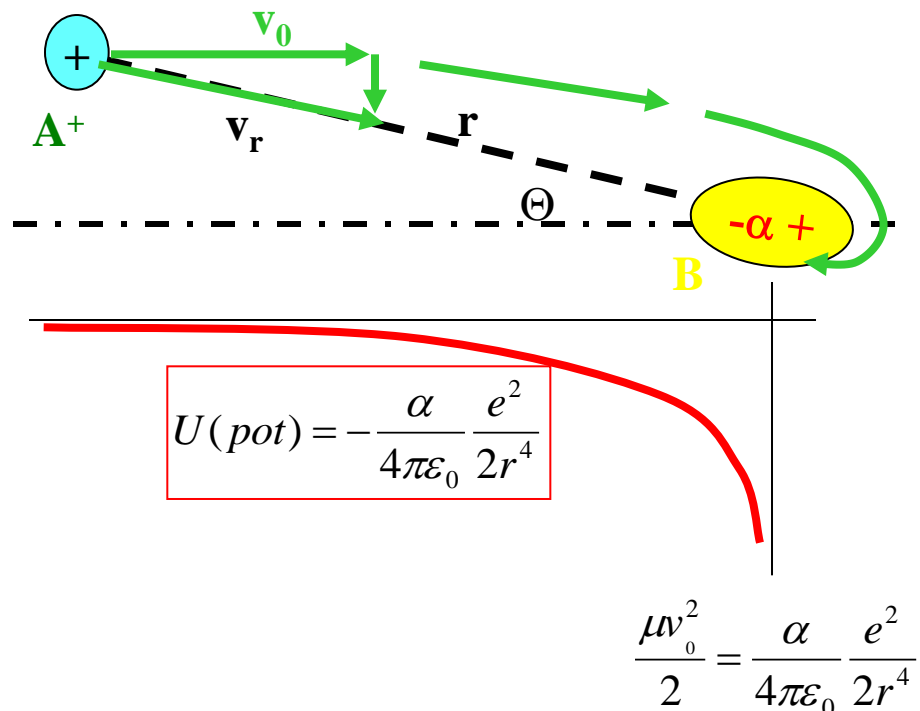
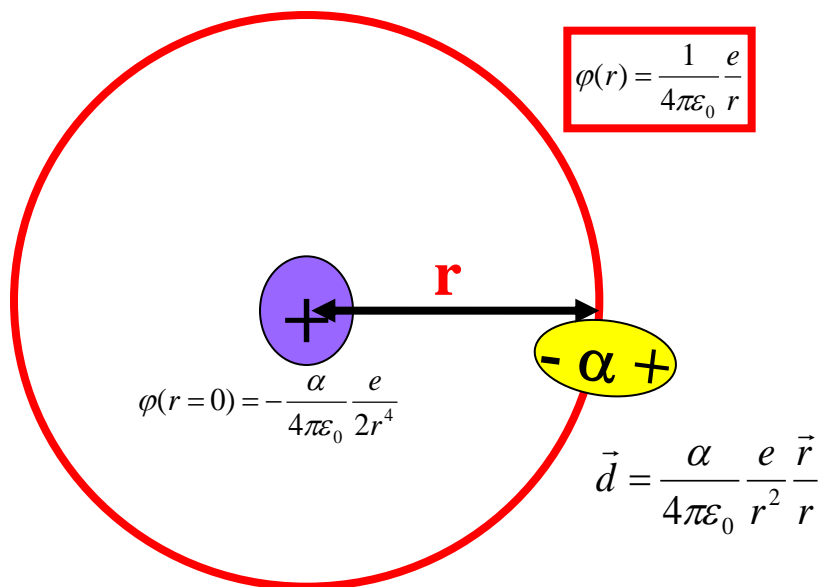
activation energy

average kinetic energy

$$\ln k = \ln A - \frac{E_a}{RT}$$

**Some experiments and data....**

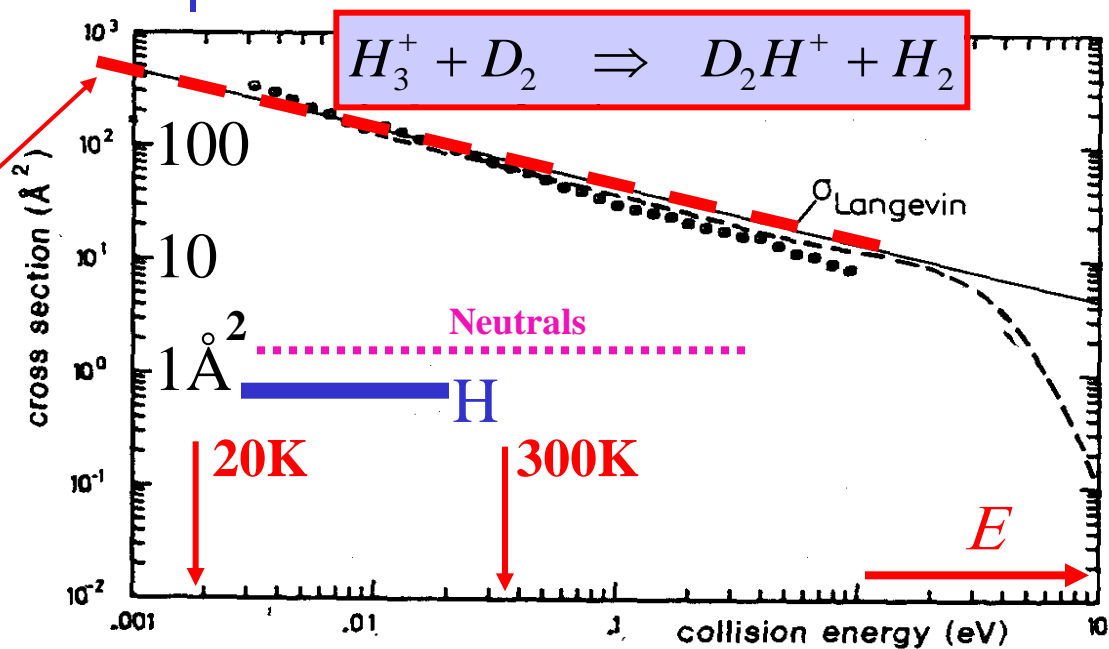
# Collision cross section of IMR



$\alpha$  - polarizability

$$\sigma = \pi \rho_0^2 = \frac{2\pi e}{v_0(4\pi\epsilon_0)} \sqrt{\frac{\alpha}{\mu}}$$

$$\sigma = \pi \rho_0^2 \sim \frac{1}{v_0} \sqrt{\frac{\alpha}{\mu}} \sim \frac{1}{\sqrt{E}}$$





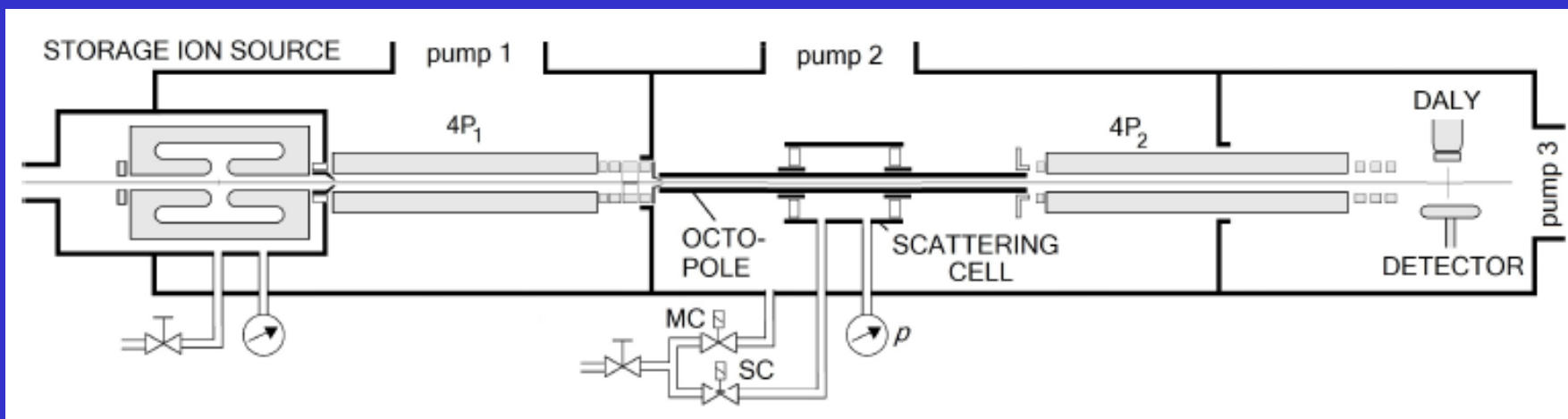
ChemPhysChem

Articles  
doi.org/10.1002/cphc.202000258Chem  
Europ  
European  
Societies P

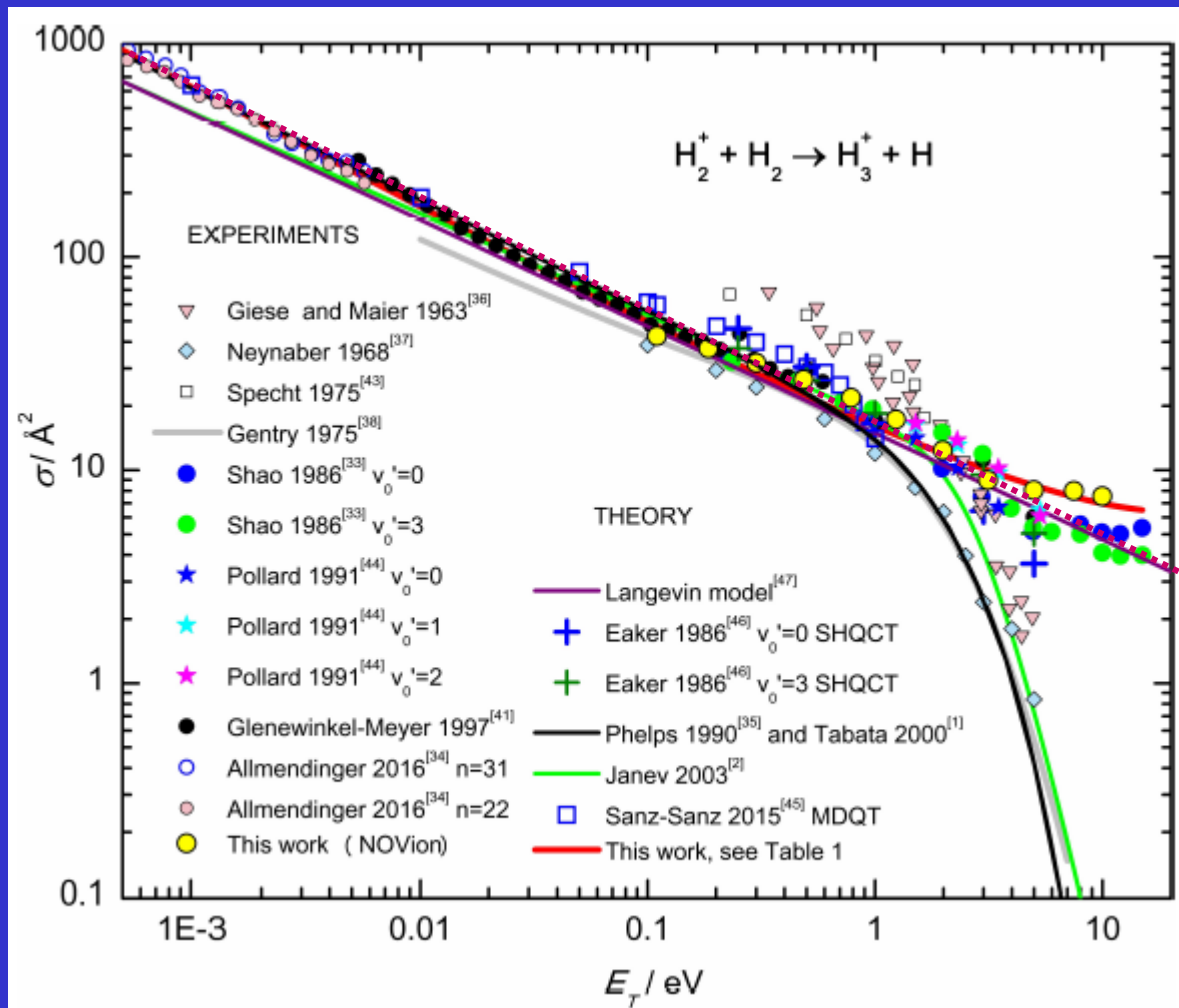
© 2020 Wiley-VCH Verlag GmbH &amp; Co. KGaA, Weinheim

VIP Very Important Paper

## Formation of $\text{H}_3^+$ in Collisions of $\text{H}_2^+$ with $\text{H}_2$ Studied in a Guided Ion Beam Instrument

Igor Savić,<sup>\*,[a]</sup> Stephan Schlemmer,<sup>[b]</sup> and Dieter Gerlich<sup>[c]</sup>

**Figure 1.** The Guided Ion Beam instrument *NOVion* consists of a storage ion source (SIS), a first quadrupole ( $4P_1$ ), an octopole, guiding the ions through a scattering cell, a second quadrupole ( $4P_2$ ), and a Daly type ion detector. Three separated vacuum chambers are pumped by turbopumps with pumping speeds of 180 l/s for hydrogen. For determining integral cross sections of ions reacting with neutrals, the target gas is leaked alternately into the scattering cell (SC) or into the main chamber (MC) containing the octopole. The net pressure  $p$  is the difference between the two values measured under these two conditions,  $p^{\text{MC}}$  and  $p^{\text{SC}}$ .



2020



$$\sigma_L(E_T)$$

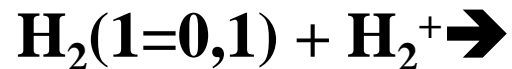
$$\sigma = \pi \rho_0^2 \sim \frac{1}{v_0} \sqrt{\frac{\alpha}{\mu}} \sim \frac{1}{\sqrt{E}}$$

Langevin

**Figure 2.** Dependence of the integral cross section for the reaction  $\text{H}_2^+ + \text{H}_2 \rightarrow \text{H}_3^+ + \text{H}$  on the collision energy  $E_T$ . In the meV and sub-meV energy range, there is good agreement between two different merged beam results, Refs. [34,41]. Note that Allmendinger et al.<sup>[34]</sup> scaled their relative cross sections to the absolute ones calculated by Sanz-Sanz et al.<sup>[45]</sup> as described in the caption of figure 10 of Ref. [34]. Between thermal energies and 1 eV, most of the published and tabulated values agree more or less with the function proposed in the compilations by Tabata<sup>[1]</sup> (black line) and Janev et al.<sup>[2]</sup> (green line). However, based on results from the sixties and seventies, a steep decline has been predicted above 2 eV. In contrary, our results (yellow filled circles) do not show this trend, in accordance with the guided ion beam results from Shao et al.<sup>[33]</sup> The data presented in Ref. [35] as tabulated values and in Ref. [1] as an analytical function are nearly identical and are represented here simply by the one black line.



# Very recent experiments and theory



THE JOURNAL OF CHEMICAL PHYSICS 145, 244316 (2016)

## Observation of enhanced rate coefficients in the $\text{H}_2^+ + \text{H}_2 \rightarrow \text{H}_3^+ + \text{H}$ reaction at low collision energies

Pitt Allmendinger,<sup>a)</sup> Johannes Deiglmayr,<sup>a)</sup> Katharina Höveler, Otto Schullian, and Frédéric Merkt<sup>b)</sup>  
Laboratory of Physical Chemistry, ETH Zurich, Zurich, Switzerland

(Received 25 October 2016; accepted 29 November 2016; published online 29 December 2016)

2016

$k/k_L$

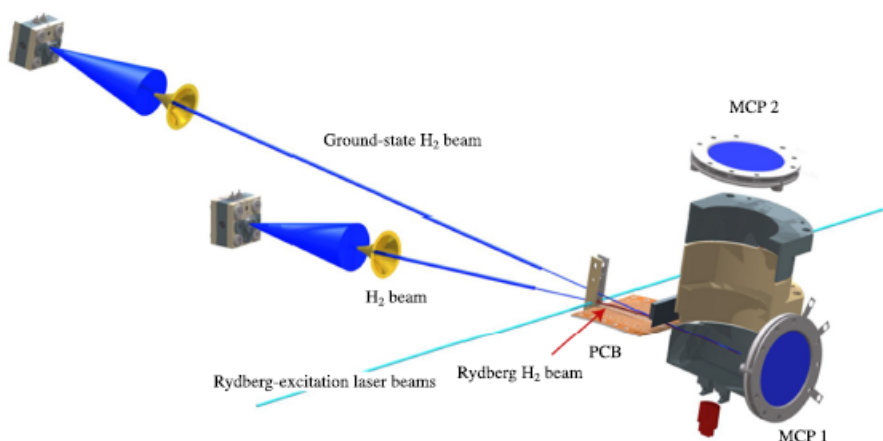
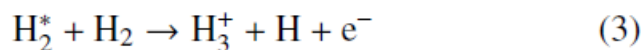


FIG. 1. Schematic representation of the merged-beam apparatus used to study ion-molecule reactions at low collision energies, with the two skimmed supersonic beams initially propagating at an angle of  $10^\circ$ , the Rydberg-Stark deflector made of a curved printed circuit board (PCB), and used to merge the beams after laser excitation, the reaction zone located within an electrode stack (gray), which constitutes the linear time-of-flight mass spectrometer used to detect reactants and products separately. (MCP1) and (MCP2) Microchannel-plate detectors to monitor the flight times of Rydberg  $\text{H}_2$  molecules and the ion-time-of-flight spectra, respectively.

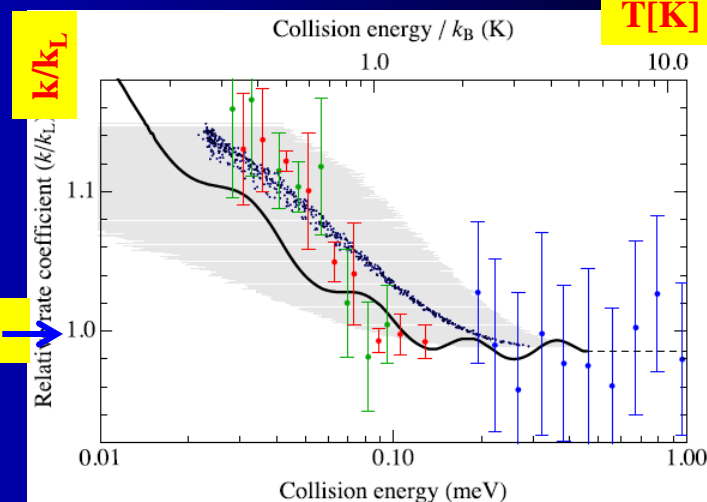


FIG. 3. Comparison of the energy-dependence of the measured relative rate coefficients  $k(E)/k_L$  (color dots) to the calculation by Dashevskaya *et al.*<sup>22</sup> for normal  $\text{H}_2$  (75%  $\text{H}_2$  in  $j = 1$  and 25%  $\text{H}_2$  in  $j = 0$ ) at fixed collision energies (solid line) and for collision energies averaged over the simulated experimental energy distributions (black dots, gray bars indicate one standard deviation). Green dots: two-pulse sequence ( $\Delta t = 7 \mu\text{s}$ ) and  $\text{H}_2^*$  Rydberg beam central velocity  $v(\text{H}_2^+) = 1800 \text{ m/s}$ . Red dots: single-pulse sequence for  $v(\text{H}_2^+) = 1700 \text{ m/s}$ . Blue dots: single-pulse sequence,  $v(\text{H}_2^+) = 1540 \text{ m/s}$ . The absolute scaling of each experimental data set was chosen to minimize the deviation from the simulation. The simulation (black dots) is based on the experimental parameters of the two-pulse measurement (green dots), but the result is very similar for the other measurements.

- Relocking of intrinsic angular momenta in collisions of diatoms with ions: Capture of  $H_2(j = 0,1)$  by  $H_2^+$

E. I. Dashevskaya,<sup>1,2</sup> I. Litvin,<sup>3</sup> E. E. Nikitin,<sup>1,2</sup> and J. Troe<sup>2,3,a)</sup>  
<sup>1</sup>Schulich Faculty of Chemistry, Technion—Israel Institute of Technology, Haifa 32000, Israel  
<sup>2</sup>Max-Planck-Institut für Biophysikalische Chemie, Am Fassberg 11, D-37077 Göttingen, Germany  
<sup>3</sup>Institut für Physikalische Chemie, Universität Göttingen, Tammannstrasse 6, D-37077 Göttingen, Germany  
 (Received 25 October 2016; accepted 30 November 2016; published online 29 December 2016)

(Received 25 October 2016; accepted 30 November 2016; published online 29 December 2016)

T[K]

 $\mathbf{k}/\mathbf{k}_L$  $\mathbf{k}/\mathbf{k}_L$ 

T[K]

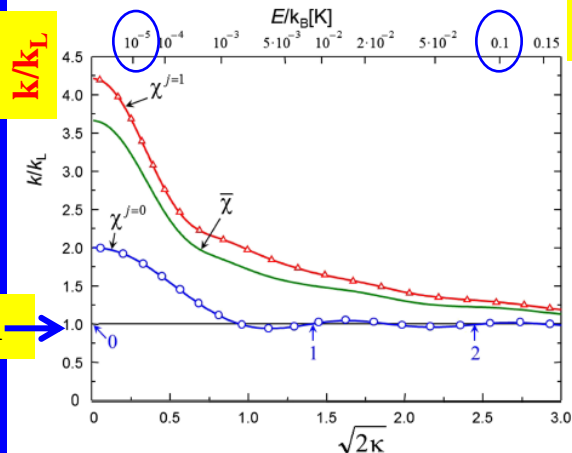

$$\mathbf{k}/\mathbf{k}_L=1 \rightarrow$$

FIG. 2. Scaled rate coefficients for capture of  $\text{H}_2(j=0,1)$  by  $\text{H}_2^+$  ( $\chi^{j=0}, \chi^{j=1}$ ) and mean rate coefficients for a para-ortho mixture  $\bar{\chi} = (1/4)\chi^{j=0} + (3/4)\chi^{j=1}$  (values are given relative to the Langevin limit  $k_L$ ; the classical opening of successive channels for a charge-induced dipole potential for  $j=0$  is marked by arrows (accurate results from the present work; ANC results are presented in Figs. 4 and 5 in the Appendix).

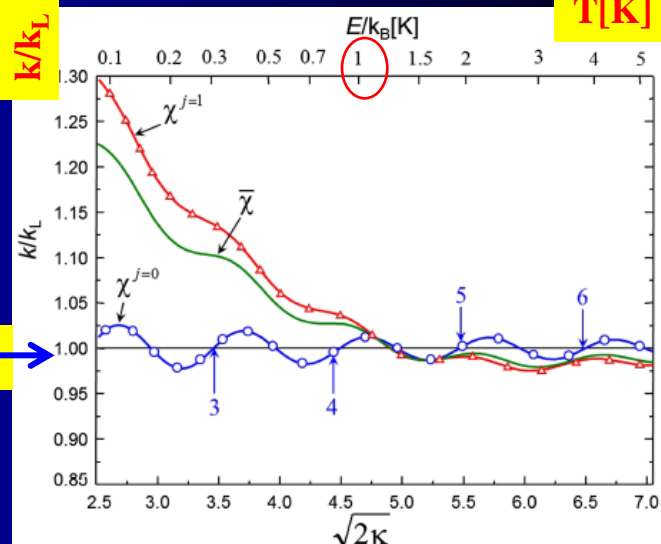
 $k/k_L = 1 -$ 

FIG. 3. As Fig. 2, but for larger energies.

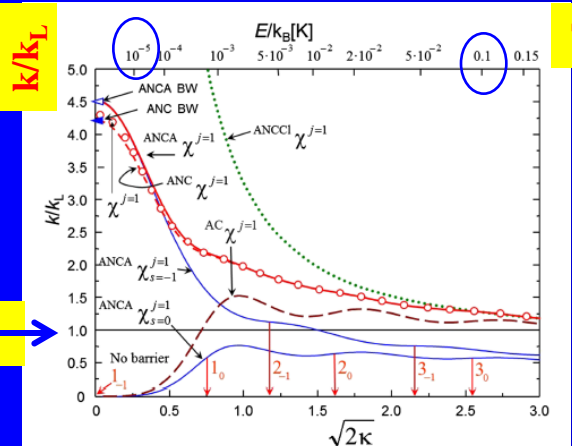

$$k/k_I = 1 \rightarrow$$

FIG. 4. Total and partial scaled rate coefficients for capture of  $H_2(j=1)$  by  $H_2^+$  in different approximations across the ultra-low (two classically open channels) and very-low (several classically open channels) energy range. (The classical opening of successive channels for ANC potentials is marked by  $J_s$  symbols and arrows. BW = Bethe-Wigner limits.)

$$k/k_L = 1 \rightarrow$$
 $k/k_p$ 

T[K]

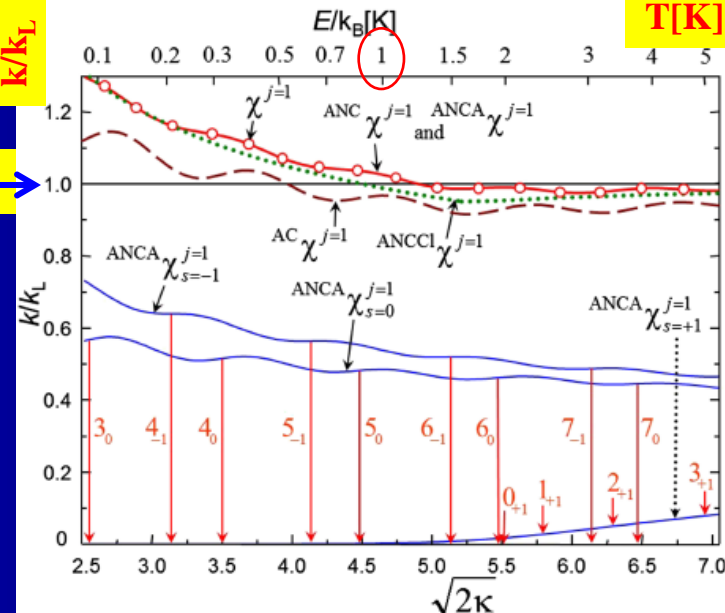
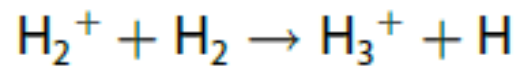


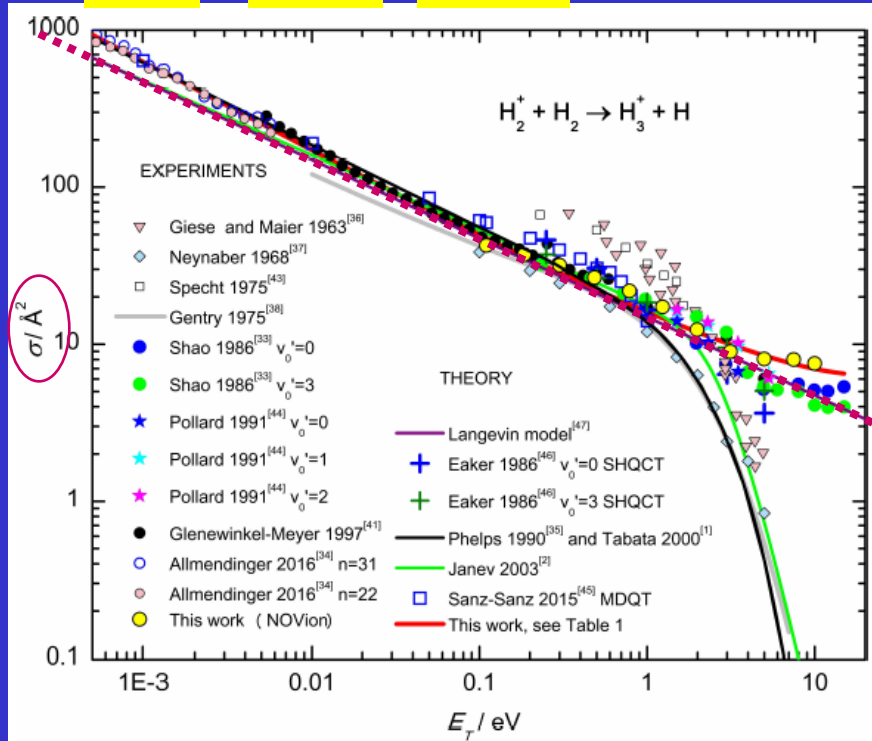
FIG. 5. As Fig. 4, but for larger energies.



10 K

100 K

1000 K



For large energies ~0.001 – 10 eV

For large energies ~10 – 100 000 K

0.1 K

1 K

T[K]

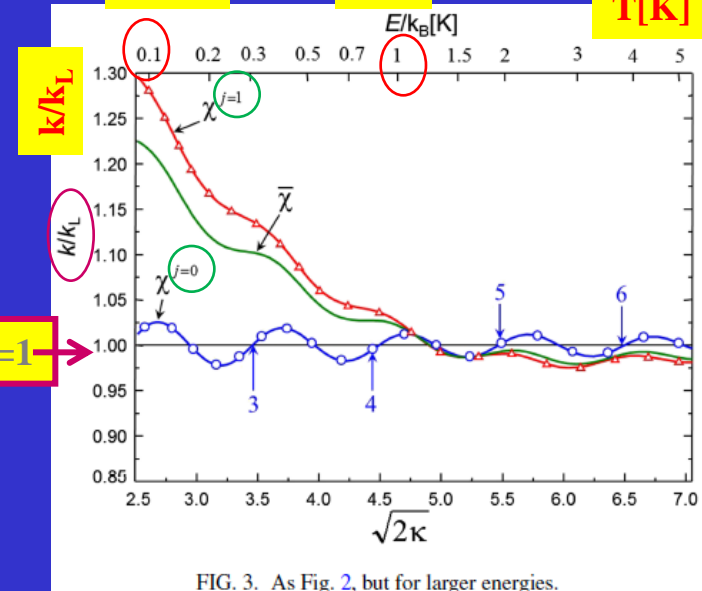


FIG. 3. As Fig. 2, but for larger energies.

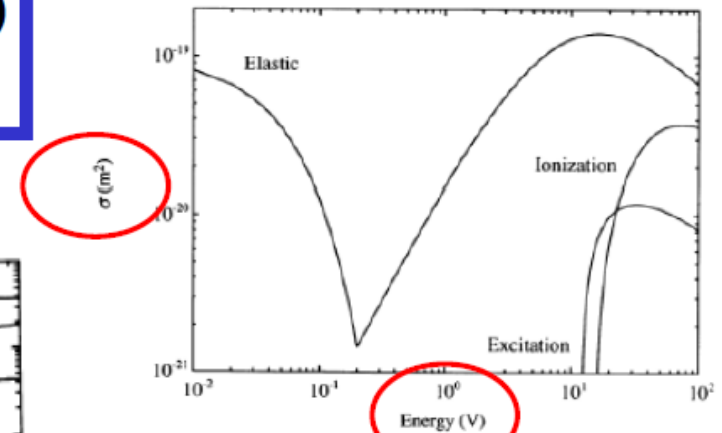
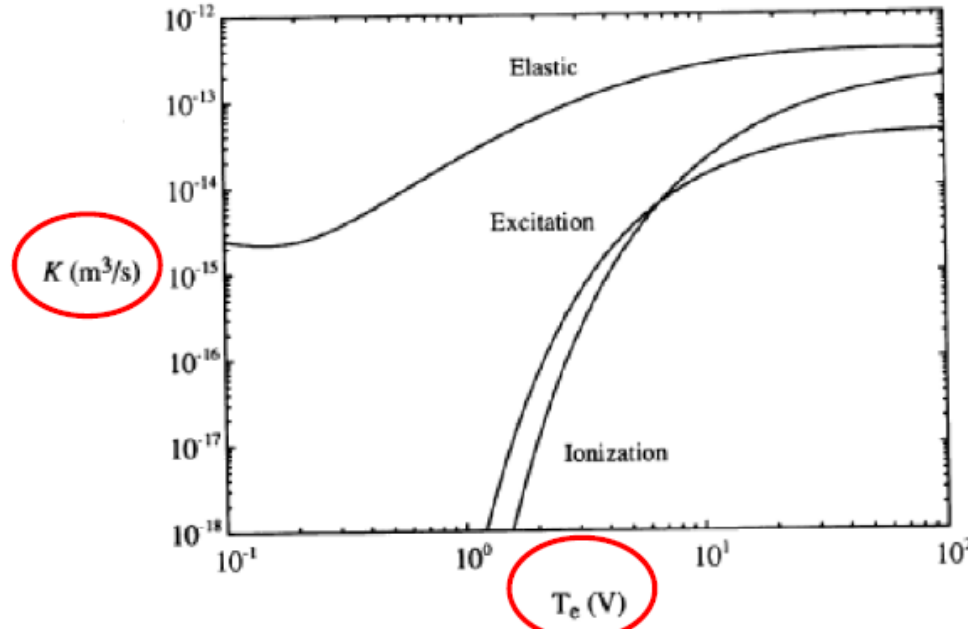
For lower energies ~ 0.1 – 5 K

# Older experiments and theory

## Electron scattering cross-section on Ar

$$k = \int_v f_T(v) \cdot v \cdot \sigma(v) dv = k(T)$$

Electrons – Boltzman distribution with  $T_e$



3. Ionization, excitation and elastic scattering cross sections for electrons in argon (compiled by Vahedi, 1993).

$$\alpha(T, T_e) \propto \int_0^\infty \sqrt{E} \sigma_w(E, T) f(E, T_e) dE$$

**FIGURE 3.16.** Electron collision rate constants  $K_{iz}$ ,  $K_{ex}$  and  $K_m$  versus  $T_e$  in argon gas (compiled by Vahedi, 1993).

What if we have metastables?

Lieberman & Lichtenberg

# IMR thermal

$$\sigma = \pi \rho_0^2 = \frac{2\pi e}{v_0(4\pi\epsilon_0)} \sqrt{\frac{\alpha}{\mu}}$$

$$k = \int_v f_T(v).v.\sigma(v)dv = k(T)$$

$$k_{\text{coll}} \sim 10^{-9} \text{cm}^3 \text{s}^{-1}$$

$$k_{\text{col}} = \langle v\rho \rangle \sim \langle v1/v \rangle = \text{const.}$$

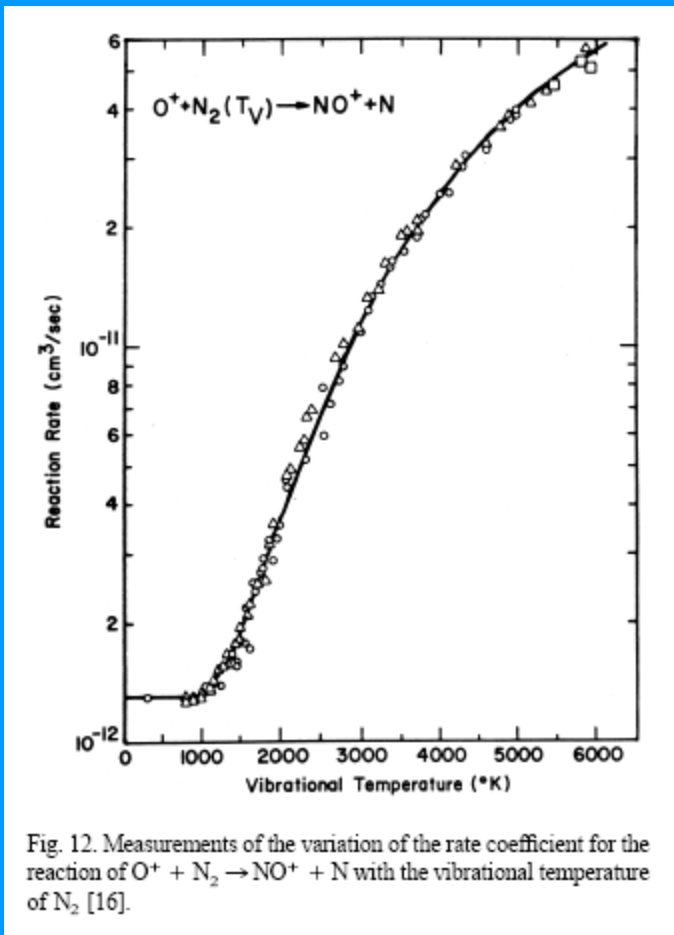
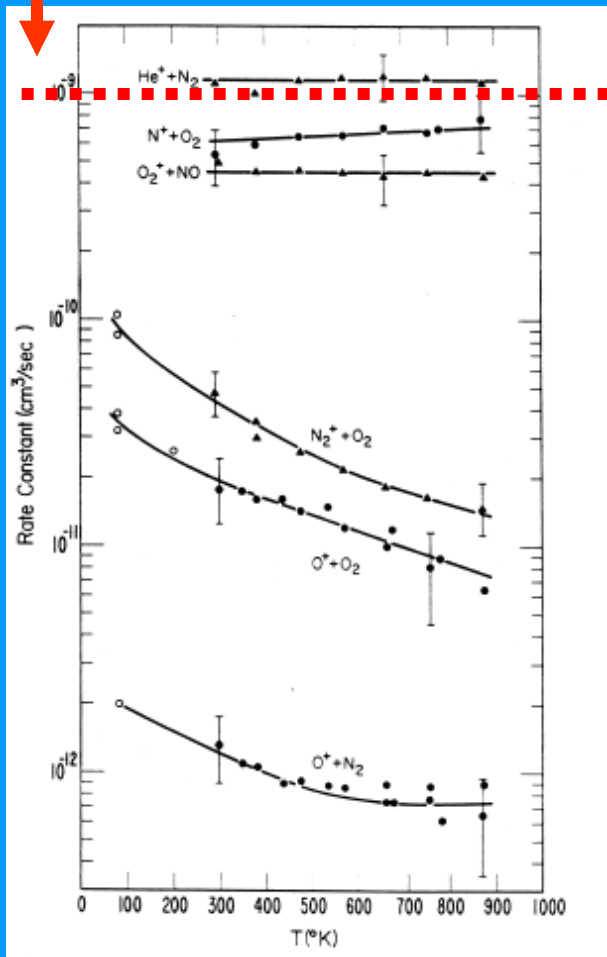
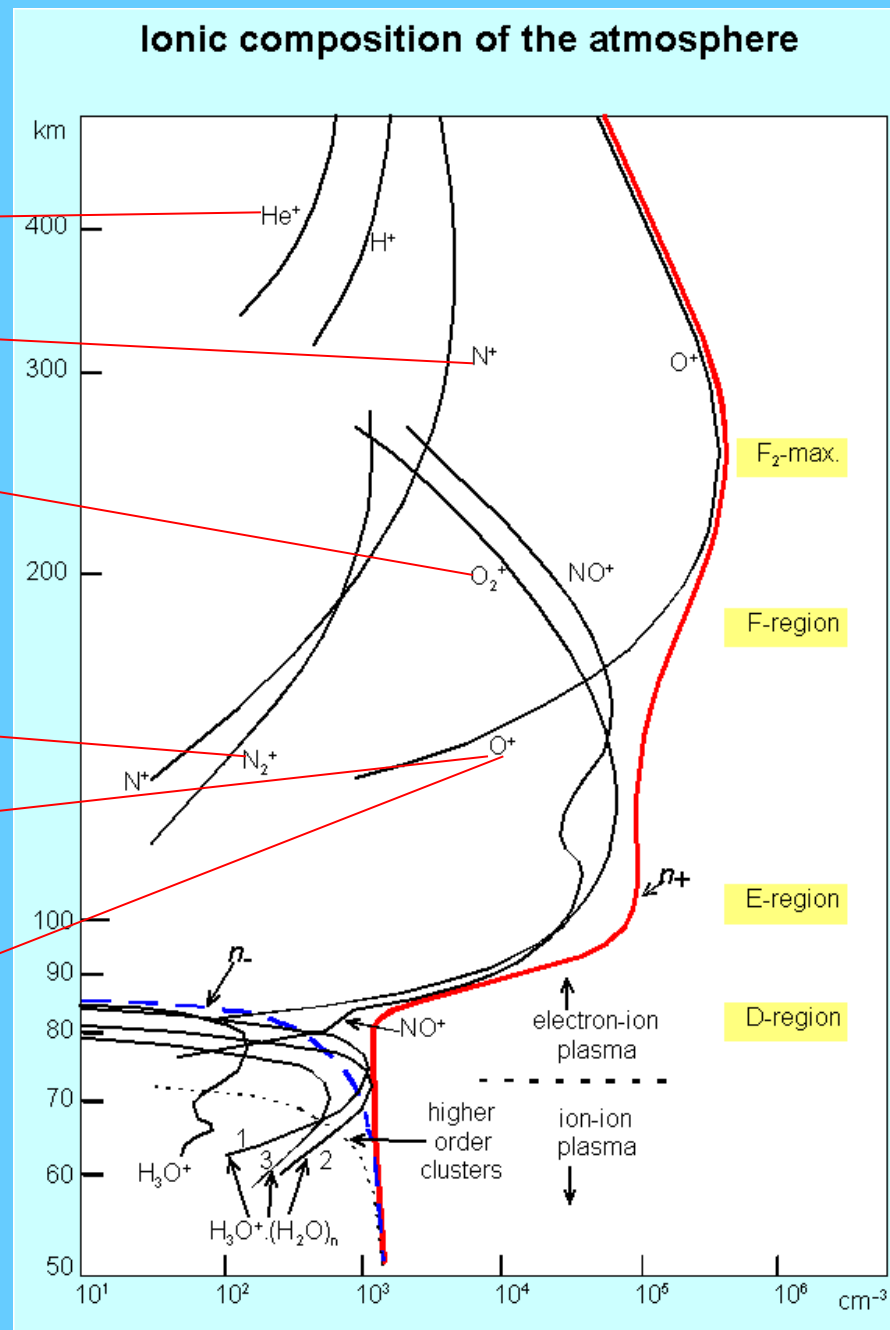
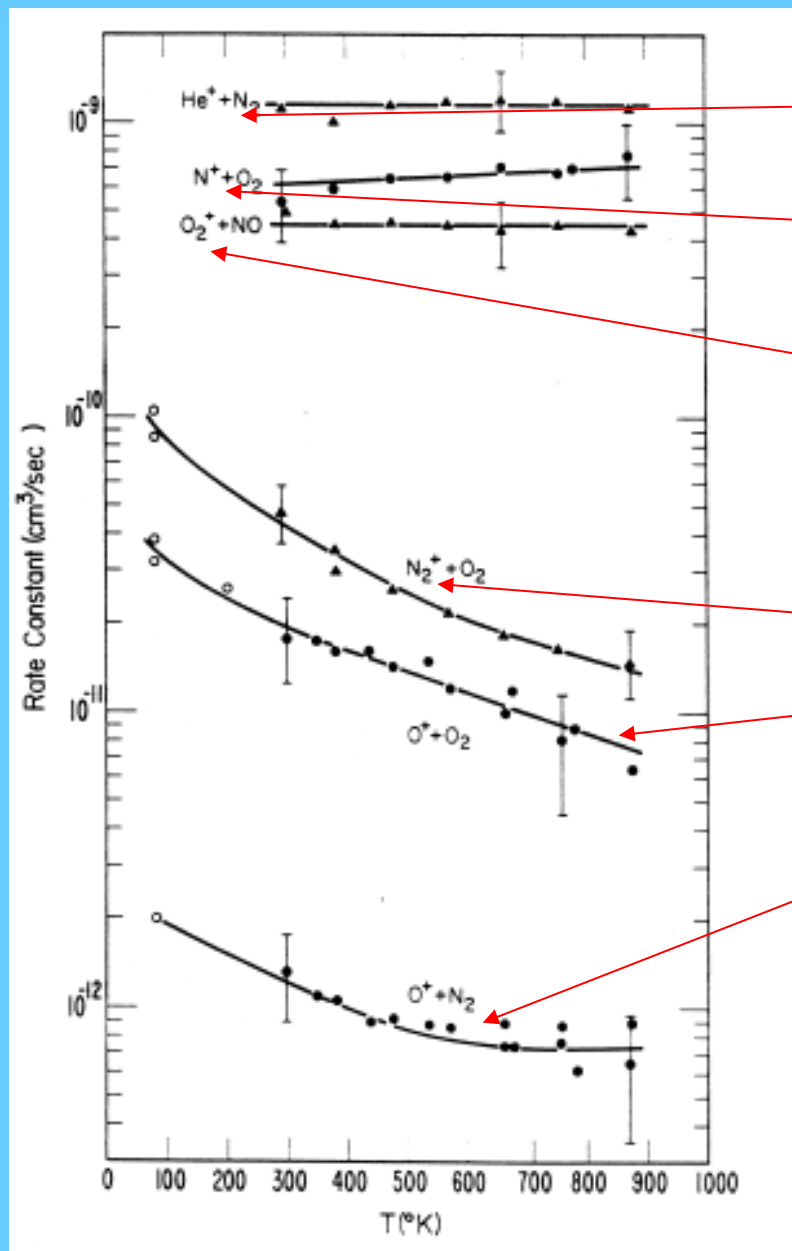


Fig. 12. Measurements of the variation of the rate coefficient for the reaction of  $\text{O}^+ + \text{N}_2 \rightarrow \text{NO}^+ + \text{N}$  with the vibrational temperature of  $\text{N}_2$  [16].

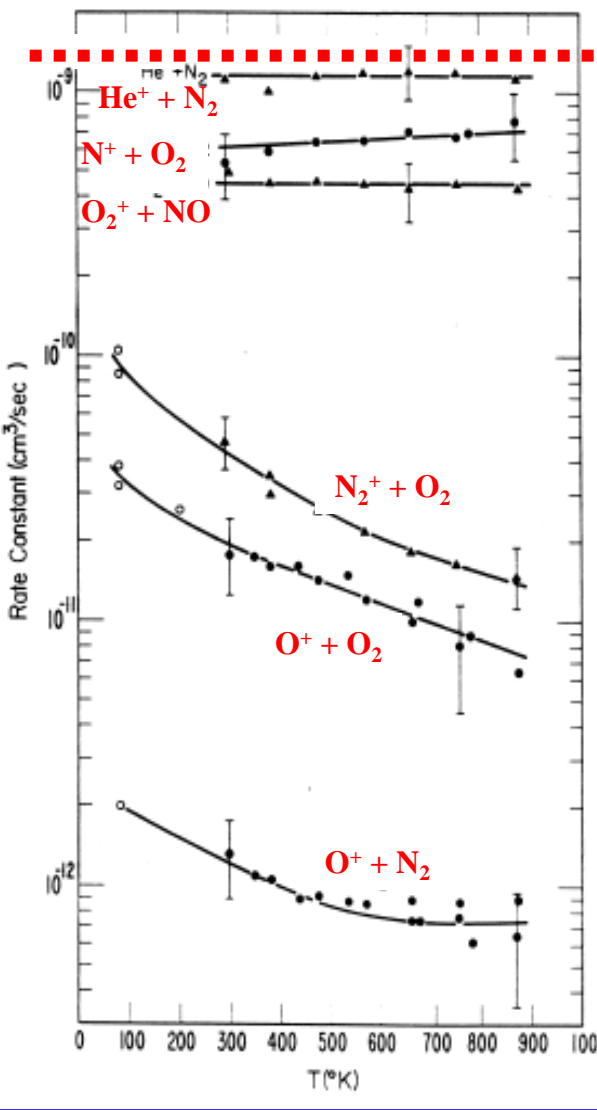
# Ionic composition of the atmosphere



# Reaction Rate of IMR relevant for ionosphere

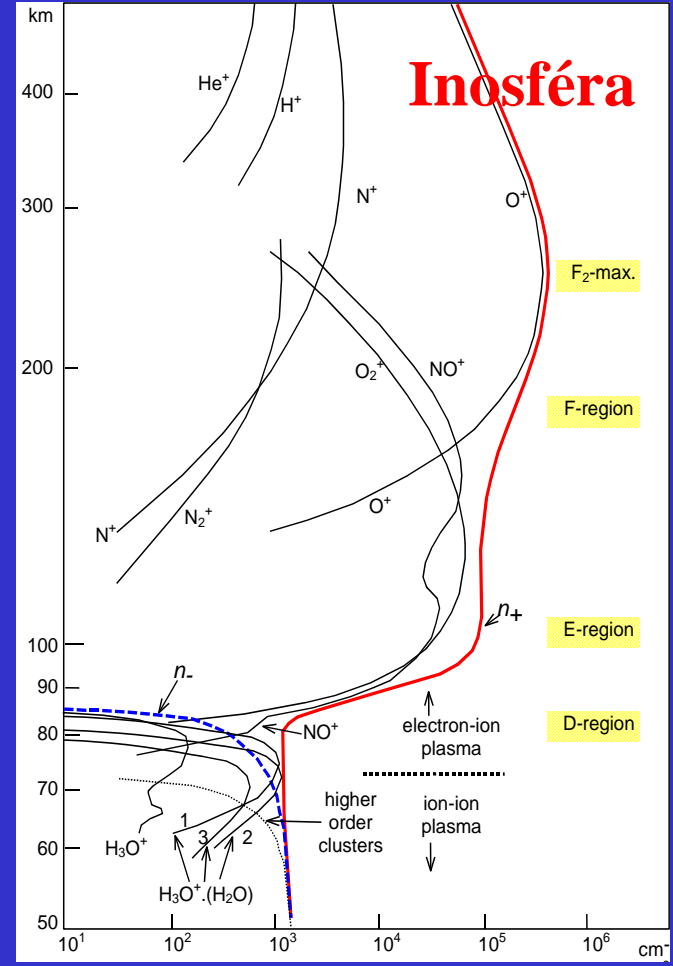
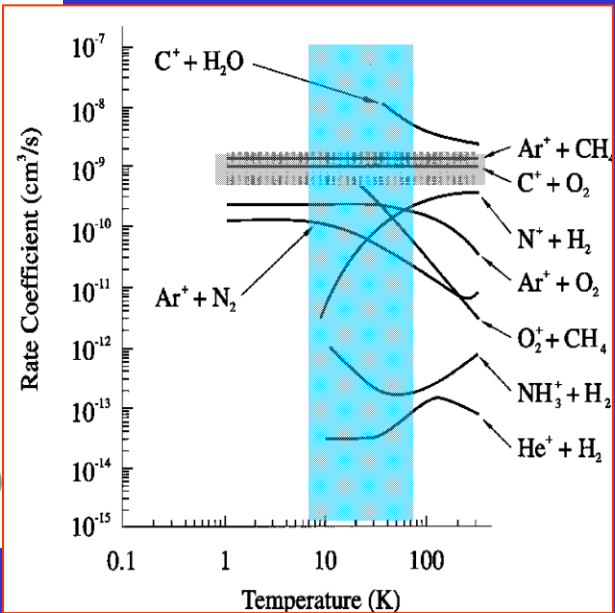
$k_{\text{IMR}}$

$k_{\text{coll}} \sim 10^{-9} \text{ cm}^3 \text{ s}^{-1}$

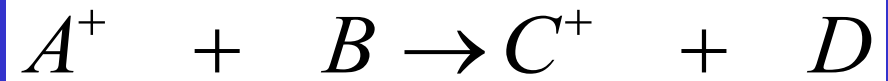


1975-90

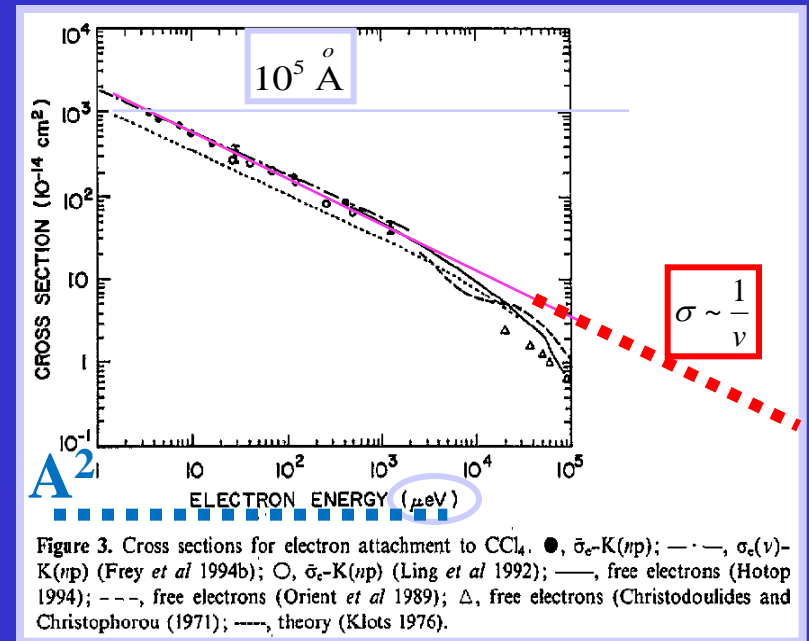
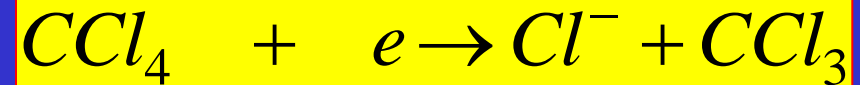
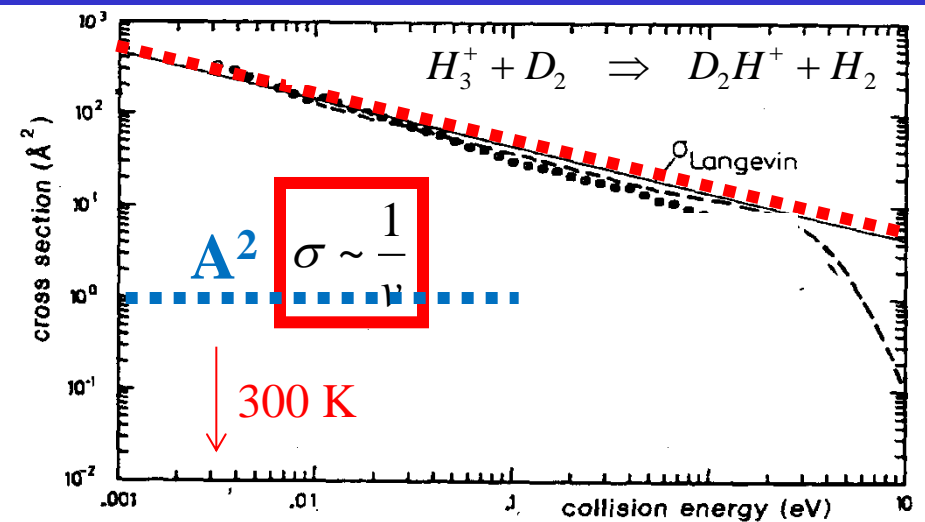
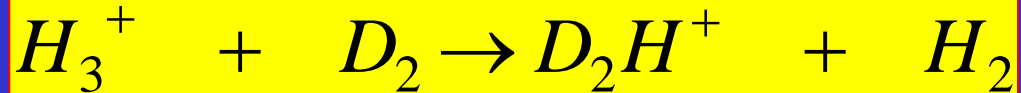
1990-00



# Reaction cross section



$$\frac{dA^+}{dt} = -k_{BIN} A^+ B$$

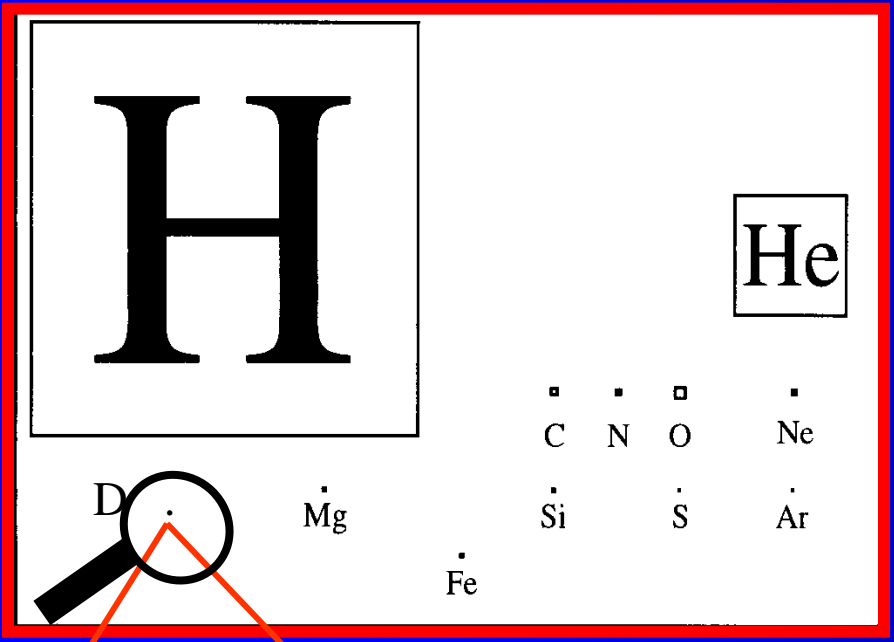




# Interstellar medium

92.1% of nucleons in the universe are protons  
7.8% are helium nuclei !  
0.1%.....C,N,O,S,Si....

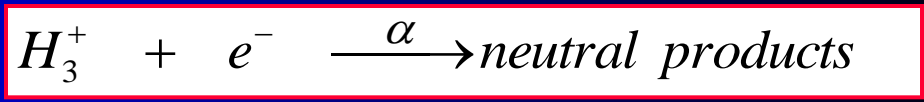
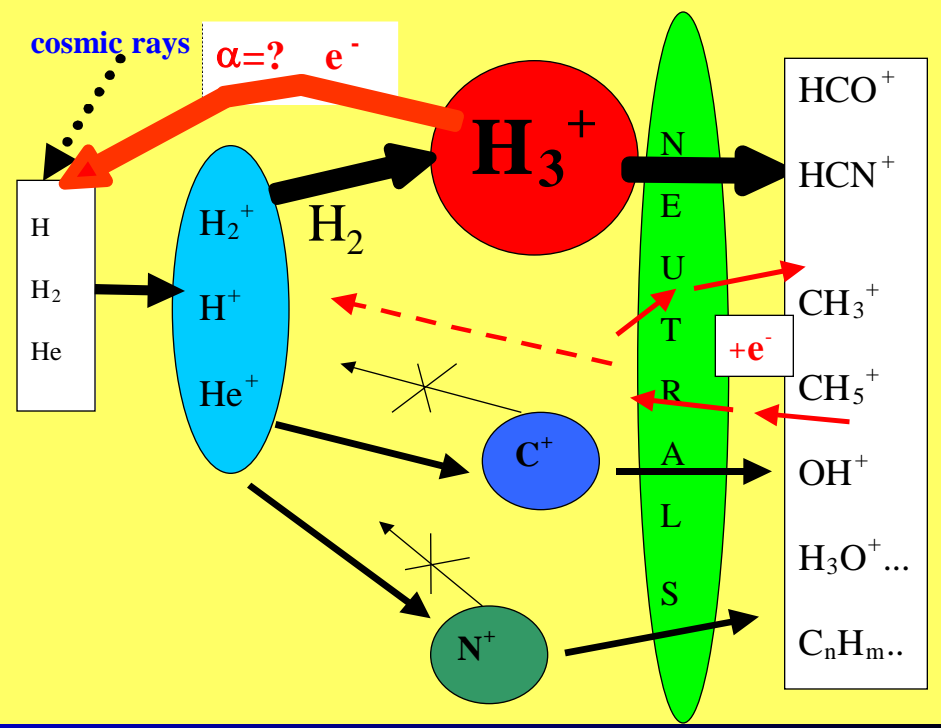
## Cosmic abundance



D/H ratio ~  $10^{-5}$

@ 10-50K

## DENSE INTERSTELLAR CLOUDS



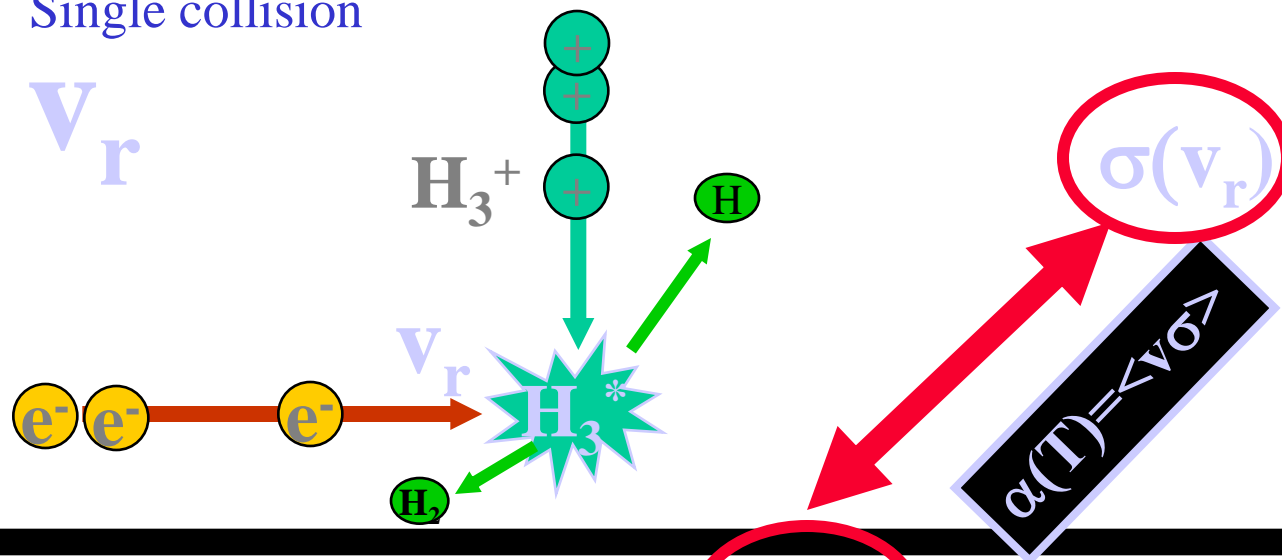
$\alpha$  (10 K) = ????



Cross section

Single collision

$\mathbf{v}_r$

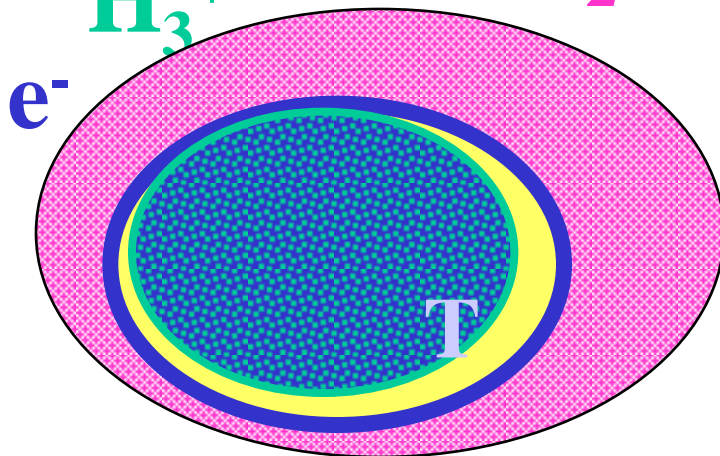


$\alpha(T)$  Rate coefficient

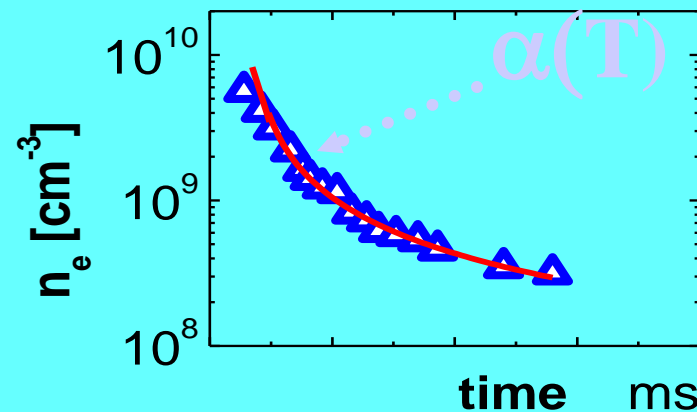
T

Multiple collisions

$\text{H}_3^+ + \text{He, H, H}_2 \text{ hv} \dots$

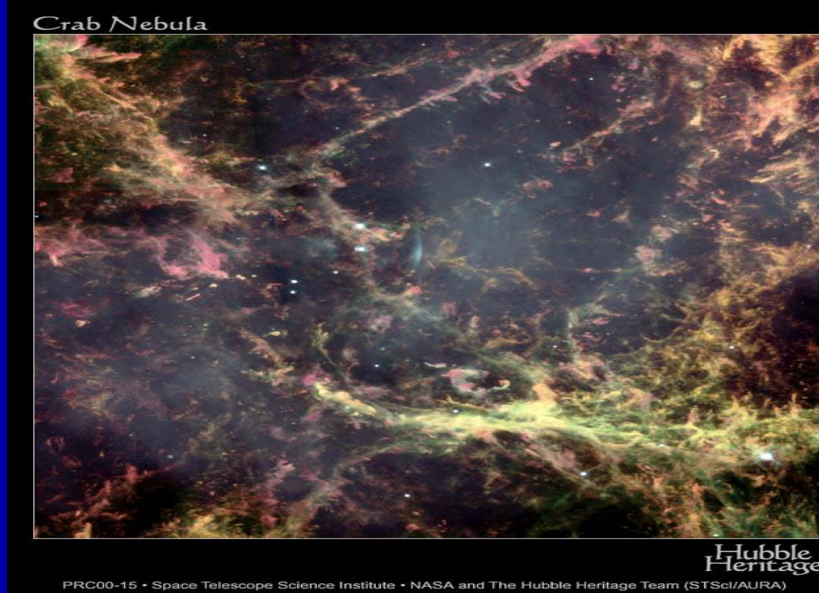
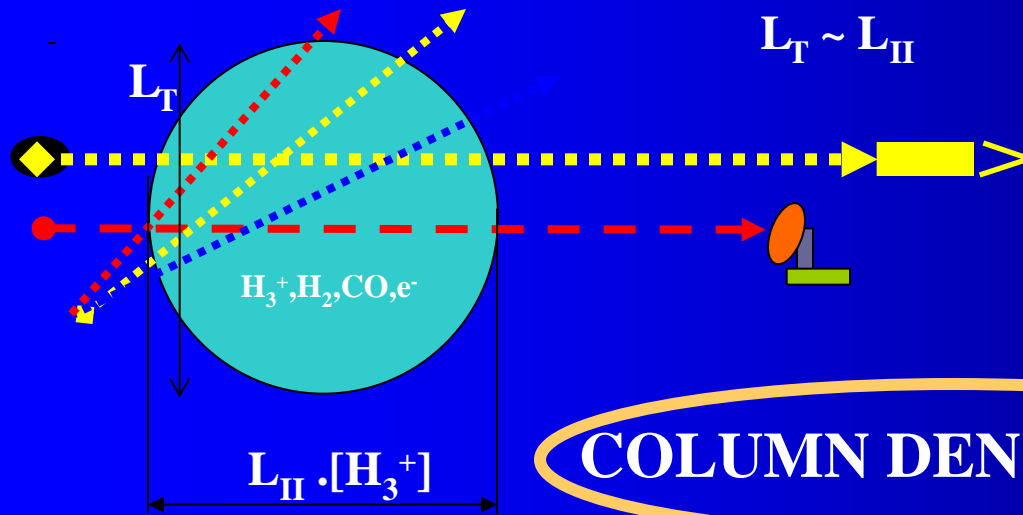


$$\frac{dn_e}{dt} = -\alpha n_i n_e = -\alpha n_e^2$$

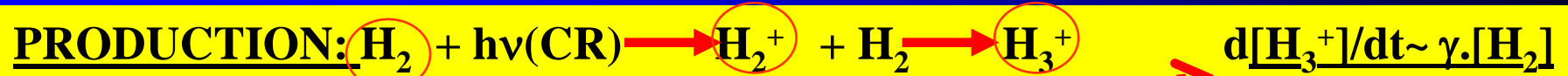


# Balance in ISM

Cosmic-ray ionisation rate  $\gamma \sim 3 \times 10^{-17} \text{s}^{-1}$



# COLUMN DENSITY $N(\text{H}_3)$



**a) DENSE CLOUDS: DESTRUCTION:**



$$\frac{d[\text{H}_3^+]/dt}{\sim -k_{\text{CO}}x[\text{H}_3^+]x[\text{CO}]}$$

$$\underline{d[H_3^+]/dt \sim \gamma \cdot [H_2]}$$

$$[\text{H}_3^+] = \gamma/k_{\text{CO}} \cdot [\text{H}_2]/[\text{CO}] = \underline{\sim 1 \times 10^{-4} \text{ cm}^{-3}}$$

## ~OK with observation

**b) DIFFUSE CLOUDS: DESTRUCTION:**  $\text{H}_3^+ + \text{e}^-$

$$\frac{d[\text{H}_3^+]/dt}{[e^-] \sim [\text{C}]} \sim -\alpha_{\text{DR}} \frac{[\text{H}_3^+][e^-]}{[\text{C}]}$$

$$d[\underline{\text{H}_3^+}]/dt \sim \gamma \cdot [\underline{\text{H}_2}]$$

$$\alpha_{DR} = 2 \times 10^{-7} \text{ cm}^3 \text{ s}^{-1} \times (T/300)^{-0.65} \text{ ?}$$

$$[\text{H}_3^+] = \gamma / \alpha_{\text{DR}} \cdot [\text{H}_2] / [\text{C}] = \sim \underline{1 \times 10^{-7} \text{ cm}^{-3}}$$

~ NO with observation

Low energy collisions with molecules

# Collisions of electrons with atoms (atomic beams)

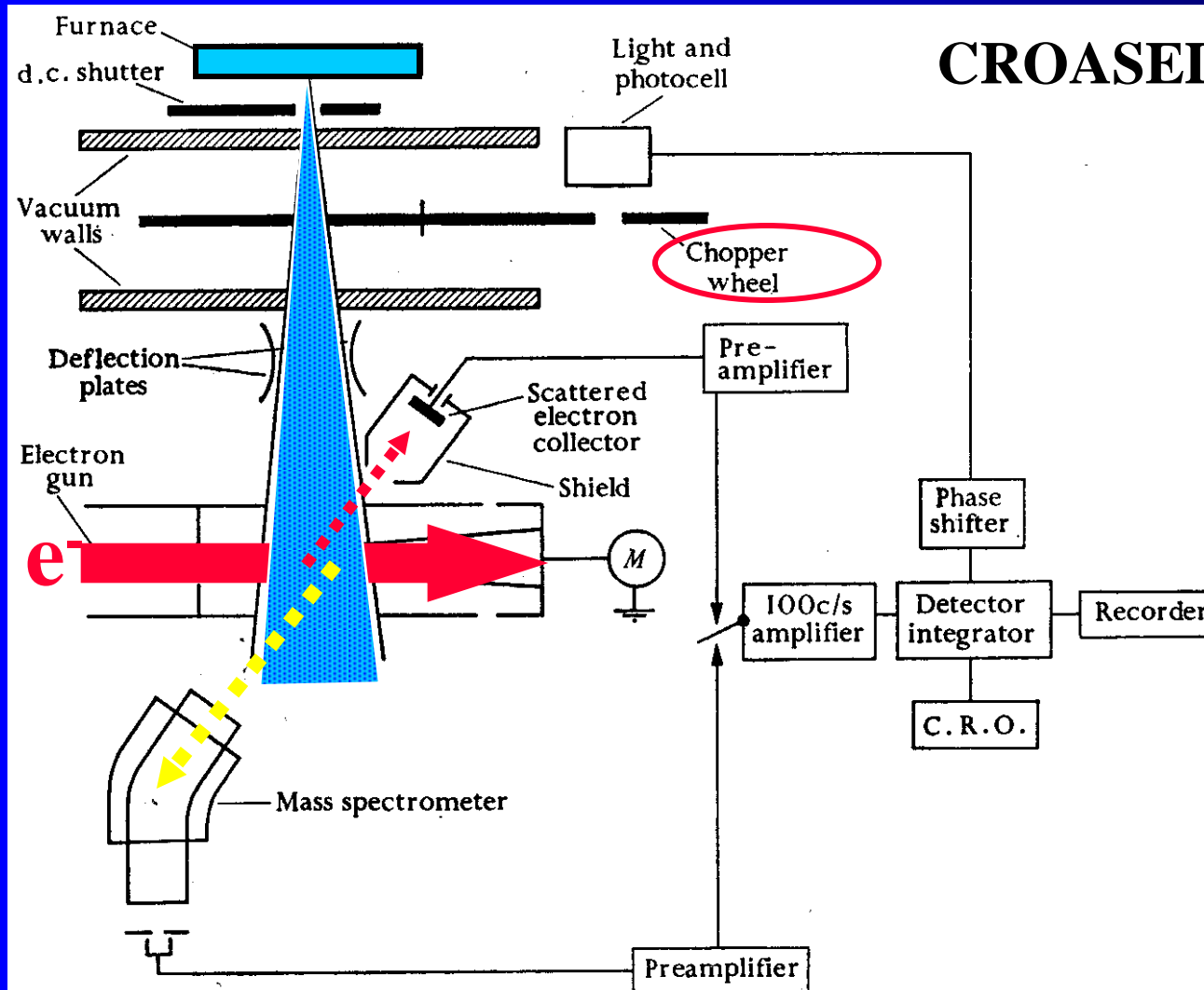
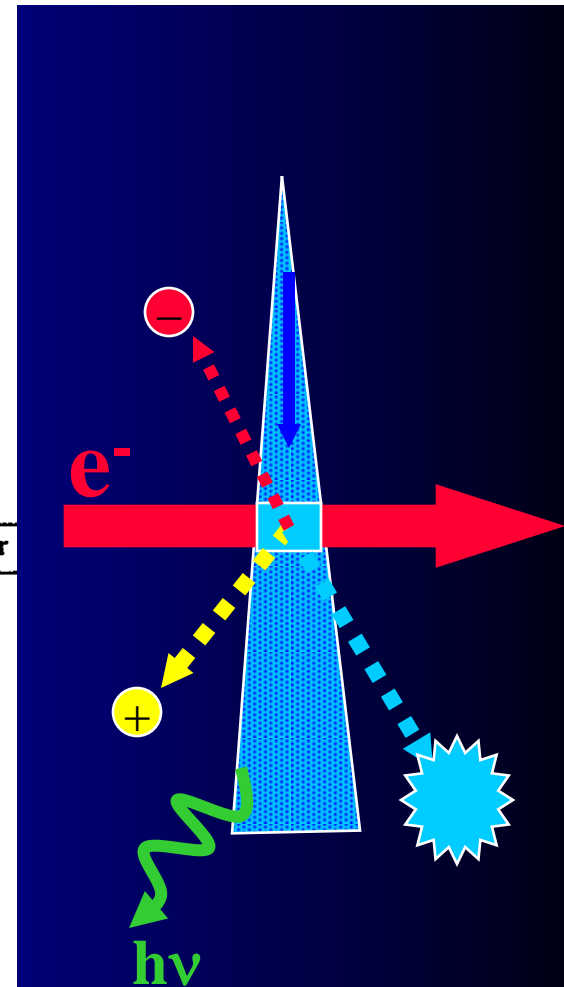


FIG. 1.2. Schematic diagram of the arrangement of apparatus used by Fite, Brackmann, and Neynaber for observation of elastic scattering of electrons by atomic hydrogen.



**Position (angle), mass and energy sensitive detectors**

# Partial cross section for excitation

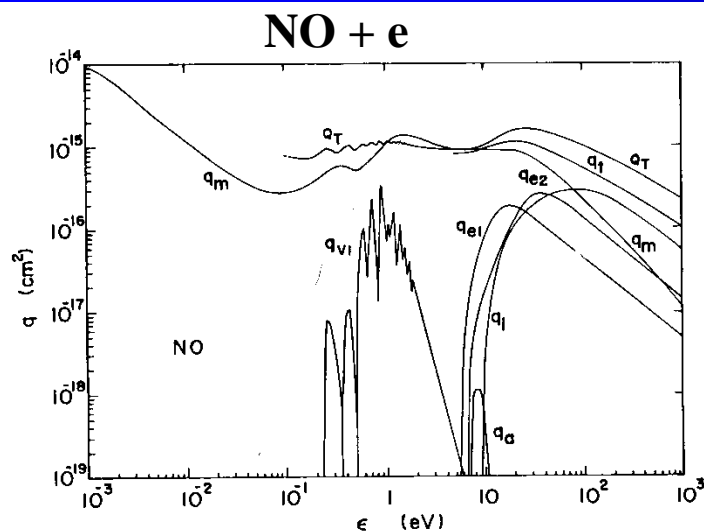


Fig. 4. Cross-section set for NO (1986).

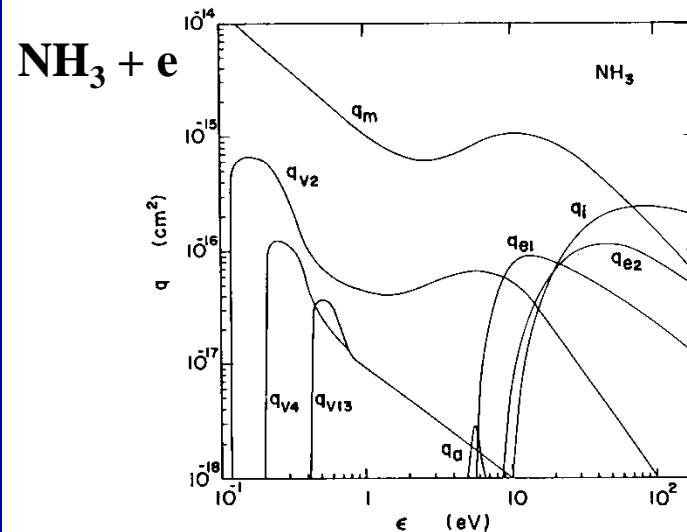


Fig. 6. Electron collision cross-section set for NH<sub>3</sub> (1986).

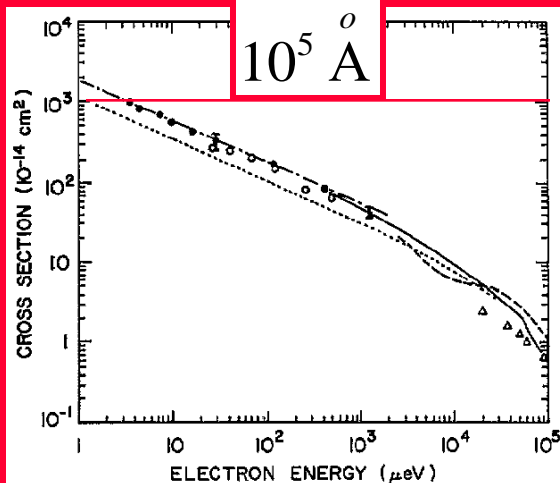
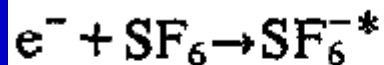
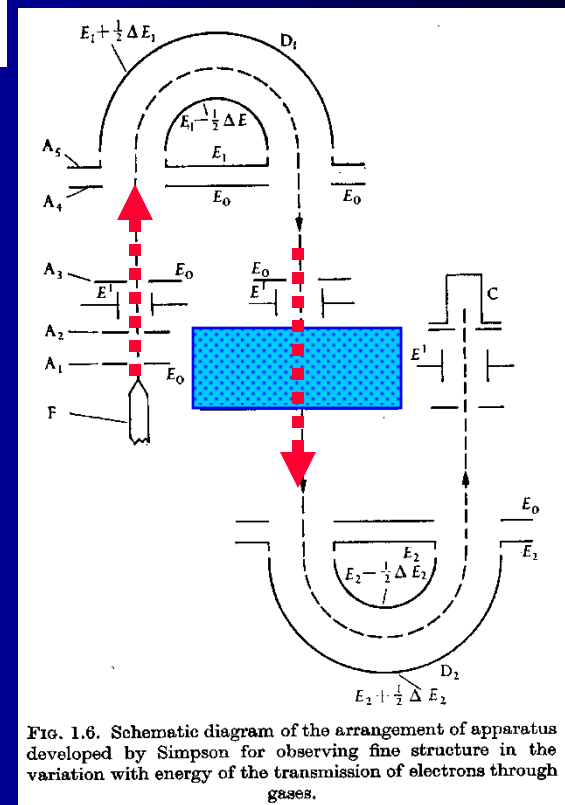
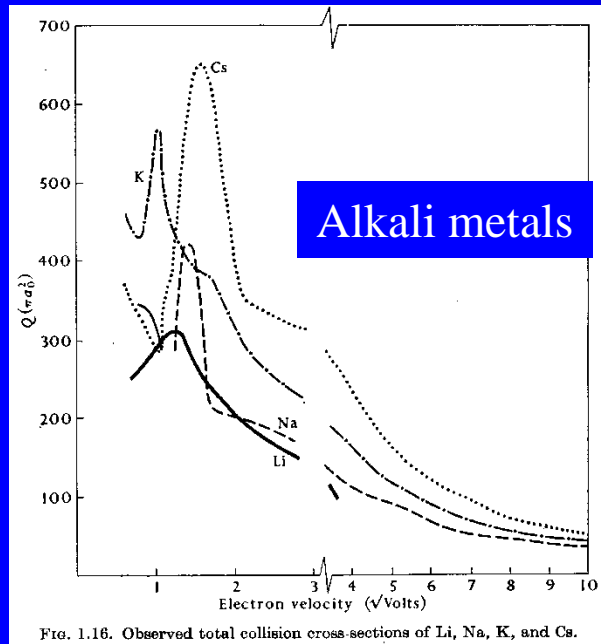


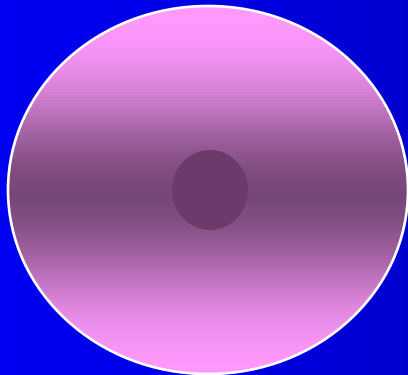
Figure 3. Cross sections for electron attachment to CCl<sub>4</sub>. ●,  $\bar{\sigma}_e$ -K( $\eta$ p); —·—,  $\sigma_e$ ( $\nu$ )-K( $\eta$ p) (Frey *et al* 1994b); ○,  $\bar{\sigma}_e$ -K( $\eta$ p) (Ling *et al* 1992); —, free electrons (Hotop 1994); ---, free electrons (Orient *et al* 1989); Δ, free electrons (Christodoulides and Christophorou (1971); —·—, theory (Klots 1976).



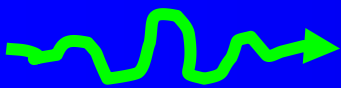
# Total collision cross sections Na, K, Cs...



Cs



$e^-_{(v)}$



# Total collision and reactive cross sections comparison

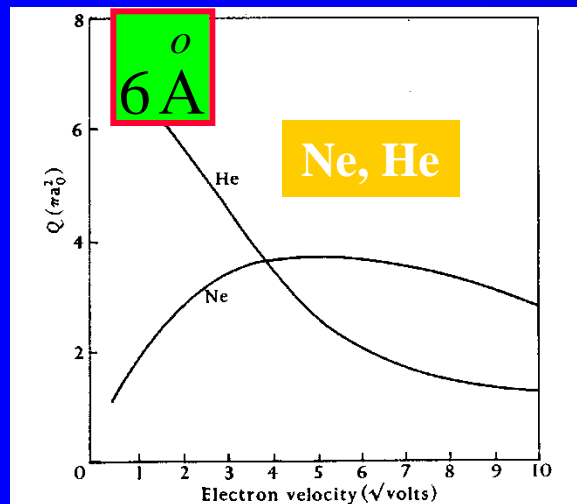


FIG. 1.10. Observed total collision cross-sections of He and Ne.

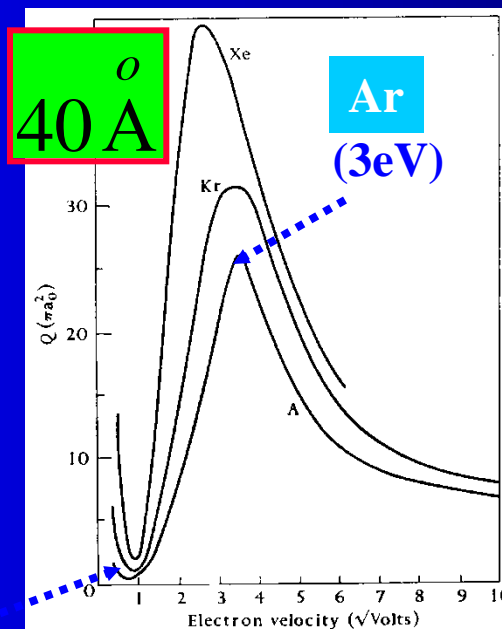


FIG. 1.9. Observed total collision cross-sections of Ar, Kr, and Xe.

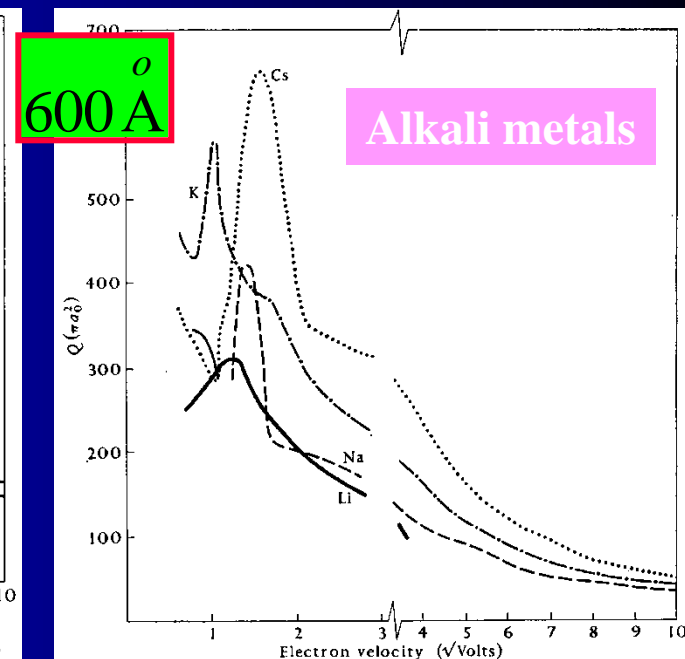


FIG. 1.16. Observed total collision cross-sections of Li, Na, K, and Cs.

(0,3eV)

$\sigma(v)$

$e^-(v)$

Ar  
(3eV)  
Ne  
Ar  
(0.3eV)

500A  
Cs  
(2eV)

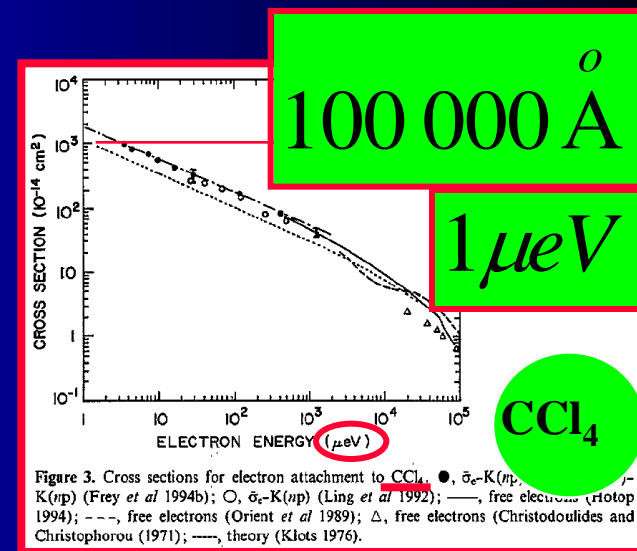


Figure 3. Cross sections for electron attachment to  $\text{CCl}_4$ .  $\bullet$ ,  $\sigma_{\text{e}}\text{-K}(np)$ ;  $\circ$ ,  $\sigma_{\text{e}}\text{-K}(np)$  (Frey *et al* 1994b);  $\Delta$ ,  $\sigma_{\text{e}}\text{-K}(np)$  (Ling *et al* 1992); —, free electrons (Hofop 1994); ---, free electrons (Orient *et al* 1989);  $\Delta$ , free electrons (Christodoulides and Christophorou (1971); —, theory (Klots 1976).



# Collisions of electrons with atoms – Ramsauer's method

Lenard 1903

Akesson 1916

Ramsauer 1921

## ATTENUATION METHOD

$$\delta I = -N\sigma I_p \delta x$$

$$I_p = I_0 \exp(-\sigma N x)$$

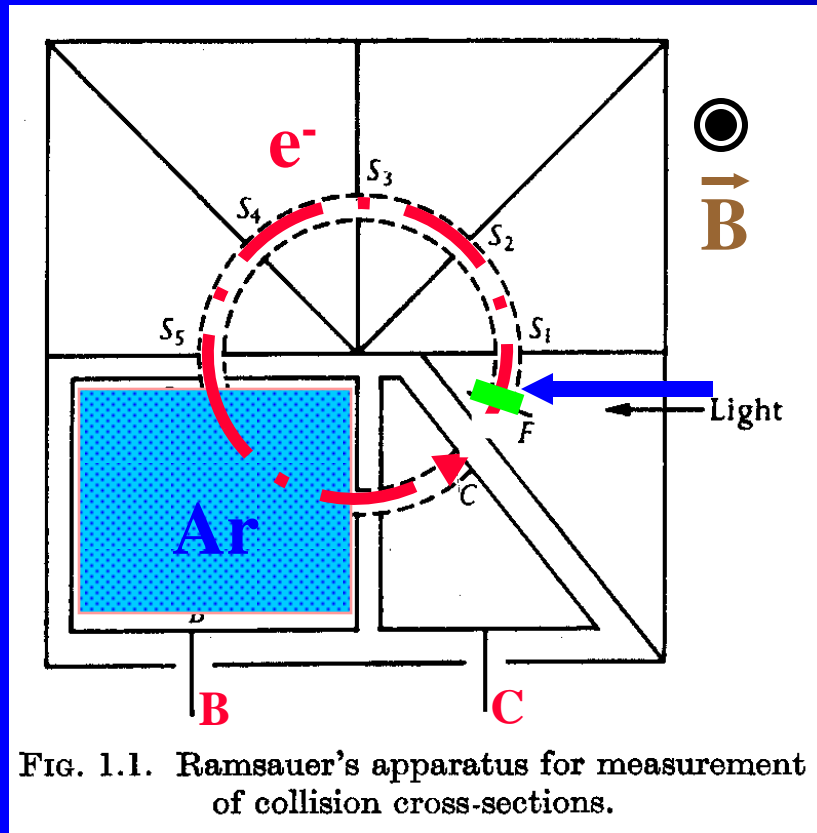
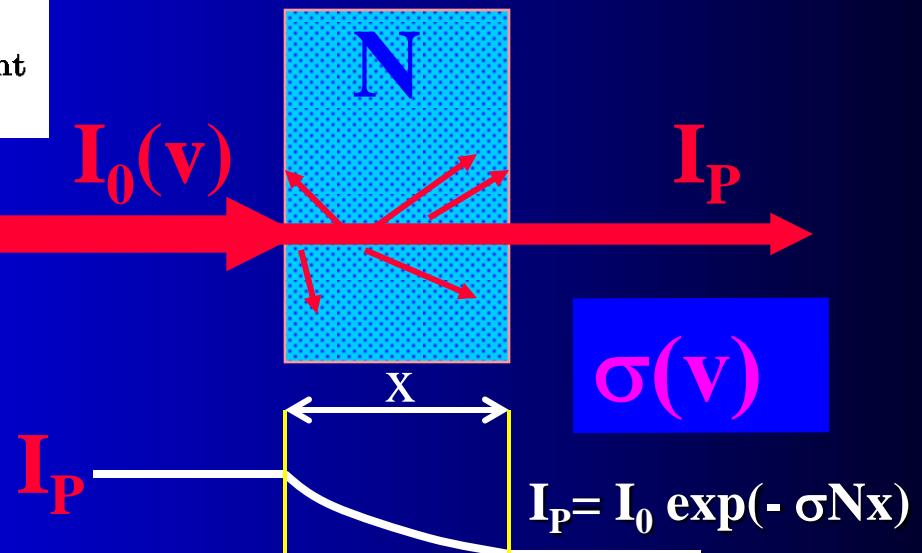
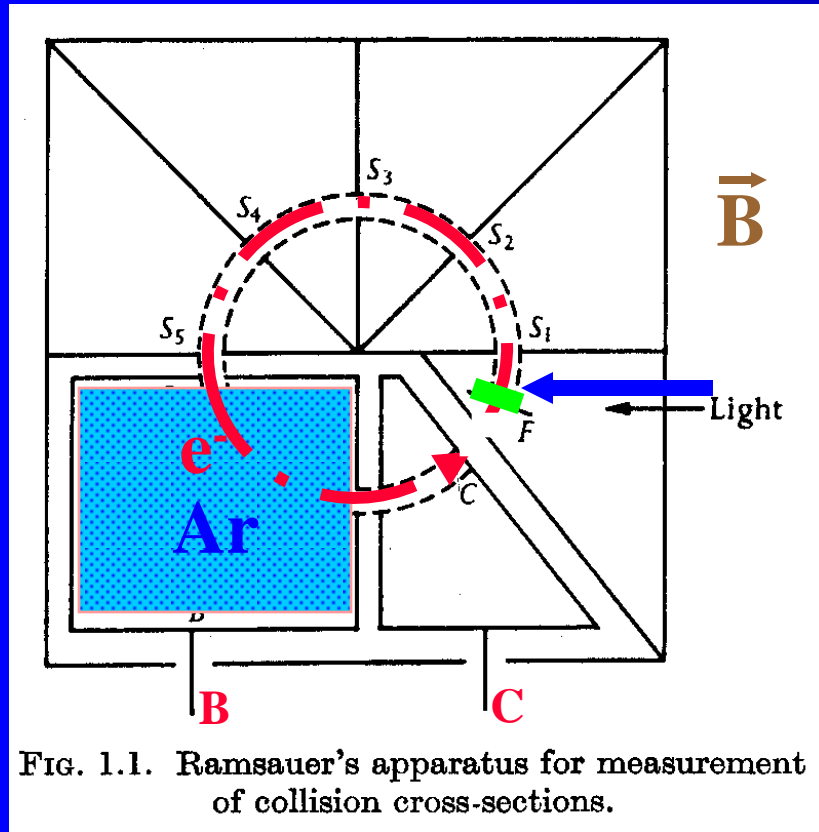


Photo cathode

Mono energetic electrons



# Collisions of electrons with atoms – Ramsauer's method



Lenard 1903  
Akesson 1916  
Ramsauer 1921

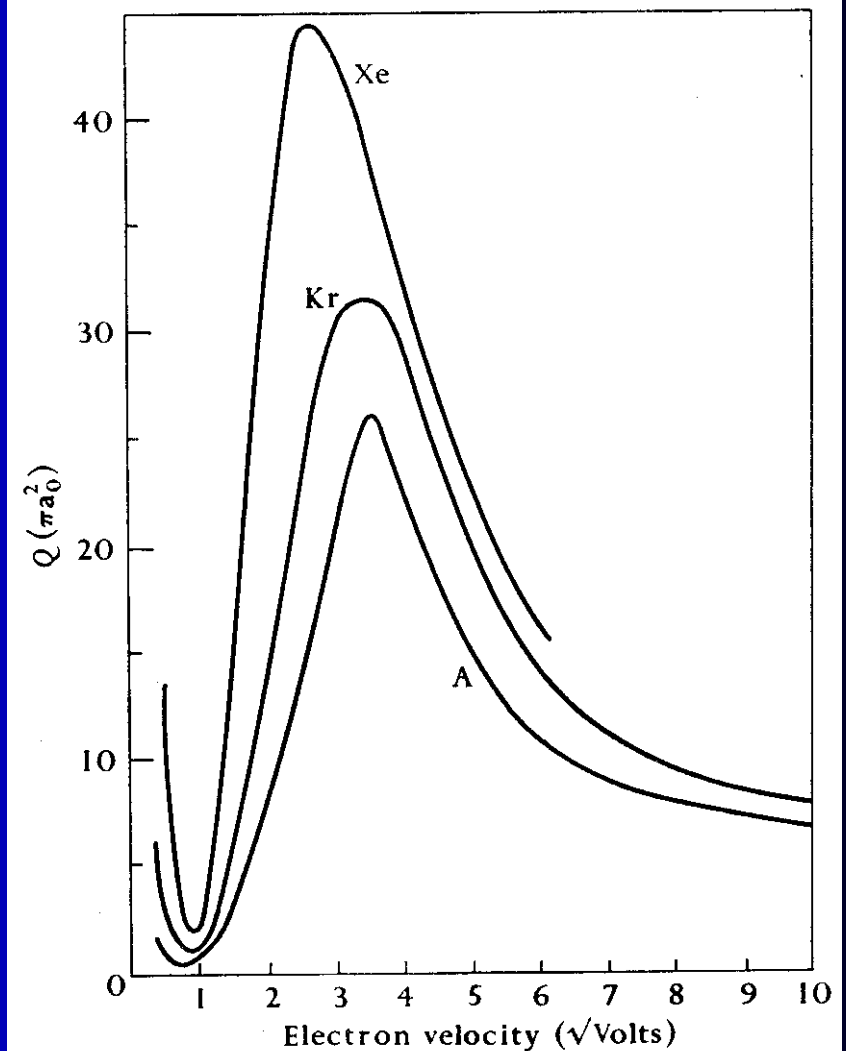


FIG. 1.9. Observed total collision cross-sections of A, Kr, and Xe.

# Total collision cross section – e/atoms

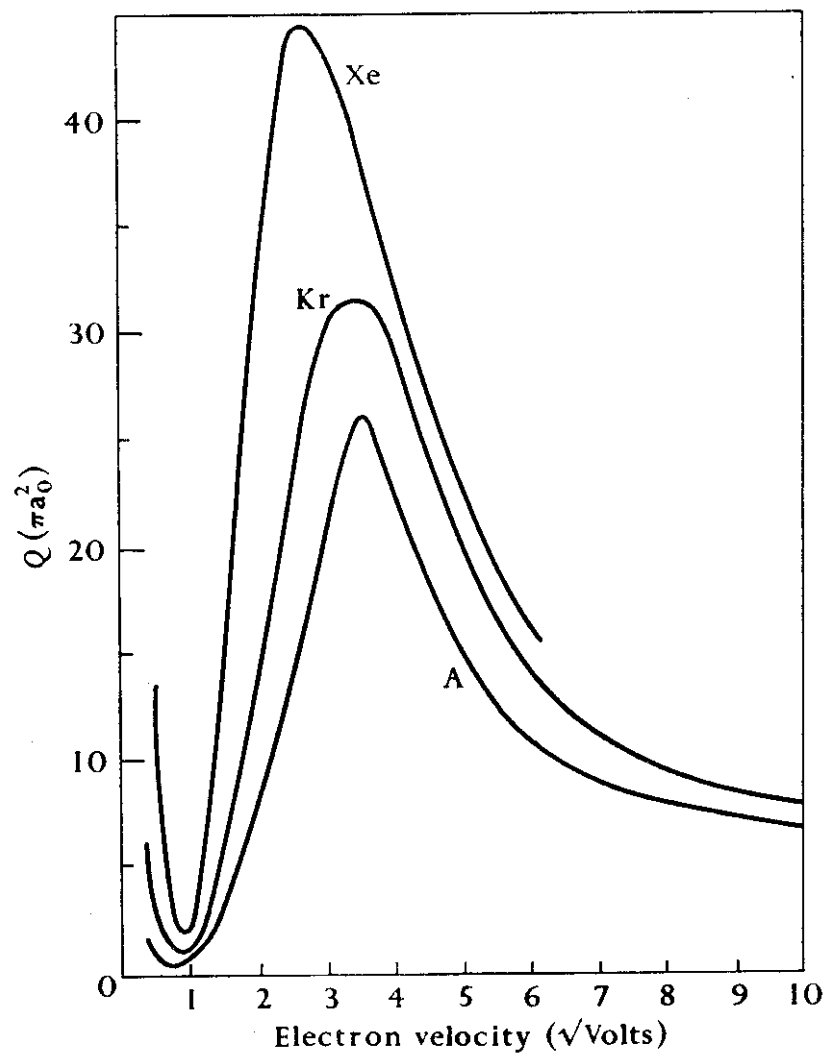


FIG. 1.9. Observed total collision cross-sections of A, Kr, and Xe.

$a_0 = 0.53 \times 10^{-8} \text{ cm} \sim 0.5 \text{ \AA}$

Radius of the first Bohr orbit of H atom

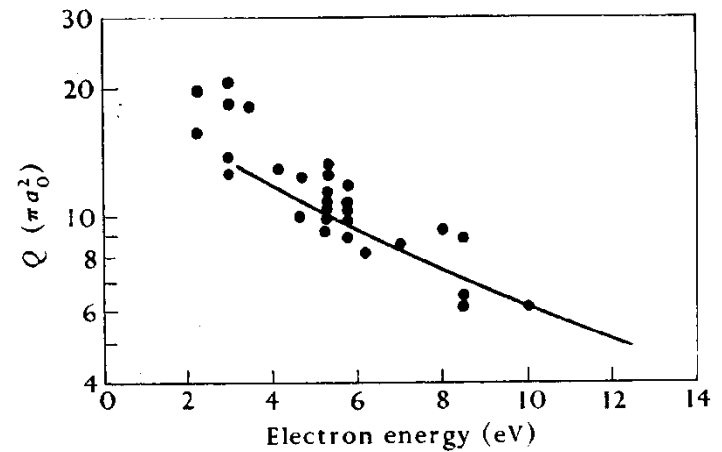


FIG. 1.11. Total collision cross-sections of atomic hydrogen. ● observed by Brackmann, Fite, and Neynaber; — observed by Neynaber, Marino, Rothe, and Trujillo.

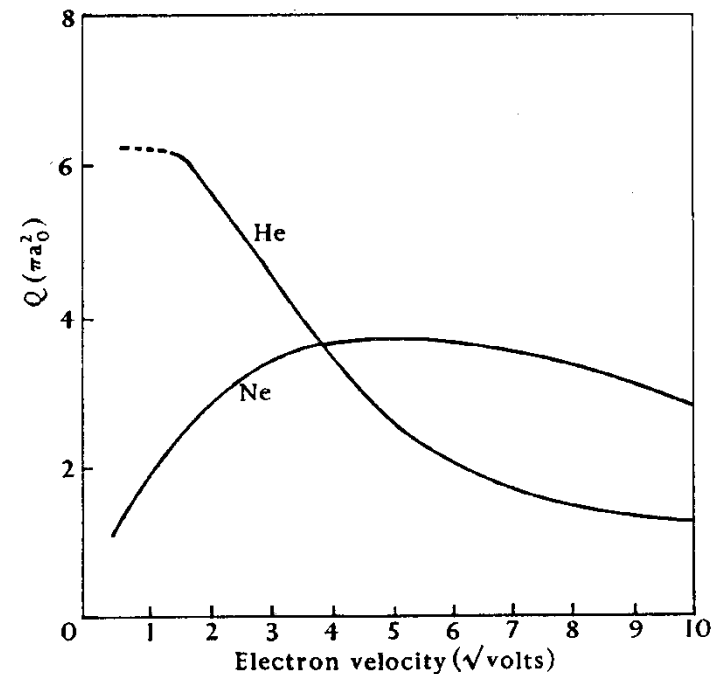


FIG. 1.10. Observed total collision cross-sections of He and Ne.

# Details of Ramsauer effect

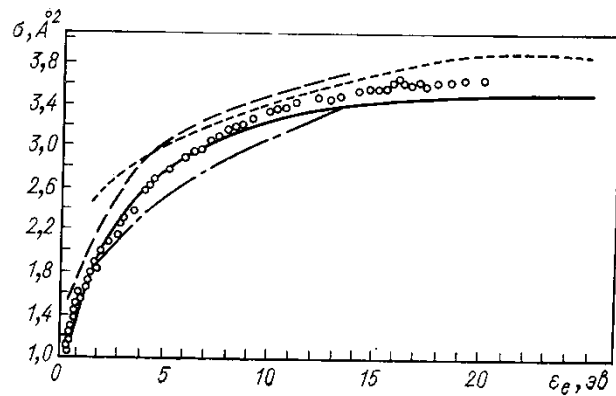


Рис. 5.8. Полное сечение рассеяния электрона на атоме неона.

Эксперимент (метод Рамзауэра):  $\circ$  — [101]; — [29]; ..... — [92]; — [95]. Теория: — [109].

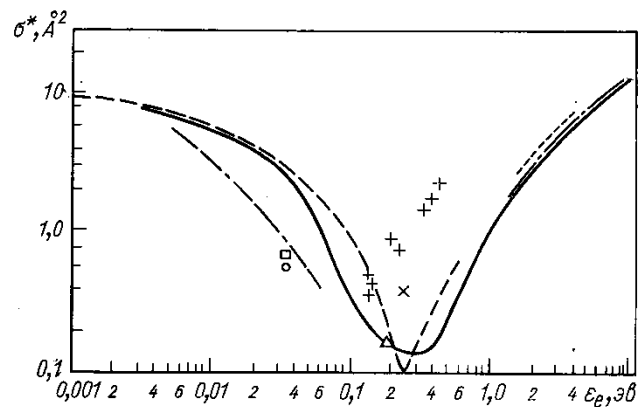


Рис. 5.9. Диффузионное сечение столкновения электрона с атомом аргона.

Эксперимент (подвижность электронов при малых полях и температурах): ..... — [21]; — [47];  $\times$  — [60];  $\circ$  — [91];  $\square$  — [112];  $\triangle$  — [44]; — [16]; — [108]; + — [43]. Теория: — [87].

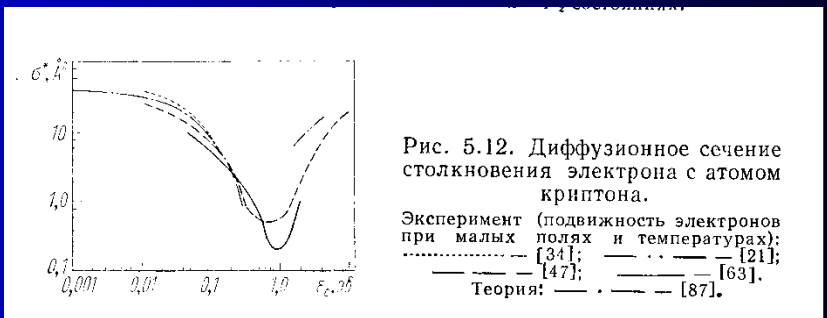


Рис. 5.12. Диффузионное сечение столкновения электрона с атомом криптона.

Эксперимент (подвижность электронов при малых полях и температурах): ..... — [34]; — [21]; — [47]; — [63]. Теория: — [87].

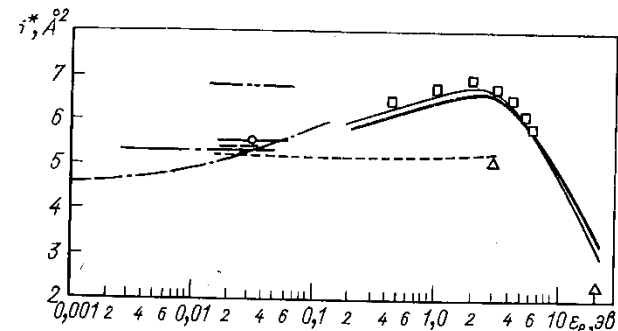


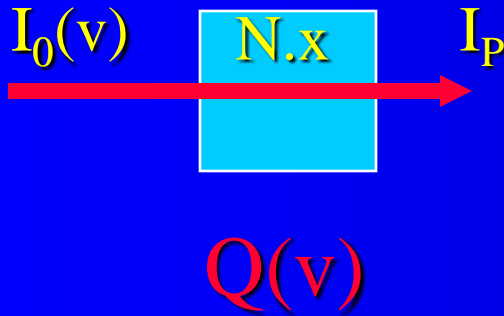
Рис. 5.3. Диффузионное сечение столкновения электрона с атомом гелия.

Эксперимент (подвижность электронов при малых полях и температурах):  $\square$  — [39];  $\triangle$  — [73]; — [88]; — [91]; ..... — [58]; — [13]; — [62]. Теория: — [75]; — [32]; — расчет по формуле (5.37).

# Frequencies of elastic collisions

$$\delta I = -NQI_p \delta x$$

$$I_p = I_0 \exp(-QNx)$$



$$a_0 = 0.53 \times 10^{-8} \text{ cm} \sim 0.5 \text{ \AA}$$

Radius of the first Bohr orbit of H atom

$$v \sim n v \sigma$$

Collision Frequencies

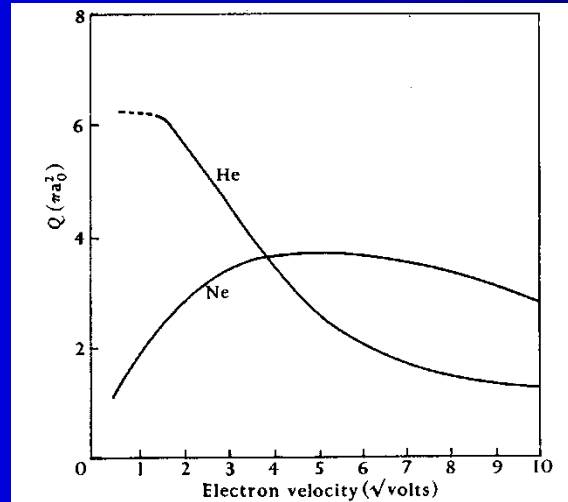


FIG. 1.10. Observed total collision cross-sections of He and Ne.

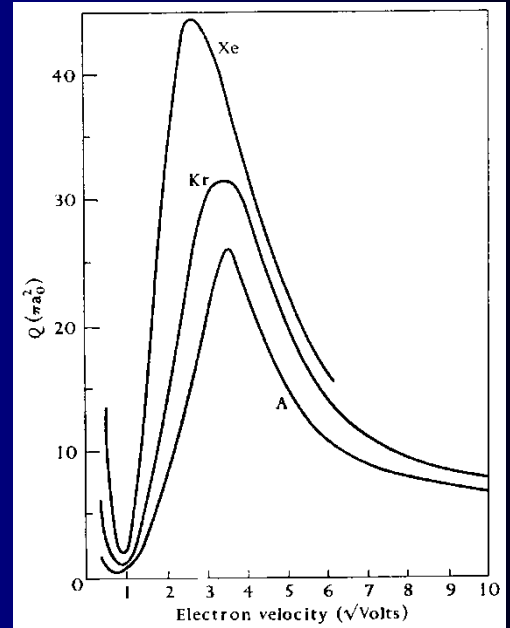
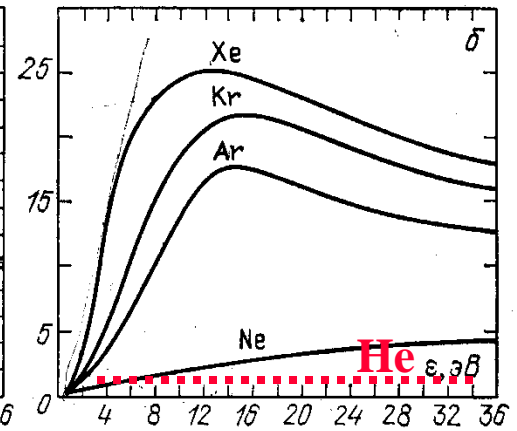
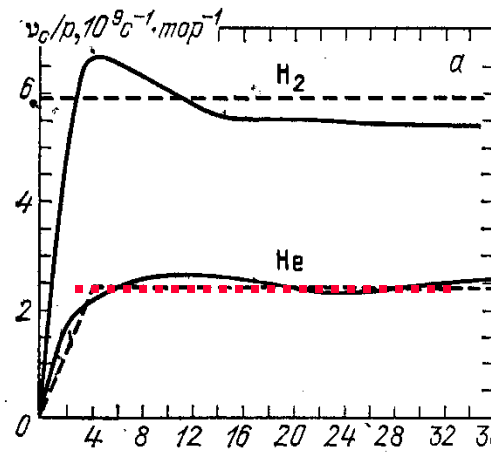


FIG. 1.9. Observed total collision cross-sections of Ar, Kr, and Xe.



Р и с. 2.5. Частоты упругих столкновений электронов,  $p=1$  топ: а — в  $H_2$  и He; б — в инертных газах; штриховые линии — удобная аппроксимация при расчетах [24]

# Total collision and reactive cross sections comparison

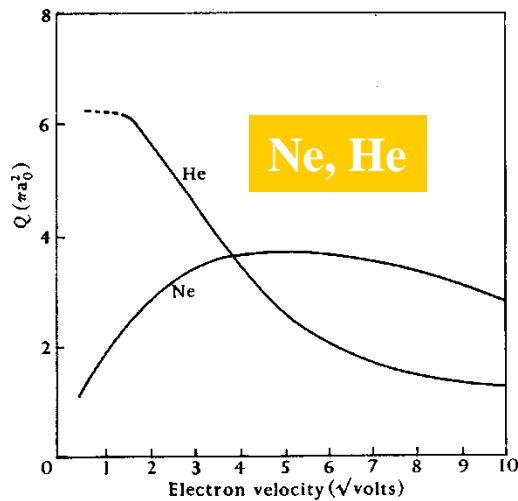


FIG. 1.10. Observed total collision cross-sections of He and Ne.

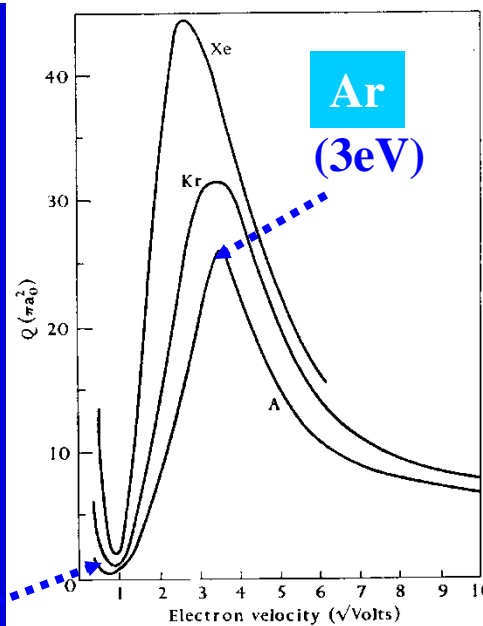


FIG. 1.9. Observed total collision cross-sections of Ar, Kr, and Xe.

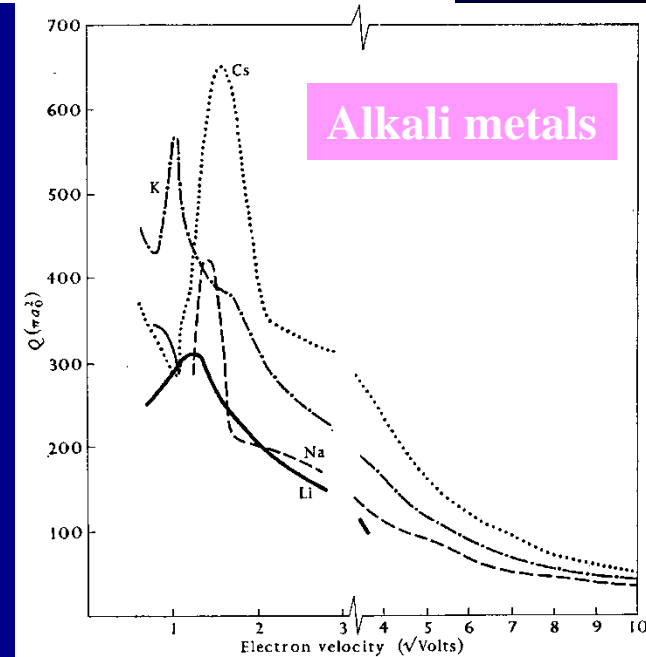


FIG. 1.16. Observed total collision cross-sections of Li, Na, K, and Cs.

$\sigma(v)$

(0,3eV)

Ar  
(3eV)

Ne

Ar  
(0.3eV)

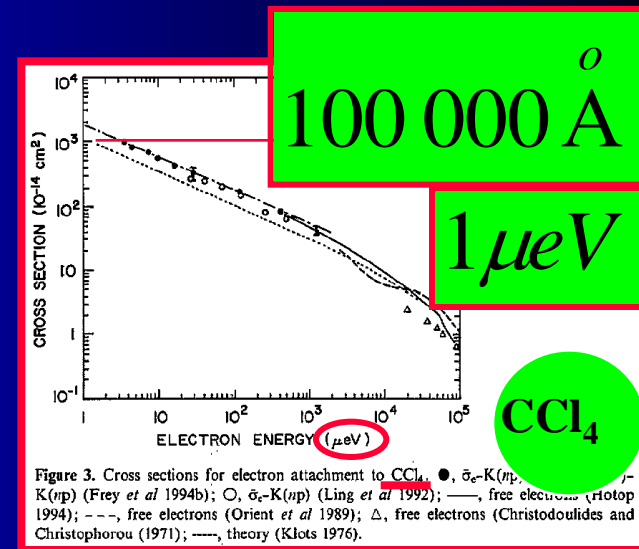
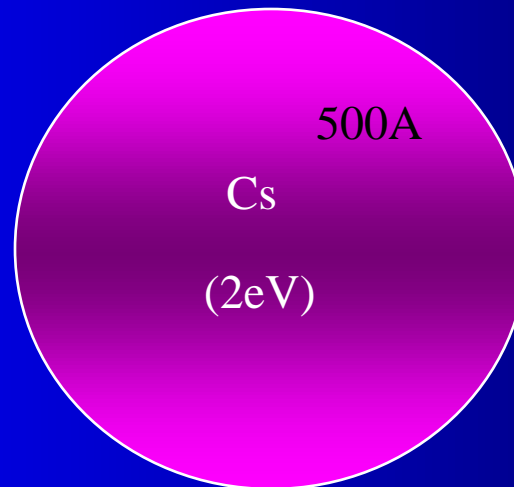
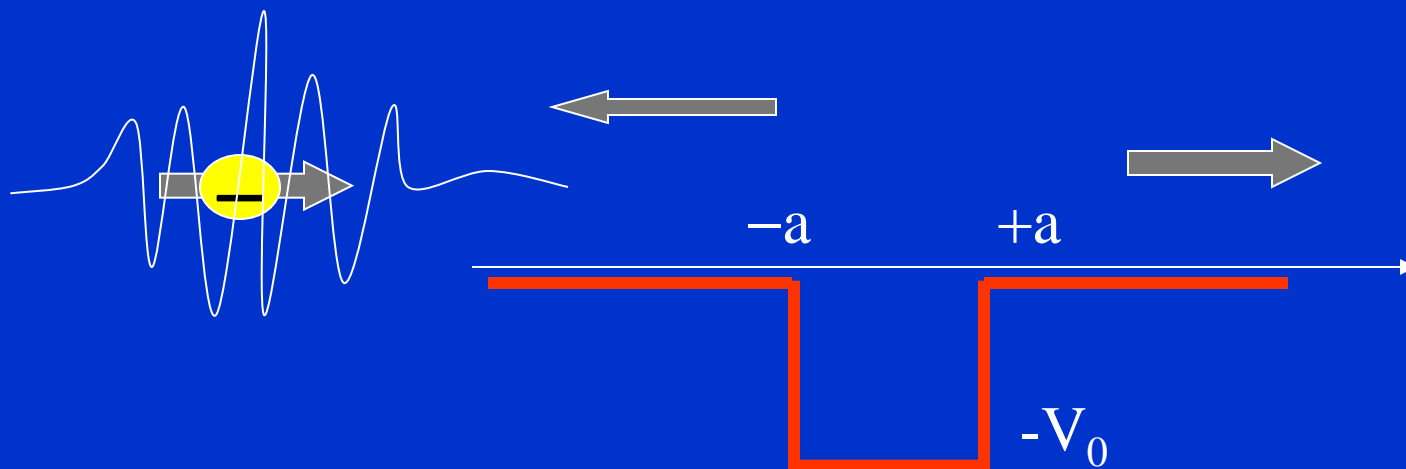


Figure 3. Cross sections for electron attachment to  $\text{CCl}_4$ .  $\bullet$ ,  $\delta_e\text{-K}(np)$ ;  $\circ$ ,  $\delta_e\text{-K}(np)$  (Frey *et al* 1994b);  $\circ$ ,  $\delta_e\text{-K}(np)$  (Ling *et al* 1992); —, free electrons (Hofop 1994); ---, free electrons (Orient *et al* 1989);  $\Delta$ , free electrons (Christodoulides and Christophorou (1971); —, theory (Klots 1976).

# Kvantová mechanika

## Jednorozměrný rozptyl



Kvantová mechanika I  
J. Klíma B. Velický  
MFF 1992

# Jednorozměrný rozptyl

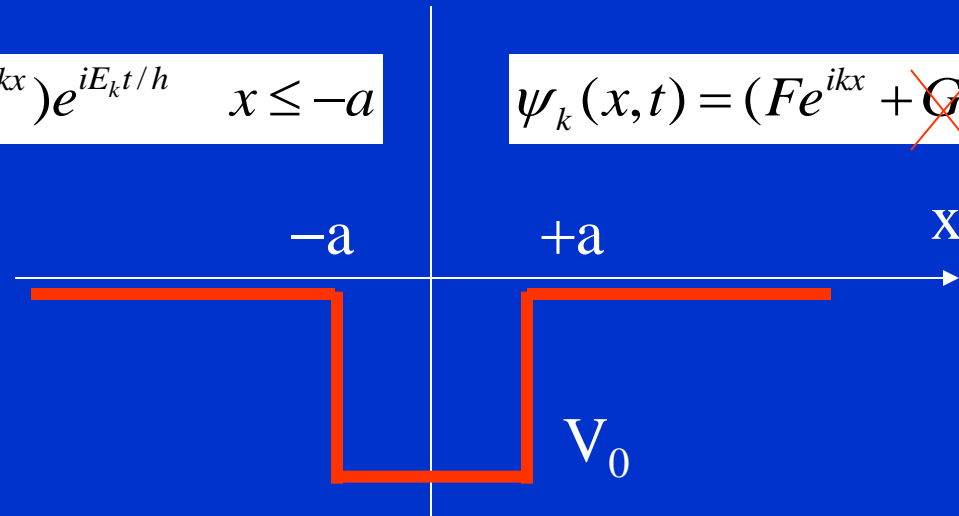
Vlnová funkce má tvar superposice Brogliových vln

$$k = \sqrt{2mE / \hbar^2}$$

$$\psi_k(x, t) = (Ae^{ikx} + Be^{-ikx})e^{iE_k t / \hbar} \quad x \leq -a$$

$$k = \sqrt{2mE / \hbar^2}$$

$$\psi_k(x, t) = (Fe^{ikx} + \cancel{G}e^{-ikx})e^{iE_k t / \hbar} \quad x > a$$



$$\psi_k(x, t) = (Ce^{ik'x} + De^{-ik'x})e^{iE_k t / \hbar} \quad |x| \leq a$$

$$k' = \sqrt{2m(E + V_0) / \hbar^2}$$

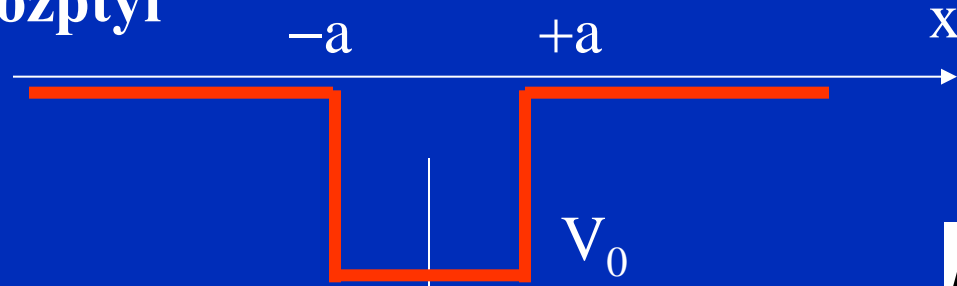
a) dopadající částice  $\rightarrow A$

b) odražená částice  $\rightarrow B$

c) procházející částice  $\rightarrow F \neq 0, G = 0$



# Jednorozměrný rozptyl



$$k = \sqrt{2mE / \hbar^2}$$

$$k' = \sqrt{2m(E + V_0) / \hbar^2}$$

$$\psi_k(x, t) = (Ae^{ikx} + Be^{-ikx})e^{iE_k t / \hbar} \quad x \leq -a$$

$$\psi_k(x, t) = (Ce^{ik'x} + De^{-ik'x})e^{iE_k t / \hbar} \quad |x| \leq a$$

$$\psi_k(x, t) = (Fe^{ikx})e^{iE_k t / \hbar} \quad x > a$$

Parametry jsou **E**, **V<sub>0</sub>**, **a**

Hladkost řešení v bodech  $\pm a$   
Urči konstanty B, C, D, G,  
Hodnota A je vstupní parametr

Tok dopadajících částic

$$j_{in} = \frac{\hbar k}{m} |A|^2$$

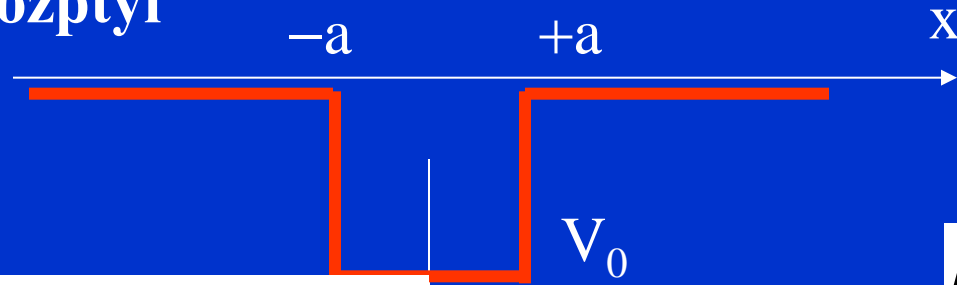
Tok odražených částic

$$j_{rf} = \frac{\hbar k}{m} |B|^2$$

Tok prošlých částic

$$j_{tr} = \frac{\hbar k}{m} |F|^2$$

# Jednorozměrný rozptyl



$$k = \sqrt{2mE / \hbar^2}$$

$$k' = \sqrt{2m(E + V_0) / \hbar^2}$$

$$\psi_k(x, t) = (Ae^{ikx} + Be^{-ikx})e^{iE_k t / \hbar} \quad x \leq -a$$

$$\psi_k(x, t) = (Ce^{ik'x} + De^{-ik'x})e^{iE_k t / \hbar} \quad |x| \leq a$$

$$\psi_k(x, t) = (Fe^{ikx})e^{iE_k t / \hbar} \quad x > a$$

Parametry jsou **E**, **V<sub>0</sub>**, **a**

**Hladkost řešení v bodech ±a**  
**Urči konstanty B, C, D, G,**  
**Hodnota A je vstupní parametr**

**Tok dopadajících částic**

$$j_{in} = \frac{\hbar k}{m} |A|^2$$

$$C = \frac{F}{2} \left(1 + \frac{k}{k'}\right) e^{i(k-k')a}$$

**Tok odražených částic**

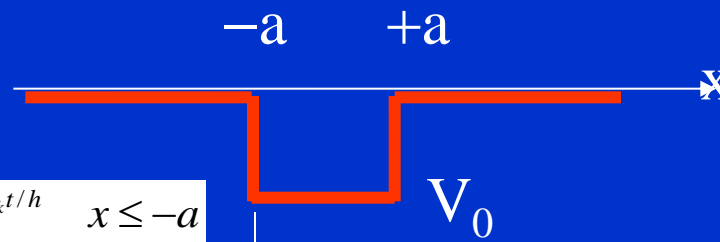
$$j_{rf} = \frac{\hbar k}{m} |B|^2$$

$$D = \frac{F}{2} \left(1 - \frac{k}{k'}\right) e^{i(k+k')a}$$

**Tok prošlých částic**

$$j_{tr} = \frac{\hbar k}{m} |F|^2$$

# Jednorozměrný rozptyl



$$k = \sqrt{2mE} / \hbar$$

$$k' = \sqrt{2m(E + V_0)} / \hbar$$

$$\psi_k(x,t) = (Ae^{ikx} + Be^{-ikx})e^{iE_k t / \hbar} \quad x \leq -a$$

$$\psi_k(x,t) = (Ce^{ik'x} + De^{-ik'x})e^{iE_k t / \hbar} \quad |x| \leq a$$

$$\psi_k(x,t) = (Fe^{ikx})e^{iE_k t / \hbar} \quad x > a$$

Parametry jsou **E**, **V<sub>0</sub>**, **a**

$$j_{in} = \frac{\hbar k}{m} |A|^2$$

$$j_{rf} = \frac{\hbar k}{m} |B|^2$$

$$j_{tr} = \frac{\hbar k}{m} |F|^2$$

**Hladkost řešení v bodech  $\pm a$**   
**Urči konstanty B, C, D, F,**  
**Hodnota A je vstupní parametr**

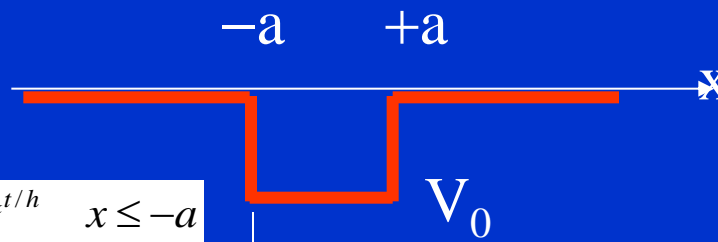
$$\varepsilon = \frac{k'}{k} + \frac{k}{k'}$$

$$A = e^{2ika} (\cos(2k'a) - i(\varepsilon/2) \sin(2k'a)) F$$

**Koeficient průchodu T, koeficient odrazu R**

$$\frac{1}{T} = \left| \frac{A}{F} \right|^2 = 1 + \frac{V_0^2}{4E(E + V)} \sin^2(2k'a)$$

# Jednorozměrný rozptyl



$$k = \sqrt{2mE} / \hbar$$

$$k' = \sqrt{2m(E + V_0)} / \hbar$$

$$\psi_k(x,t) = (Ae^{ikx} + Be^{-ikx})e^{iE_k t/\hbar} \quad x \leq -a$$

$$\psi_k(x,t) = (Ce^{ik'x} + De^{-ik'x})e^{iE_k t/\hbar} \quad |x| \leq a$$

$$\psi_k(x,t) = (Fe^{ikx})e^{iE_k t/\hbar} \quad x > a$$

Parametry jsou **E**, **V<sub>0</sub>**, **a**

$$j_{in} = \frac{\hbar k}{m} |A|^2$$

$$j_{rf} = \frac{\hbar k}{m} |B|^2$$

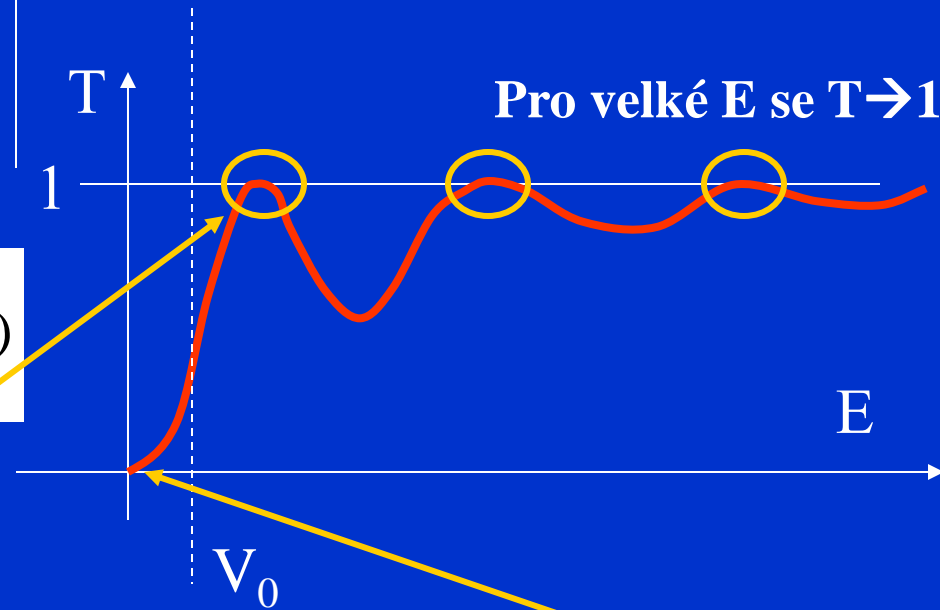
$$j_{tr} = \frac{\hbar k}{m} |F|^2$$

Koeficient průchodu T, koeficient odrazu R

$$\frac{1}{T} = \left| \frac{A}{F} \right|^2 = 1 + \frac{V_0^2}{4E(E + V_0)} \sin^2(2k'a)$$

T=1 pro

$$2k_n' a = n\pi$$



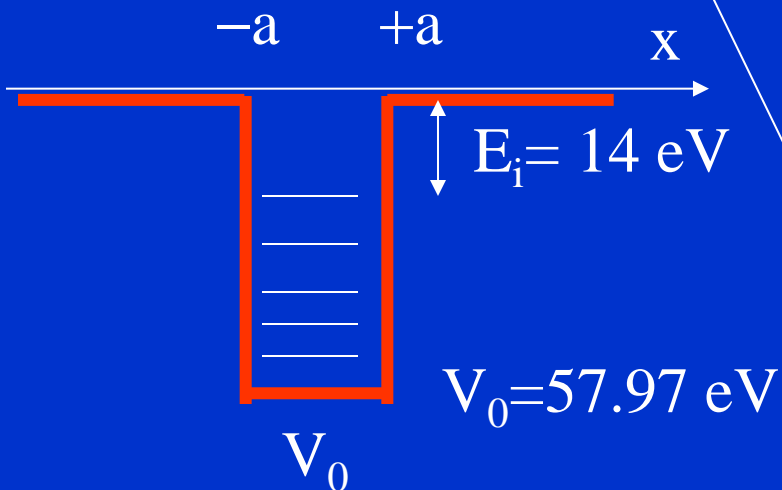
$$\lim_{E \rightarrow 0} \frac{1}{T} \sim 1 + \frac{V_0^2}{4EV_0} \sin^2(2k'a) \sim 1 + \frac{V_0}{4E} \sin^2(2\sqrt{2mV_0}/\hbar^2 a) \sim 1 + \frac{V_0}{4E} \text{const} \sim \infty \quad \lim_{E \rightarrow 0} T \sim 0$$

# Efekt Ramsauera - Kr

Parametry jsou  $E, V_0, a$

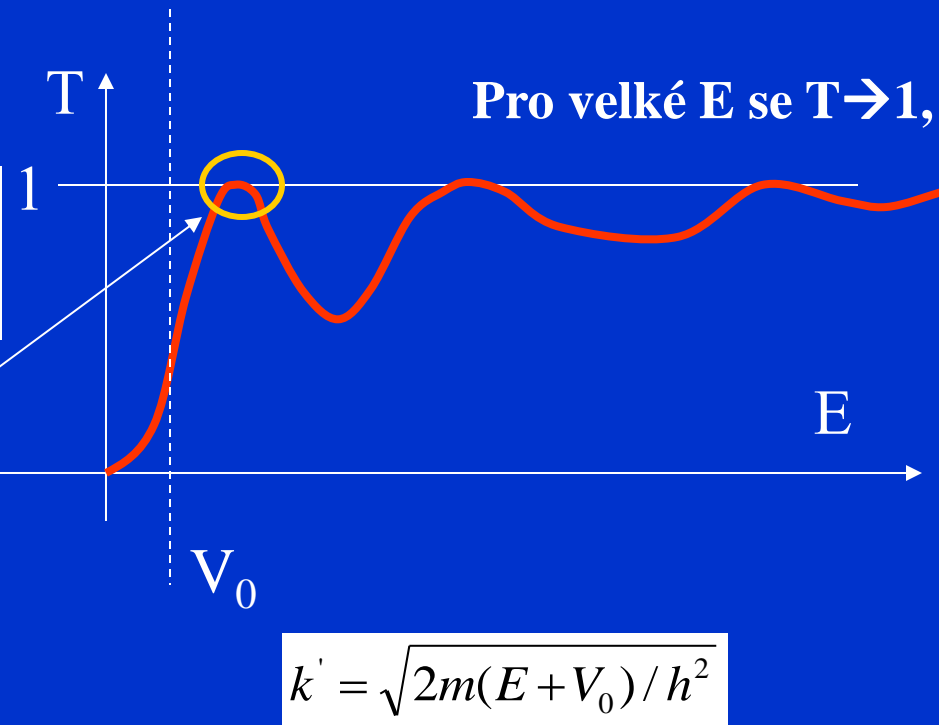
$$\frac{1}{T} = \left| \frac{A}{F} \right|^2 = 1 + \frac{V_0^2}{4E(E + V_0)} \sin^2(2k'a)$$

$T=1$  pro  $2k_n'a = n\pi$



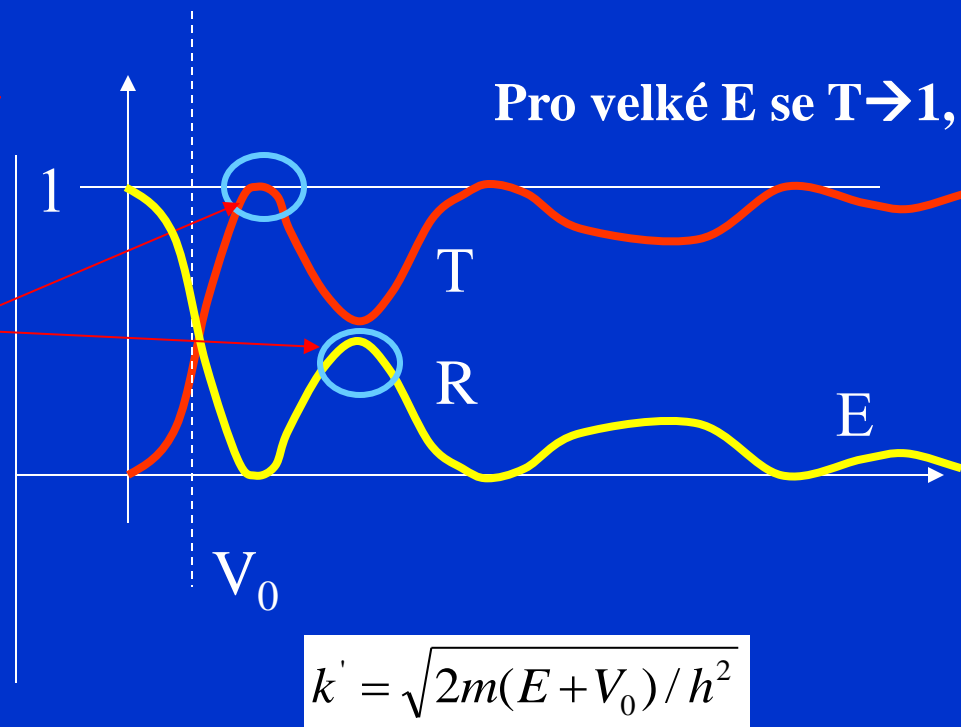
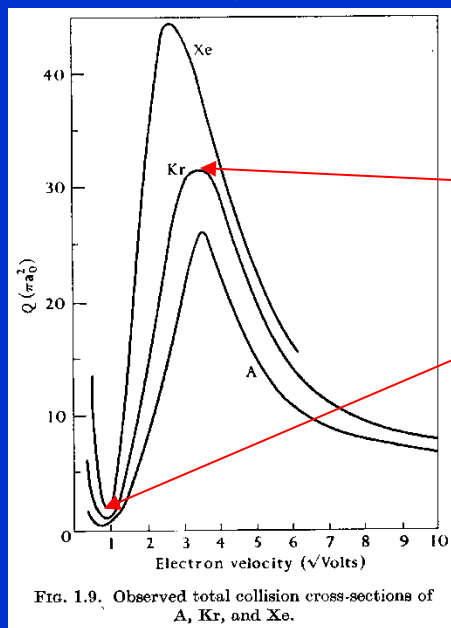
Kr;  $a = 2 \text{ \AA}$   
 $E_i = 14 \text{ eV} \rightarrow V_0 = 57.97 \text{ eV}$

$E = 0.013 \text{ eV}$   $V_0 = 0.75 \text{ eV}$



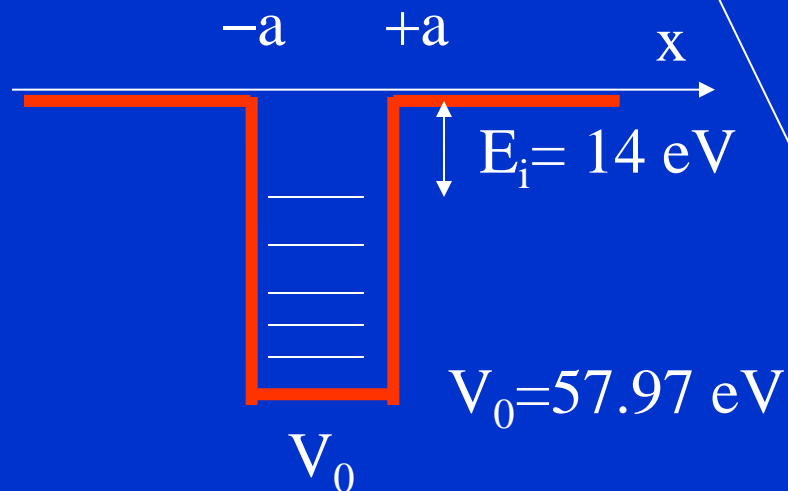
# Jednorozměrný rozptyl

Parametry jsou  $E, V_0, a$   $T+R=1$



$$2k_n' a = n\pi$$

$$k' = \sqrt{2m(E + V_0) / \hbar^2}$$



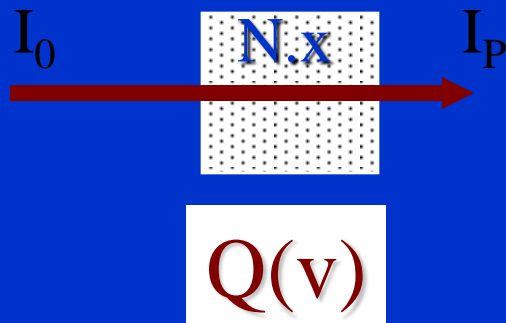
Kr;  $a = 2 \text{ \AA}$   
 $E_i = 14 \text{ eV} \rightarrow V_0 = 57.97 \text{ eV}$

$$E = 0.013 \quad V_0 = 0.75 \text{ eV}$$

# Frequencies of elastic collisions

$$\delta I = -NQI_p \delta x$$

$$I_p = I_0 \exp(-QNx)$$



**Collision  
Frequencies**

$$\nu \sim n v \sigma$$

$a_0 = 0.53 \times 10^{-8} \text{ cm} \sim 0.5 \text{ \AA}$   
Radius of the first Bohr orbit of H atom

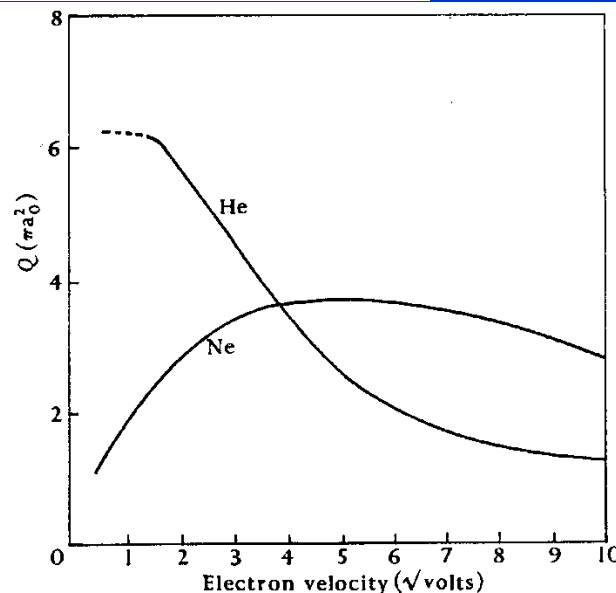


Fig. 1.10. Observed total collision cross-sections of He and Ne.

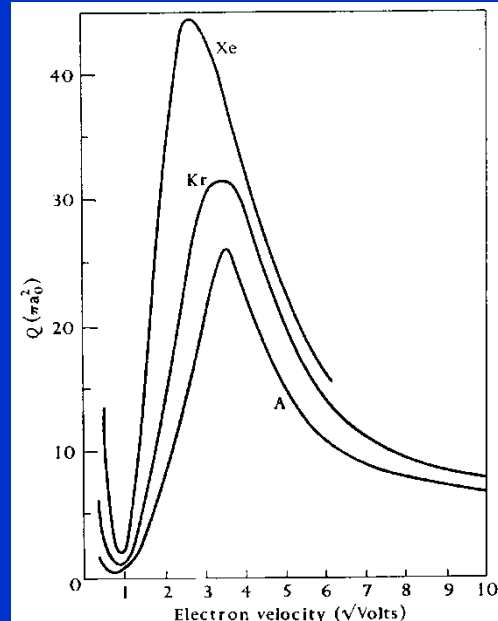


Fig. 1.9. Observed total collision cross-sections of A, Kr, and Xe.

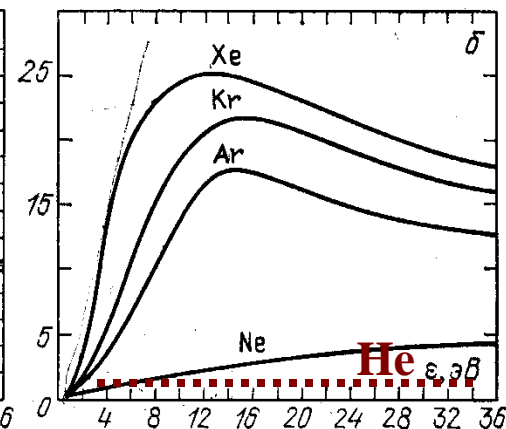
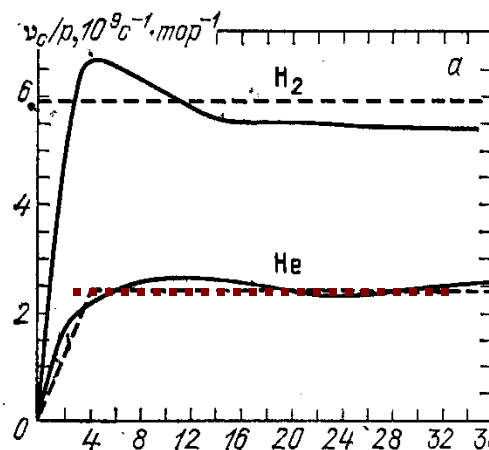


Рис. 2.5. Частоты упругих столкновений электронов,  $p=1$  топ: а — в  $H_2$  и He; б — в инертных газах; штриховые линии — удобная аппроксимация при расчетах [24]

# Very low collision energies

1995

TOPICAL REVIEW

## Electron-molecule collisions at very low electron energies

F B Dunning

Department of Physics and the Rice Quantum Institute, Rice University, PO Box 1892, Houston, TX 77251, USA

J. Phys. B: At. Mol. Opt. Phys. 28 (1995) 1645-1672. Printed in the UK

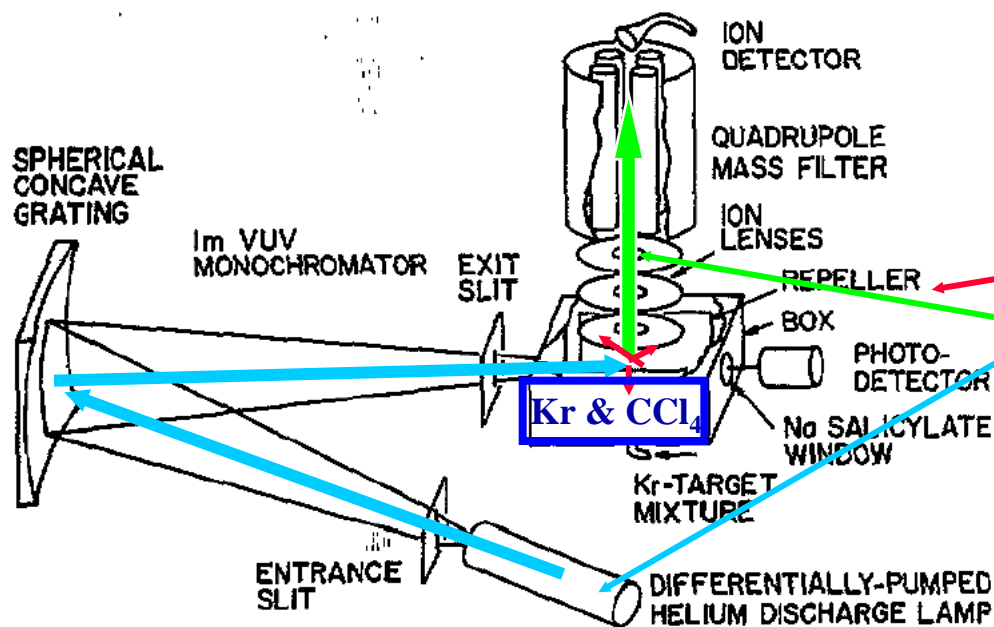
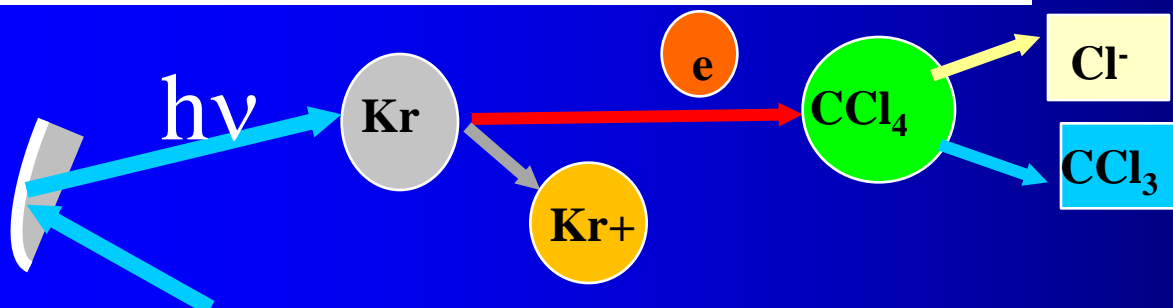
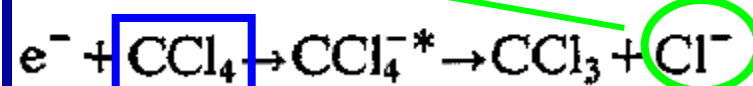
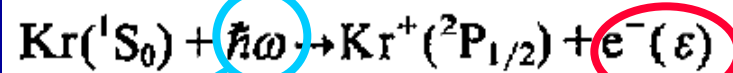


Figure 1. Schematic diagram of the VUV photoionization apparatus used for attachment studies (Chutjian and Alajajian 1985a, b).





## Electron-molecule collisions at very low electron energies

F B Dunning

Department of Physics and the Rice Quantum Institute, Rice University, PO Box 1892,  
Houston, TX 77251, USA

J. Phys. B: At. Mol. Opt. Phys. 28 (1995) 1645-1672. Printed in the UK

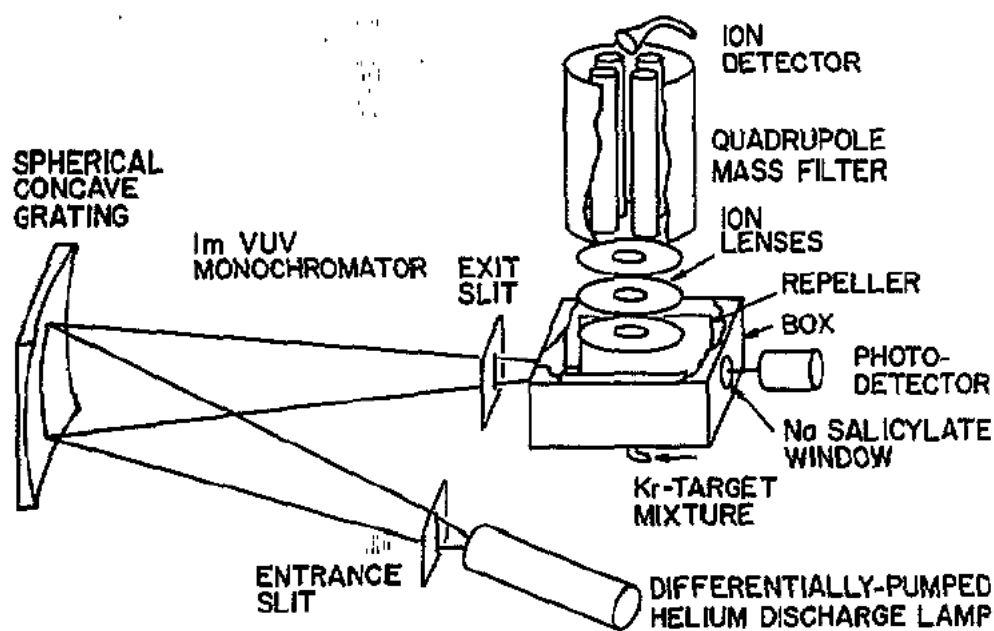
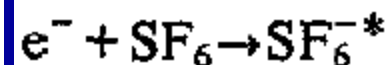


Figure 1. Schematic diagram of the VUV photoionization apparatus used for attachment studies (Chutjian and Alajajian 1985a, b).



# Very low collision energies

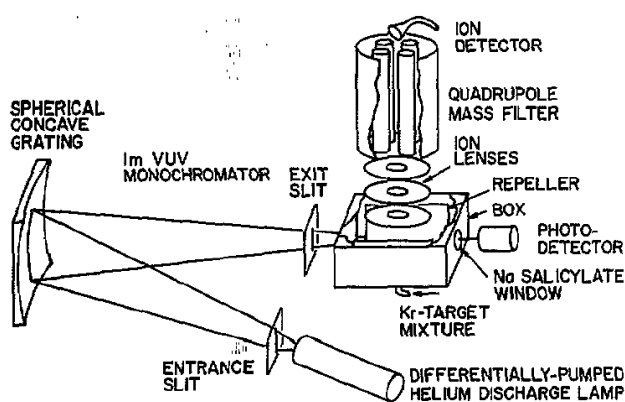
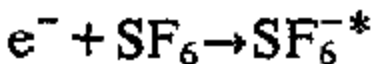
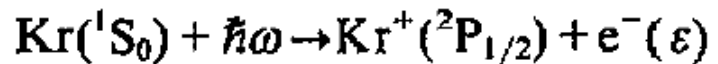


Figure 1. Schematic diagram of the VUV photoionization apparatus used for attachment studies (Chutjian and Alajajian 1985a, b).

## TOPICAL REVIEW

J. Phys. B: At. Mol. Opt. Phys. 28 (1995) 1645–1672. Printed in the UK

## Electron-molecule collisions at very low electron energies

F B Dunning

Department of Physics and the Rice Quantum Institute, Rice University, PO Box 1892, Houston, TX 77251, USA

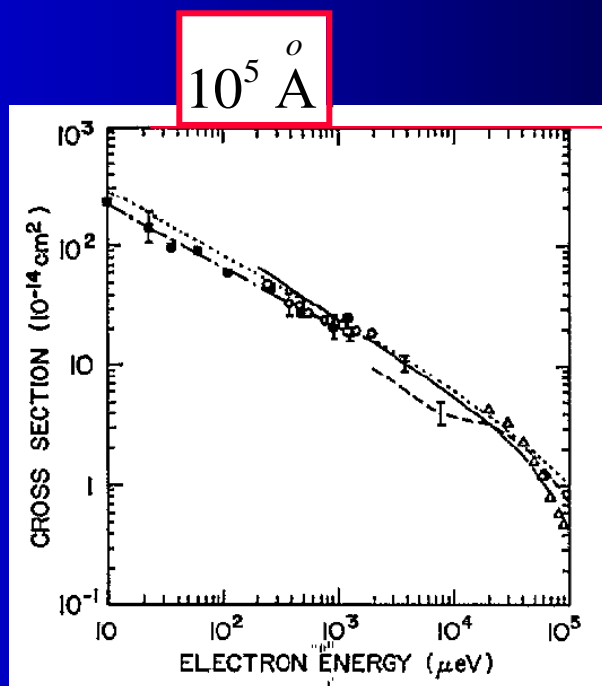


Figure 2. Cross section for electron attachment to  $\text{SF}_6$ . ■,  $\sigma_e\text{-K}(np)$ ; — · —,  $\sigma_e(v)\text{-K}(np)$  (Ling *et al* 1992). ○,  $\sigma_e\text{-Rb}(ns)$  (Zollars *et al* 1985); —, free electrons (Klar *et al* 1992a, b); ---, free electrons (Chutjian and Alajajian 1985); △, free electrons (Pai *et al* 1979, Chutjian and Alajajian 1985a); ----, theory (Klots 1976).

# Electron attachment at very low electron energies

$10^5 \text{ } ^\circ \text{A}$

$10^5 \text{ } ^\circ \text{A}$

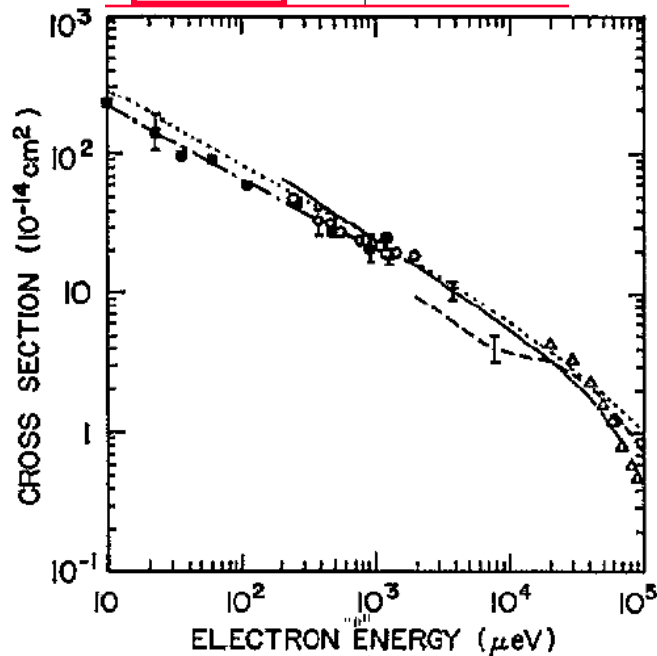


Figure 2. Cross section for electron attachment to  $\text{SF}_6$ . ■,  $\sigma_e\text{-K}(np)$ ; — · —,  $\sigma_e(v)\text{-K}(np)$  (Ling *et al* 1992). ○,  $\sigma_e\text{-Rb}(ns)$  (Zollars *et al* 1985); —, free electrons (Klar *et al* 1992a, b); ---, free electrons (Chutjian and Alajajian 1985); △, free electrons (Pai *et al* 1979, Chutjian and Alajajian 1985a); ----, theory (Klots 1976).

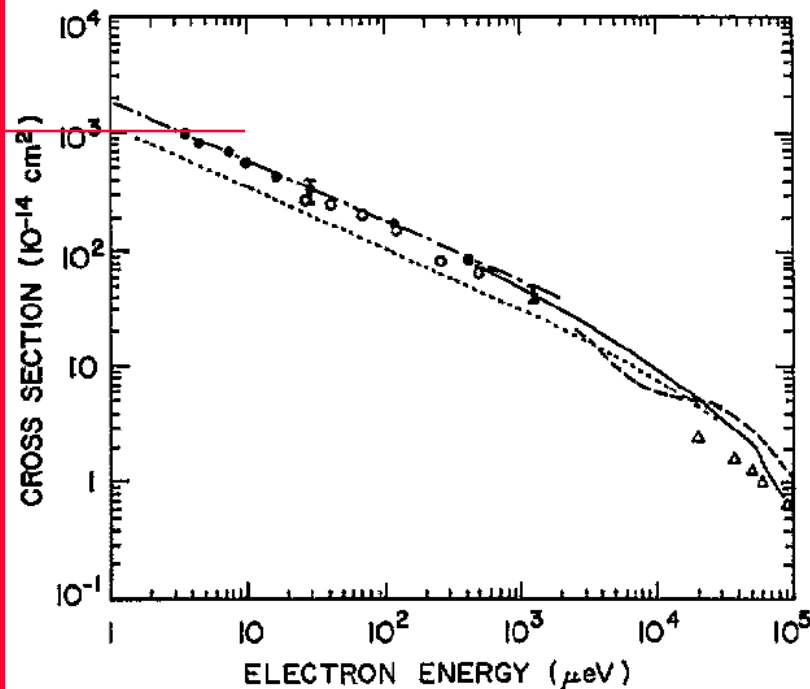


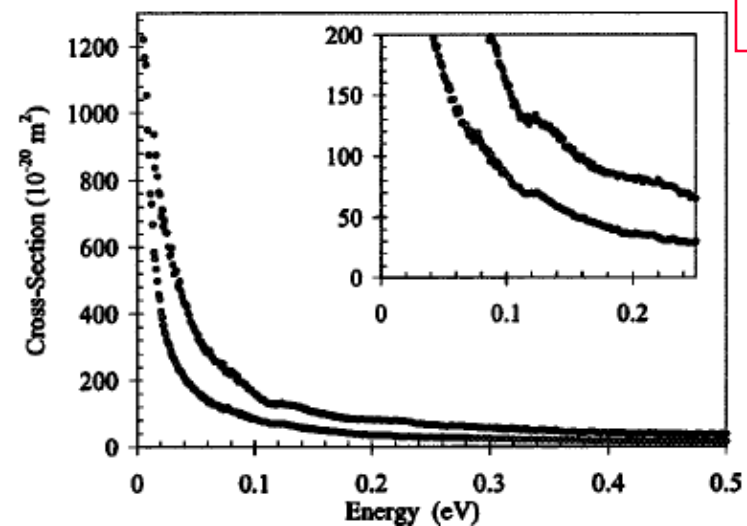
Figure 3. Cross sections for electron attachment to  $\text{CCl}_4$ . ●,  $\sigma_e\text{-K}(np)$ ; — · —,  $\sigma_e(v)\text{-K}(np)$  (Frey *et al* 1994b); ○,  $\sigma_e\text{-K}(np)$  (Ling *et al* 1992); —, free electrons (Hotop 1994); ---, free electrons (Orient *et al* 1989); △, free electrons (Christodoulides and Christophorou (1971); ----, theory (Klots 1976).

## Cold electron scattering in SF<sub>6</sub> and C<sub>6</sub>F<sub>6</sub>: Bound and virtual state channels

 D. Field,<sup>1,\*</sup> N. C. Jones,<sup>1</sup> and J.-P. Ziesel<sup>2</sup>
<sup>1</sup>Department of Physics and Astronomy, University of Aarhus, DK- 8000 Aarhus C, Denmark

<sup>2</sup>Laboratoire Collisions Agrégats Réactivité (CNRS UMR5589), Université Paul Sabatier, 31062 Toulouse, France

(Received 26 November 2003; published 20 May 2004)



The general process which we study involves electron attachment,

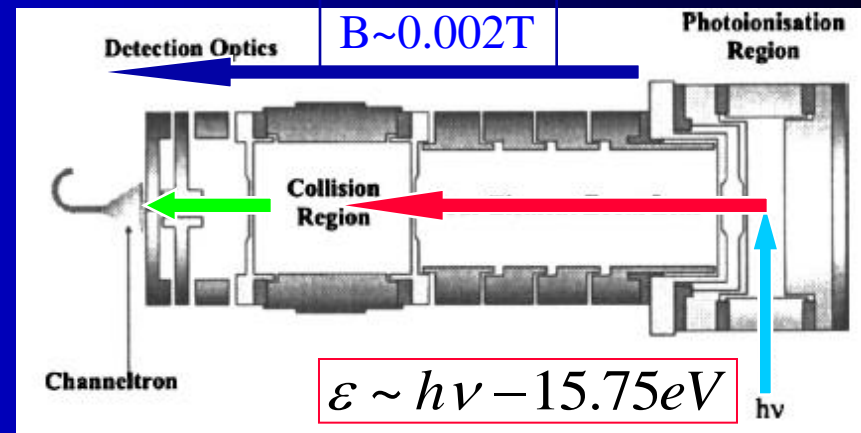
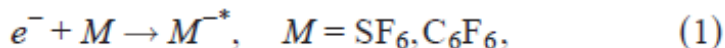
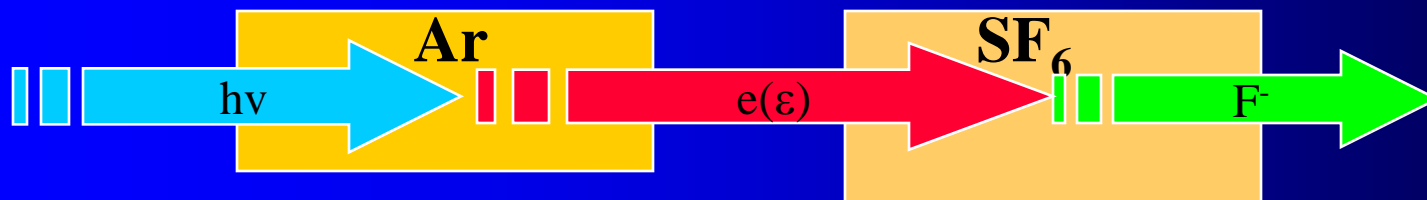
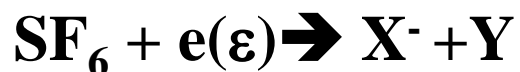


FIG. 1. A scale diagram of the apparatus. Monochromatic synchrotron radiation from ASTRID ( $h\nu$ ) enters a photoionization region containing Ar. Photoelectrons, expelled by a weak electric field, are focused by a four-element lens [38] into a collision chamber containing the target gas. Transmitted electrons are detected at the channel electron multiplier (channeltron) situated beyond some further electron optics. The apparatus may be immersed in an axial magnetic field of  $2 \times 10^{-3}$  T.

**B=0.002T**



$$\epsilon \sim h\nu - 15.75 \text{ eV}$$



## Scattering of cold electrons by ammonia, hydrogen sulfide, and carbonyl sulfide

N. C. Jones,<sup>1</sup> D. Field,<sup>2,\*</sup> S. L. Lunt,<sup>3</sup> and J.-P. Ziesel<sup>4</sup><sup>1</sup>*Institute for Storage Ring Facilities (ISA), University of Aarhus, DK-8000 Aarhus C, Denmark*<sup>2</sup>*Department of Physics and Astronomy, University of Aarhus, DK-8000 Aarhus C, Denmark*<sup>3</sup>*Kittiwake Developments Ltd, Littlehampton, West Sussex BN17 7LU, United Kingdom*<sup>4</sup>*Laboratoire Collisions Agrégats Réactivité (CNRS-UPS UMR5589), Université Paul Sabatier, 31062 Toulouse, France*

(Received 2 July 2008; published 29 October 2008)

Experimental data obtained with a high-resolution transmission experiment are presented for the scattering of electrons in the energy range 20 meV–10 eV for  $\text{NH}_3$ , 25 meV–10 eV for  $\text{H}_2\text{S}$ , and 15 meV–2.5 eV for OCS. Data include cross sections for both integral scattering and scattering into the backward hemisphere, the latter up to 650 meV impact energy, with an electron energy resolution of between 1.6 and 3.5 meV. The new data allow the first detailed comparison with theory for the energy regime dominated by rotationally inelastic and elastic scattering for these species. It is evident that theory still lacks quantitative predictive power at low energy, although qualitative agreement is consistently good for all three species. A discussion is given of the possible presence of a virtual state in OCS scattering as recently proposed on theoretical grounds.

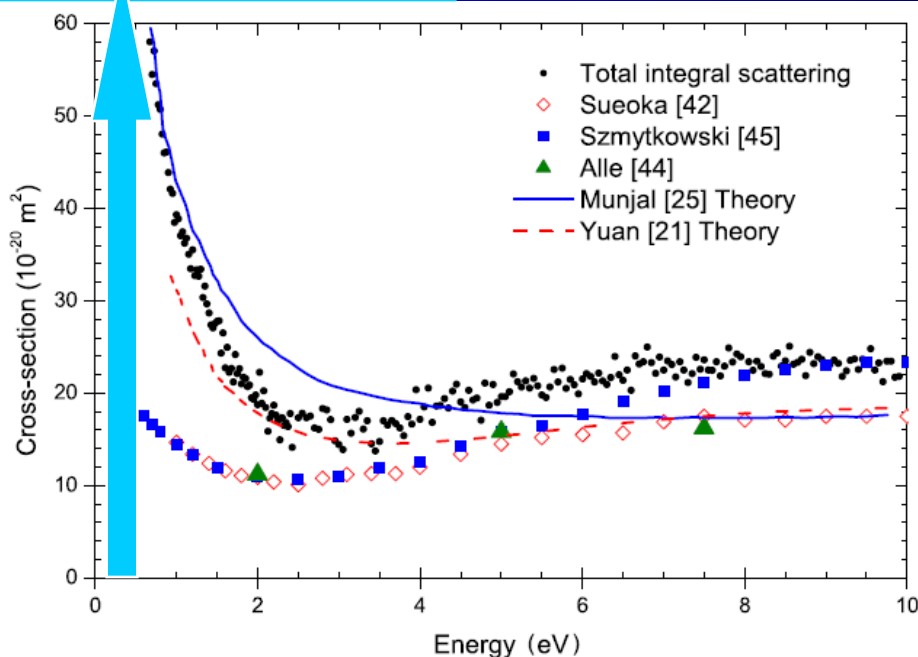
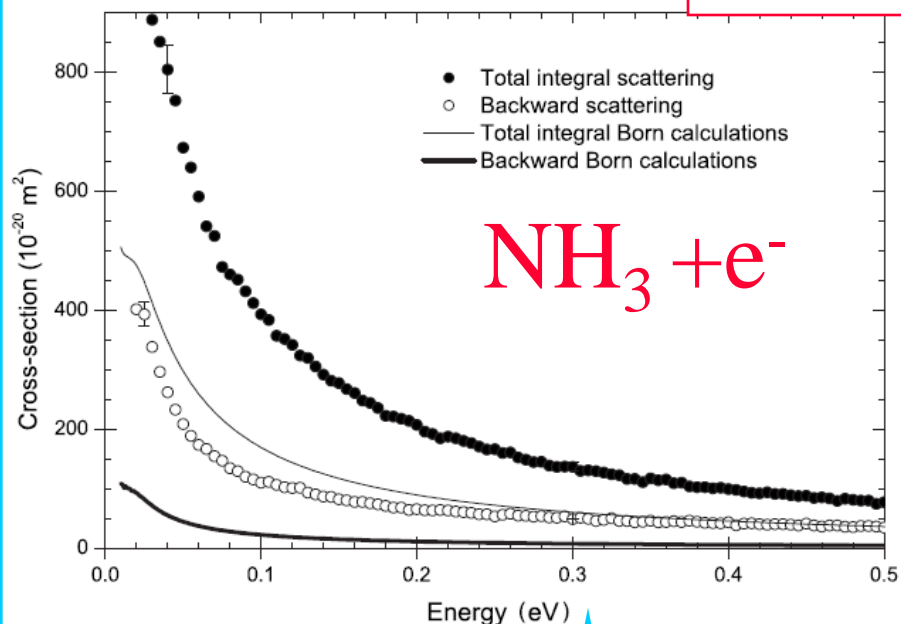


FIG. 1. (Color online)  $\text{NH}_3$ : the variation of the sum of the integral elastic and inelastic cross sections,  $\sigma_{T,I}$ , between 0.675 and 10 eV. Also shown are experimental data from Sueoka *et al.* [42], Szmytkowski *et al.* [45], and Alle *et al.* [44] and theoretical values from Munjal *et al.* [25] and Yuan *et al.* [21].

# Molecules cross section for interaction with electrons

2008

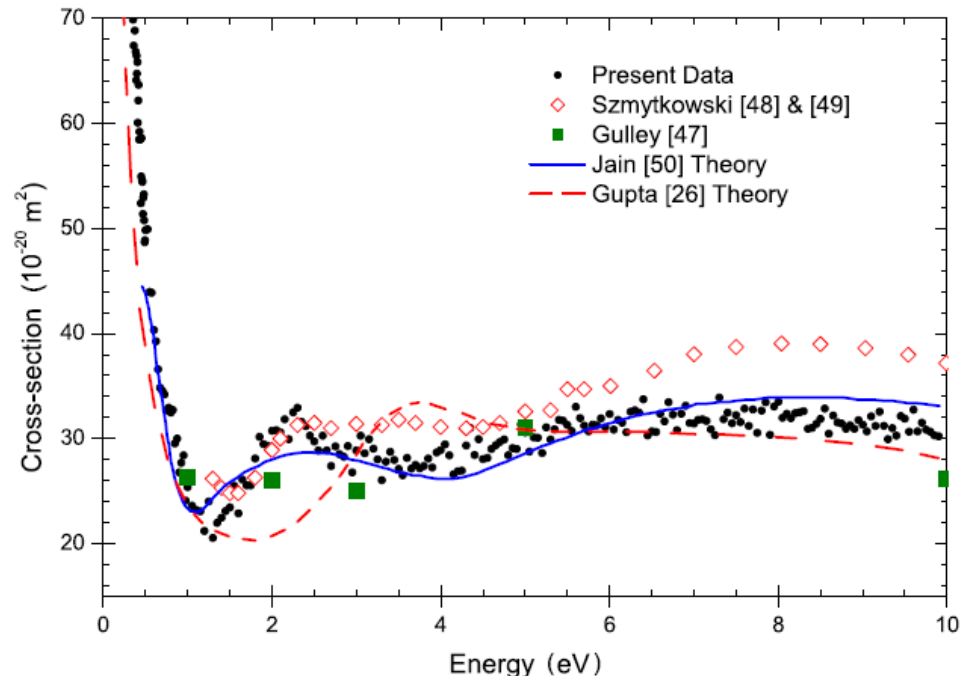


FIG. 3. (Color online)  $\text{H}_2\text{S}$ : the variation of the sum of the integral elastic and inelastic cross sections,  $\sigma_{T,I}$ , between 380 meV and 10 eV. Also shown are experimental data in Szmytkowski *et al.* [48,49] and Gulley *et al.* [47] and theoretical values from Jain *et al.* [50] and Gupta *et al.* [26].

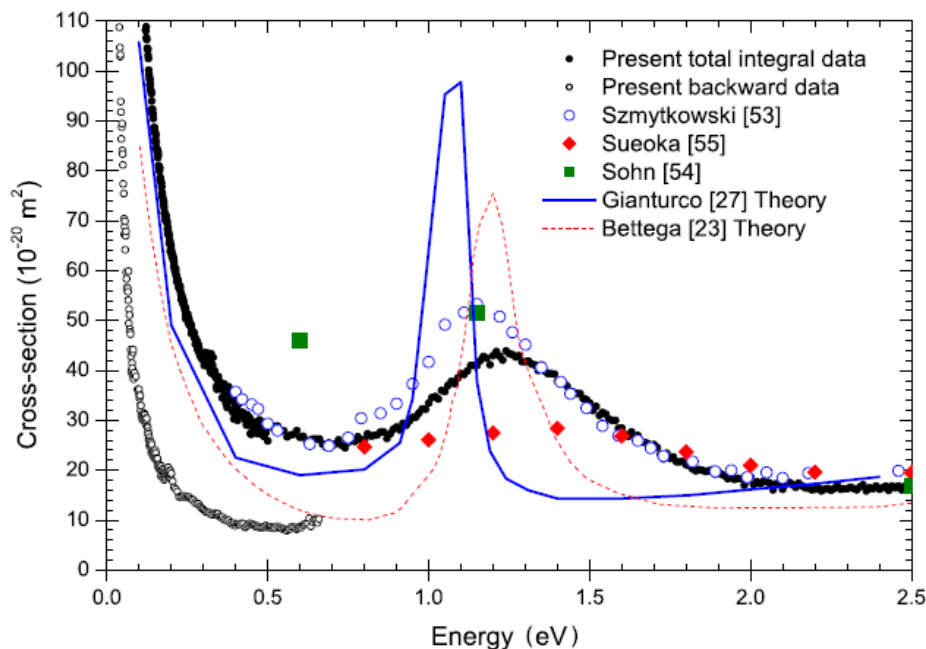
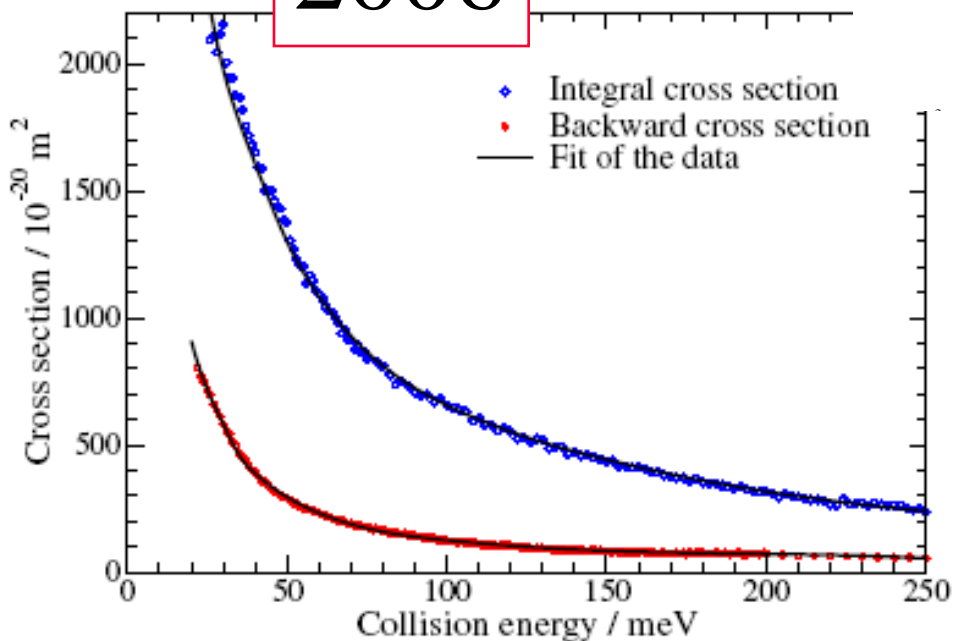
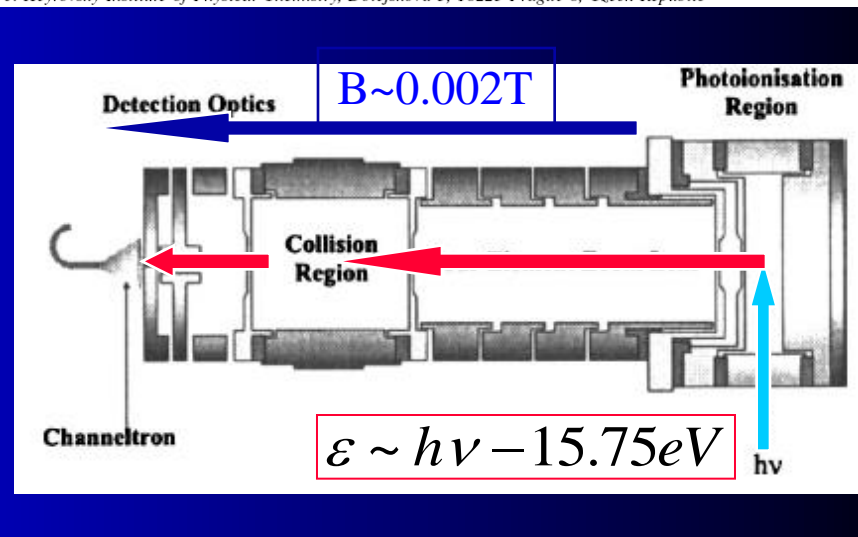
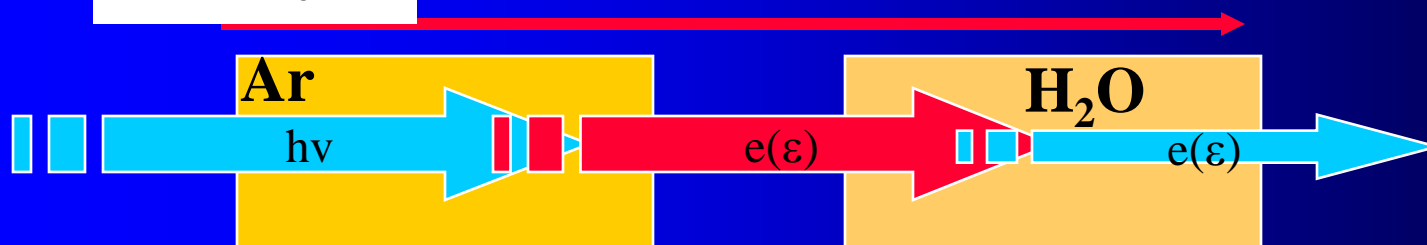


FIG. 5. (Color online)  $\text{OCS}$ : the variation of the sum of the integral elastic and inelastic cross sections,  $\sigma_{T,I}$ , between 120 meV and 2.5 eV, and the elastic and inelastic backward scattering cross section into the backward  $2\pi$  sr, between 39 and 650 meV. Also shown are experimental values from Szmytkowski *et al.* [53], Sueoka *et al.* [55], and Sohn *et al.* [54] and theoretical values of integral cross sections from Gianturco *et al.* [27] and Bettega *et al.* [23].

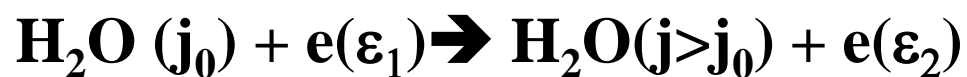
Rotational Excitation of H<sub>2</sub>O by Cold ElectronsR. Čurík,<sup>1</sup> J. P. Ziesel,<sup>2</sup> N. C. Jones,<sup>3</sup> T. A. Field,<sup>4</sup> and D. Field<sup>3,\*</sup><sup>1</sup>J. Heyrovský Institute of Physical Chemistry, Dolejšková 3, 18223 Prague 8, Czech Republic

Experimental data are presented for the scattering of electrons by H<sub>2</sub>O between 17 and 250 meV impact energy. These results are used in conjunction with a generally applicable method, based on a quantum defect theory approach to electron-polar molecule collisions, to derive the first set of data for state-to-state rotationally inelastic scattering cross sections based on experimental values.

$$B = 2 \times 10^{-3} \text{ T}$$



$$\epsilon \sim h\nu - 15.75 \text{ eV}$$



# Molecules

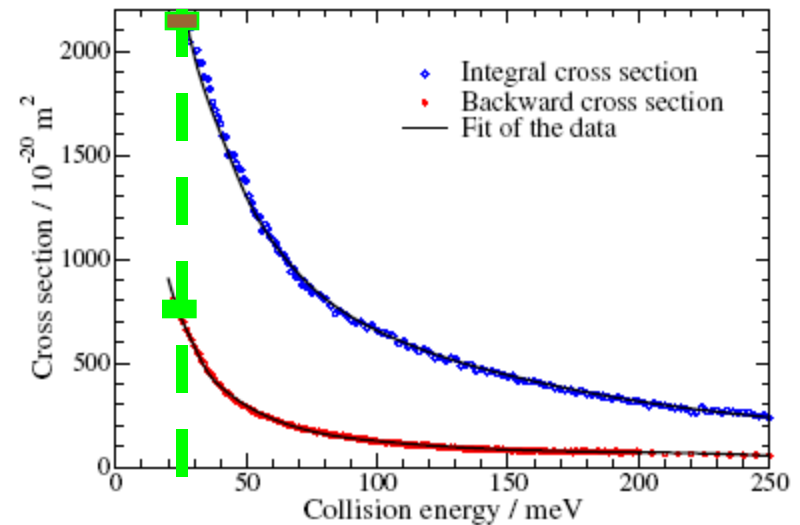
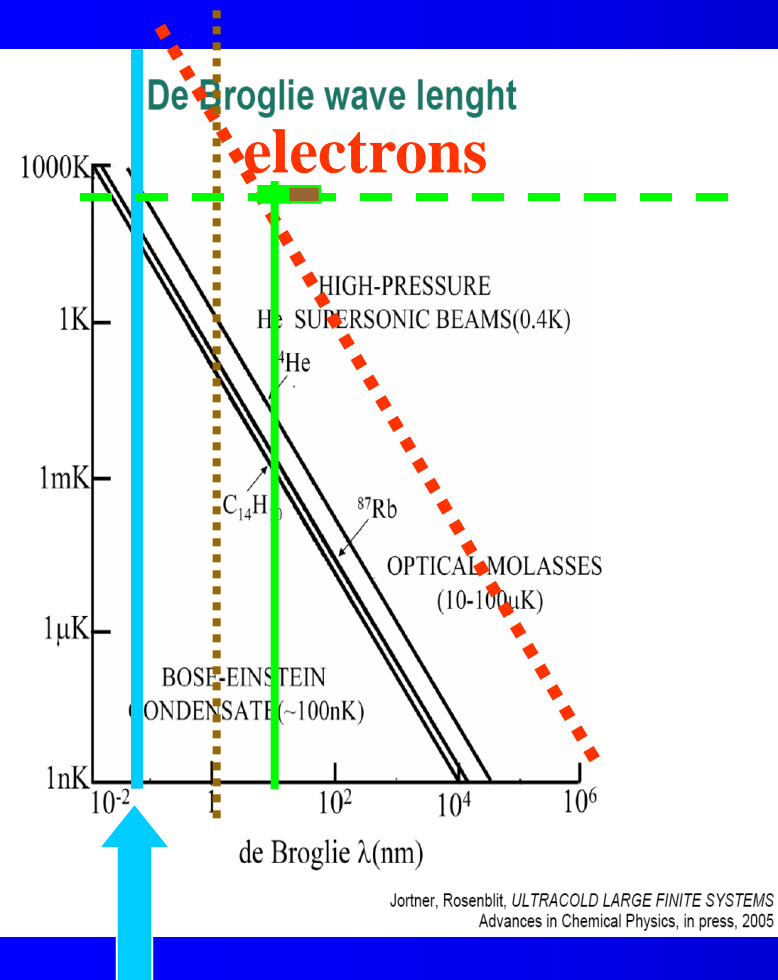


FIG. 1 (color online). Integral (upper set) and backward cross sections (lower set) for scattering of electrons by  $\text{H}_2\text{O}$  as a function of electron impact energy. Values are  $\pm 5\%$ . The solid lines are fits to theory (see text).

$$\lambda = \frac{h}{p} = \frac{h}{mv} \sqrt{1 - \frac{v^2}{c^2}}$$

$$\sigma \sim \pi \lambda^2 \sim 1/\varepsilon$$



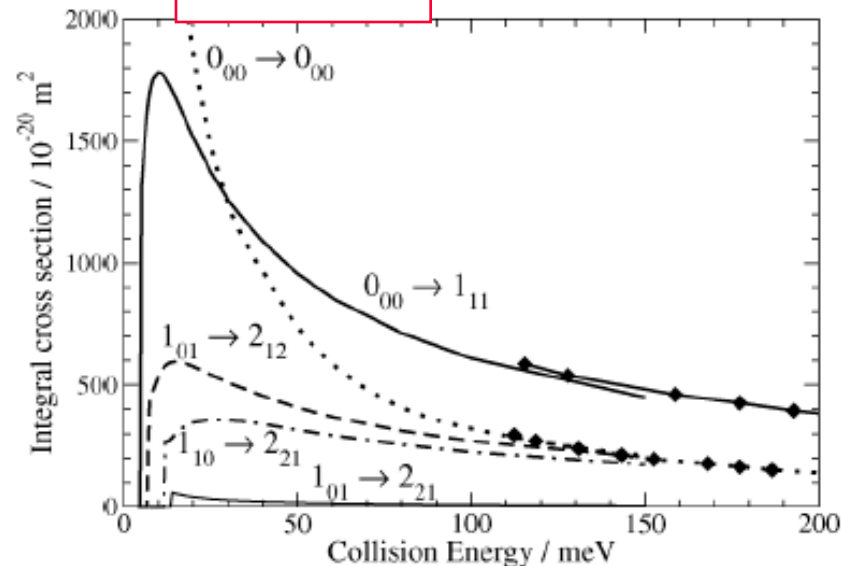
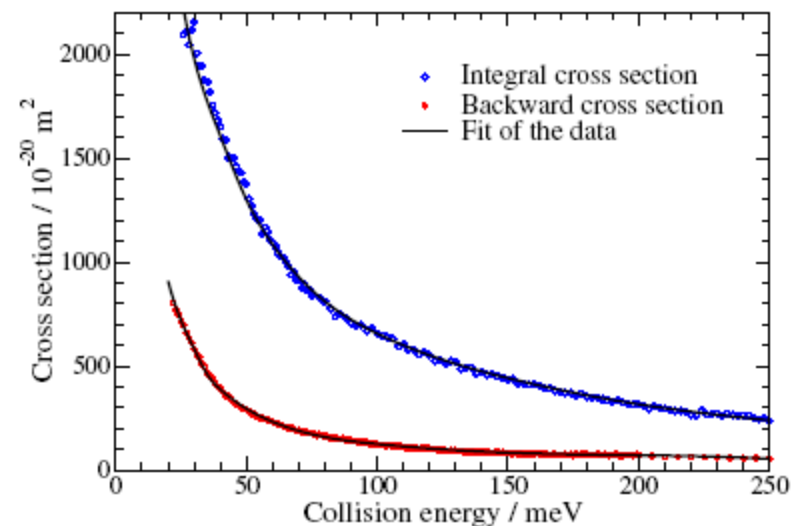
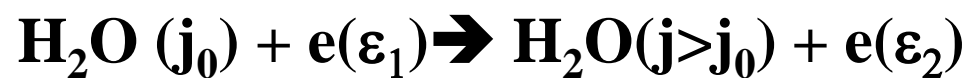


FIG. 3. Selected state-to-state integral cross sections for rotational excitation of the  $\text{H}_2\text{O}$  molecule determined from experimental data. Full curves represent results for para- $\text{H}_2\text{O}$  and dashed for ortho- $\text{H}_2\text{O}$ . The dotted curve represents elastic scattering for para- $\text{H}_2\text{O}$  in its lowest rotational state. Curves with diamonds show the results of  $R$ -matrix calculations in Ref. [12].



**End of story 25 10 2021**















# Collisions of electrons with atoms

Classical or quantum approach?

**Electron:**

$$\begin{aligned} 1\text{eV} &\rightarrow v = 5.9 \times 10^7 \text{ cm s}^{-1} \\ \tau &\sim a_0/v \sim 10^{-8} / 5.9 \times 10^7 = 2 \times 10^{-16} \text{ s} \\ \lambda &\sim 2\text{\AA} = 2 \times 10^{-8} \text{ cm} \text{ de Broglie} \end{aligned}$$

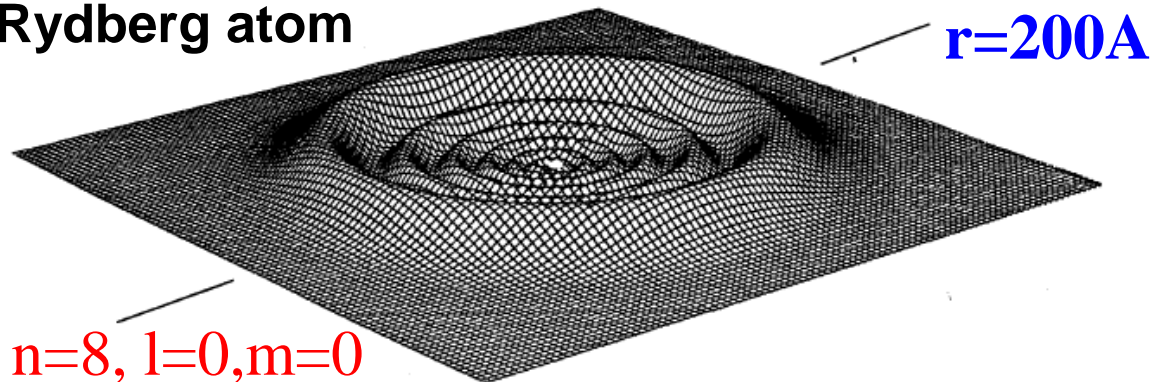
**Ar+:**

$$\begin{aligned} 1\text{eV} &\rightarrow v = 2 \times 10^5 \text{ cm s}^{-1} \\ \tau &\sim a_0/v \sim 10^{-8} / 2 \times 10^5 \sim 6 \times 10^{-14} \text{ s} \\ \lambda &\sim 9 \times 10^{-11} \text{ cm} \text{ de Broglie} \end{aligned}$$

$\text{H}_3^* + e$  at 10 K ????

$$\lambda_e(4\text{K}) \sim 540 \text{ \AA} \sim 54 \times 10^{-9} \text{ m}$$

Rydberg atom



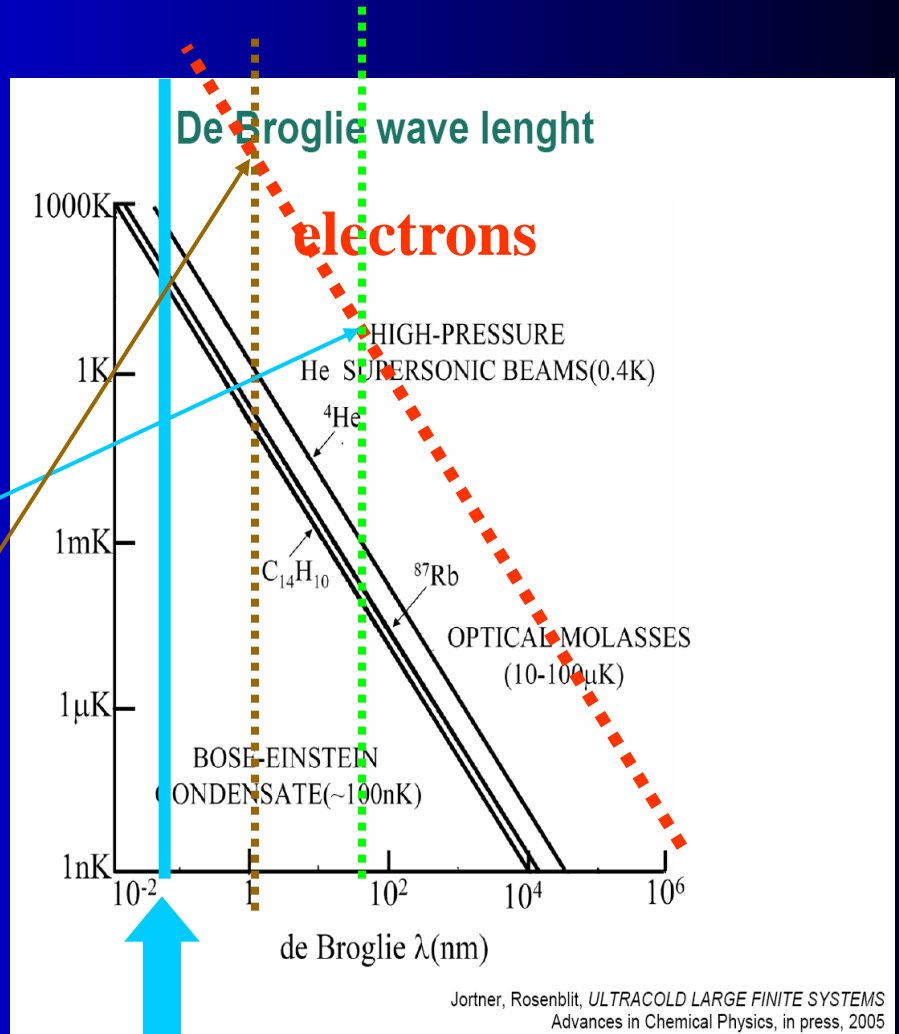
# Low energy collisions of electrons with molecules

## De Broglie wave length

$$\lambda = \frac{h}{p} = \frac{h}{mv} \sqrt{1 - \frac{v^2}{c^2}}$$

$$\lambda_e(4K) \sim 540 \text{ \AA} \sim 54 \times 10^{-9} \text{ m}$$

$$\lambda_e(1eV) \sim 11.6 \text{ \AA} \sim 1.16 \times 10^{-9} \text{ m}$$

 $a_0$